The Impact of Loricrin Deficiency on *Porphyromonas gingivalis* Induced Periodontitis

by

Karen K Ho

A thesis submitted in partial fulfillment of the requirements for the degree of

Master of Science

Medical Sciences – Oral Biology
University of Alberta

ABSTRACT

Background: According to the 2017 periodontal classification, severe forms of periodontitis (SvP) are characterized as stage 4, grade C, and hold the greatest extent of destruction to the tissues and bones surrounding teeth. Underlying mechanisms in the etiology of SvP remain to be discovered. Some studies suggest that the causative factor(s) is related to host defense, while others suggest it is related to the pathogenic bacteria. We have focused on the cornified epithelium (CE), which is the outermost layer of the skin and oral mucosa. Within this epithelial layer, an insoluble protein, called loricrin, comprises 70-80% of the total protein mass, and helps maintain the barrier between the external and internal environments. Down regulation of loricrin has been shown to be involved in inflammatory skin disorders, which suggests that this protein plays a key role in the barrier function of the CE. An animal model used to study these skin disorders, Signal Transducer and Activator of Transcription 6 VT (Stat6VT) transgenic mice, overexpress the transcription factor Stat6, causing higher levels of T Helper Cell Type 2 (Th2) cytokines and consequently, decreased loricrin expression. **Hypothesis:** Stat6VT mice, due to an impaired epithelial barrier as a result of loricrin deficiency, will develop an exaggerated immune response and much greater bone loss compared with littermate control mice, both in response to normal bacteria in the oral cavity, and even more so in response to a periodontal disease pathogen challenge. **Specific Aims:** Aim 1. To determine if there is a reduction in the expression of loricrin in the oral epithelium of Stat6VT mice compared to controls. Aim 2. To investigate Stat6VT mice for alveolar bone loss, histological evidence of inflammation, and changes in tissue structure in the oral epithelium. Aim 3. To infect Stat6VT and control mice with *Porphyromonas gingivalis (Pg)* and compare alveolar bone loss, histological evidence of inflammation, and changes in tissue structure in the oral epithelium. **Methods and Expected Outcomes**: A longitudinal study was performed on unchallenged Stat6VT mice and controls to

determine whether, similar to skin loricrin, there is a down-regulation of oral loricrin that corresponds with disease development. Based on the literature, mice were euthanized at weeks 6-8-, 10-13-, and 18-week time points and gingiva, palate, heads and blood were collected for experimentation. Cardiac puncture was performed to draw blood for analysis of Th2 cytokines and systemic inflammatory status (cytokine array). An enzyme-linked immunosorbent assay (ELISA) was used to determine loricrin expression in gingival tissue. Alveolar bone loss was assessed using microcomputed tomography (microCT) and tissue morphology of the palate was qualitatively assessed by histological examination. Additionally, we performed immunohistochemical assessments of leukocyte infiltration (antibody to cluster of differentiation 45 or CD45), antigen KI-67 (Ki67 antibody), keratin (cytokeratin 1 and 14 antibodies) and loricrin expression (loricrin antibody). Based on information from Aim 1, a time frame was chosen to orally infect mice with *Pg* by oral lavage every other day for 2 weeks. At endpoint, blood, heads and tissue were collected for assessment using methods similar to those in Aim 1.
Results: The longitudinal study was made up of 9-11 male and 9-11 female Stat6VT and control mice for each time point. Phenotypical observations confirmed that the time points (6-8-, 10-13-, and 18 weeks) were appropriate for our study. Lesion onset occurred at 10-13-weeks; therefore, this time point was chosen for *Pg* infection. In both the uninfected and *Pg* infected groups, microCT analysis demonstrated a reduction in alveolar bone levels in the Stat6VT mice when compared to controls. Additionally, histological examination demonstrated increased signs of inflammation in the Stat6VT mice compared to controls. The ELISA did not demonstrate any significant differences in the 10-13- or 18-week time point. Cytokine array profiling identified 5 cytokines in the uninfected group: Cluster of Differentiation 30 Ligand (CD30L), Eotaxin 2, Monocyte Chemotactic Protein 5 (MCP5), Monokine Induced Gamma Interferon (MIG) and B

Lymphocyte Chemoattractant (BLC). 3 cytokines were identified in the *Pg*-infected group: Osteopontin (OPN), Insulin-like Growth Factor Binding Protein 2 (IGFBP2), and Intercellular Adhesion Molecule 1 (ICAM1). **Significance:** Our studies suggested increased inflammation/bone loss in some cases that could be a result of an impaired epithelial barrier. SvP studies have been greatly hindered by the lack of a suitable animal model, and Stat6VT mice showed aspects of the disease, such as accelerated bone loss in response to a periodontal pathogen. Further study is necessary, but our results suggest that they could provide an important new tool in the field.

PREFACE

This thesis is an original work by Karen Ho. All animal procedures were approved in 2018 by the University of Alberta Animal Care and Use Committee, AUP00002935.

Development of experiments and techniques, as well as editorial and intellectual contributions to this dissertation was done in collaboration with Dr. Febbraio. Dr. Raisa Catunda developed and created the microCT approach used in this dissertation, and she also collaborated with me on all experiments performed. Dr. Maria Alexiou assisted in scanning all the mice heads for the microCT analysis and Shrushti Patel assisted in the analysis of these results. CD45 and Ki67 cell count analysis was assisted by Sara Moradipoor and Ramesh Mahdavifar. In Chapter 3, cytokine array experiment was performed by Sara Moradipoor and analyzed by Dr. Febbraio. I collected the samples for the experiment but had no part in performing the experiment or analyzing this data.

ACKNOWLEDGEMENTS

I would like to begin by extending my greatest gratitude and appreciation to my supervisor, Dr. Maria Febbraio. As a clinical student with minimal lab experience, you were patient with my lack of expertise and mentored me every step of the way. The lessons you've taught me these two and a half years extends beyond the lab, as I've learned to not only be a better scientist, but a better critical thinker and problem solver too. I will never thank you enough for all your support and your efforts to help me chase my dreams, no matter what they were. I would also like to thank my co-supervisor Dr. Liran Levin and my supervisory committee member Dr. Ava Chow. Thank you for the support and advice along the way.

I would also like to give a special mention to my lab mate and my dear friend, Dr. Raisa Catunda. This project would not have been possible without her dedication and hard work. I am forever grateful for the support and friendship she provided me throughout my Master's.

I am grateful for past and current lab members: Umar Rehki, Konrad Lehmann, Julia Piche, Linnet Immaraj, Yuli Berlin-Broner, Danielle Clark, Mohamed Omar and DongDong Fang. It was a pleasure working with all of you throughout my Master's. And thank you to all my colleagues in the Biomedical Oral and Maxillofacial Research Unit, especially Dr. Maria Alexiou, for the support throughout my graduate studies. Thank you to the summer/undergraduate students: Zahra Mantaka, Aneesh Bhardwaj, Shrushti Patel, Ramesh Mahdavifar and Kelli-Ann Sharun for the assistance throughout the project. Lastly, I would like to thank all my funding sources for supporting my studies: University of Alberta Hospital Foundation Fund, CIHR, FoMD (Graduate Recruitment and AGES Scholarship), SoD (Fund for Dentistry, Dental Hygiene Research Grant and Student Stipend).

TABLE OF CONTENTS

LIST OF TABLES

LIST OF FIGURES

CHAPTER 1: INTRODUCTION

1.1 Periodontitis

Periodontitis is defined as an inflammatory disease that results in irreversible destruction to the soft and hard tissue structures in the oral cavity that can lead to tooth loss (Caton *et al*., 2018). This disease occurs as a result of an interaction between the plaque biofilm (which contains bacteria) that accumulates on tooth surfaces, and the body's efforts to fight this infection (Armitage & Cullinan, 2000; Caton *et al*., 2018). The 2017 Global Periodontal Health Project Report, released by The World Dental Federation, notes that up to 50% of the global adult population is affected by periodontitis (Tonetti *et al*., 2017). Symptoms of periodontitis include gingival swelling, redness and bleeding (Armitage, 2002). If left unmanaged, loss of bone supporting the tooth structure can occur, which can lead to further gingival recession, periodontal pocketing, tooth mobility or even complete loss of the tooth. Periodontitis is commonly accompanied by heavy buildup of plaque and dental calculus, sometimes leading to exudate (Armitage, 2002).

There are many risk factors that have been identified for periodontitis. Demographic differences, such as age, sex and socioeconomic status can influence likelihood of periodontitis (Armitage, 2002; Caton *et al*., 2018). Furthermore, medical history such as tobacco use, diabetes, osteoporosis, HIV/AIDs and genetic predisposition can also influence likelihood. In addition, dental history, such as family history of early tooth loss, frequency of dental visits, previous history of periodontitis and oral homecare habits can determine risk of contracting periodontitis (Caton *et al*., 2018).

There are various ways to manage periodontal disease. First, a comprehensive oral examination and radiographs can be taken to determine the severity of the condition (Clark *et al*.,

2017). This may be followed by treatment planning and referral to an endodontist or periodontist, if indicated. Periodontitis can sometimes be managed with nonsurgical periodontal therapy (Badersten *et al*., 1981). This entails oral health education, smoking cessation and nutritional counseling, dental hygiene treatment (scaling and root planing, fluoride therapy) and adjunctive therapy (rinses and antimicrobial treatment). In more severe cases, surgical therapy may also be performed, such as periodontal or endodontic surgery or dental implant placement (Caton & Nyman, 1980). And finally, periodontal maintenance, by ongoing dental hygiene treatment, should be implemented in order to stabilize the treated conditions (Famili & Short, 2010).

At the proceedings of the 2017 World Workshop on the Classification of Periodontal and Peri-implant Diseases and Conditions (WWDC), a new classification system for periodontitis was developed. Specifically, the previously recognized "chronic" and "aggressive" forms of periodontitis are now characterized based on a multidimensional staging and grading system (Caton *et al*., 2018). Staging includes severity, complexity, extent and distribution of the disease. Grading includes the time frame of progression of the disease (Caton *et al*., 2018).

1.2 Severe forms of periodontitis

In the former 1999 Classification of Periodontal Disease and Conditions, aggressive periodontitis was a distinct disease entity that was distinguished from other more typical forms of periodontitis by its early age of onset, advanced rate of progression and familial aggregation (Albandar, 2014). Indeed, aggressive periodontitis was commonly observed in those under 30 years of age and affected 2% of the world's population (Susin *et al*., 2014). A characteristic of this distinct disease is very minimal plaque and calculus buildup that is oddly coupled with a rapid rate of tissue destruction. Studies have suggested genetic predisposition to this condition

and having a family history of periodontitis (Albandar, 2014). Management strategies available are similar to those for treating periodontal disease, however, there is more of a need for surgical therapy, as well as increased patient compliance for maintenance care (Clark *et al*., 2017). Additionally, use of systemic antibiotics may be more effective in these patients. With the new proceedings of the 2017 WWDC which recognizes periodontitis as a spectrum disorder, what was previously characterized as aggressive periodontitis has now been placed at the end of the disease spectrum and falls into the category of grade C stage IV periodontitis (Caton *et al*., 2018). For simplicity, in this thesis we have used the term "severe periodontitis" (SvP).

The underlying mechanism in the etiology of SvP is still unknown (Clark D *et al*., 2017; Nibali L, 2015), however, studies suggest that genetic factors (Gandhi & Kothiwale, 2012; Schork *et al*., 2000; Vieira & Albandar, 2014) and bacteria, especially those in the red complex, play a role (Casarin *et al*., 2010; Chahboun *et al*., 2015; Herbert *et al*., 2016). The red complex is a combination of periodontal pathogens which include *Porphyromonas gingivalis (Pg)*, *Treponema denticola*, and *Tannerella forsythia*, that are found within the periodontal pocket, and are known to cause destruction of the hard and soft tissues (Suzuki *et al*., 2013). Nonetheless, an apparent commonality amongst all types of periodontitis is that the hosts' response to bacteria is essential to the inflammatory response (Tapashetti *et al*., 2013; Zhang *et al*., 2003).

This commonality is important especially when considering the etiology of SvP. As mentioned, the minimal amount of plaque bacteria does not correlate with the severity of damage and heightened inflammatory response (Albandar, 2014). In this thesis, we consider that a compromised oral epithelial barrier leads to a change in perception of pathogenic threat. If the integrity of the oral barrier is compromised, then the exposure of the host to even a small amount

of plaque would be altered, producing a response that would appear exaggerated, but in fact in line with what the host perceived.

1.3 The etiology of barrier dysfunction

1.3.1 Cornified epithelium

The cornified epithelium (CE) is the outermost epidermal layer of the skin and sometimes known as keratinized epithelium in the oral mucosa (Candi *et al*., 2005; Darlenski & Tsankov, 2011). The major cell type present is the keratinocyte, that helps maintain barrier function. These cells produce keratins, which provide mechanical strength for the epithelia. Keratins work with other structural proteins to join adjacent cells tightly together to create a barrier from external physical and chemical forces (Candi *et al*., 2005; Darlenski & Tsankov, 2011).

Creation of the cornified epithelium is through a tightly regulated differentiation process (Candi *et al*, 2005; Darlenski & Tsankov, 2011; Nemes & Steinhert, 1999). Cells lose their nucleus and all other cytoplasmic organelles, and the plasma membrane becomes highly reinforced with keratin. Proteins from the granular layer such as loricrin, involucrin, filaggrin and small proline rich (SPR) proteins, form a scaffold under the cell membrane in which the keratins are embedded (Proksch *et al*., 2008). These proteins are hydrophobic—which means water resistant, and are highly cross-linked, forming a tight mesh (Candi *et al*., 2005, Darlenski & Tsankov, 2011; Nemes & Steinhert, 1999). Lipids also become part of the cornified layer, to prevent water loss. As a result of this process, our skin and oral mucosa provide a shield against the environment and bacteria, while preventing dehydration (Candi *et al*., 2005; Darlenski & Tsankov, 2011; Nemes & Steinhert, 1999).

1.3.2 Loricrin

Of the proteins mentioned, loricrin is the most abundant in the CE. Loricrin is a 26 kilodalton (kDa) insoluble protein that comprises approximately 70-80% of the CE (Nithya *et al*., 2008). It has the highest level of expression in humid tissues, such as the oral mucosa. Loricrin is only expressed in keratinized epithelia and reinforces the CE by providing flexibility and protection against mechanical stress (Hohl *et al*., 1991; Kalinin *et al*., 2001; Steinhert *et al*., 1998; Steinhert & Marekov, 1995; Steven & Steinhert, 1994). Furthermore, loricrin contains many transglutaminase crosslinking sites, which allows it to act as a strong barrier between the external and internal environment. Studies have shown that when loricrin is not expressed appropriately in the CE, the barrier function can become compromised, leading to skin diseases such as Vohwinkel syndrome, psoriasis, and atopic dermatitis (AD) (Agrawal & Woodfolk 2014; Guttman-Yassky *et al*., 2009; Koch PJ *et al*., 2000; O'Driscoll J *et al*., 2002). These conditions suggest that any issues that arise during the process of cornification or transglutamination can lead to a change in barrier function and manifestation of disease.

1.4 Barrier function in skin disorders

In humans, defects in loricrin or filaggrin are associated with skin disorders such as AD (O'Driscoll *et al*., 2002; Koch *et al*., 2000). AD is a chronic inflammatory skin disease characterized by acute flare-ups of red, itchy lesions over dry skin. It has been estimated that approximately 20% of children and 3% of adults are affected by AD globally (Nutten, 2015). AD has been shown to be caused by a T Helper Cell Type 2 (Th2) immune response, similar to that observed in SvP (Garlet *et al*., 2003; Bartova *et al*., 2000; Lappin *et al*., 2001; Sehra *et al*., 2016). The expression of IL-4, IL-13 and basophil infiltration then leads to a dramatic inflammatory response that manifests as skin lesions of the epithelial layer. There is currently no evidence of association between SvP and AD, but this has not been specifically studied, which

may be due to the low prevalence of SvP globally. Additionally, structural proteins such as filaggrin and loricrin have not specifically been studied in periodontal research, which may also explain the lack of available literature. However, the parallels observed between the diseases in terms of onset and immune response suggest that research into an association could have merit.

Another skin disorder, psoriasis, is a chronic disease that is also affected by downregulation of CE proteins (Bilal *et al*., 2018). Individuals who suffer from psoriasis present with scaly, erythematous plaques on the skin. Although its exact mechanism is still being investigated, it is considered to be a T Helper Cell Type 1 (Th1) autoimmune disease. Additionally, a protein called psoriasin has most recently attracted study (Son *et al*., 2016). Research has shown that psoriasin is upregulated in psoriasis and AD and may play a role in regulation of epithelial cell differentiation. Recent epidemiological studies have shown an association between psoriasis and periodontal disease (Holmstrup *et al*., 2017; Nakib *et al*., 2013; Painsi *et al*., 2017; Sarac *et al*., 2017; Su *et al*., 2017).

Both AD and psoriasis are elicited by an apparent combination of factors, including immune dysregulation, skin barrier disruption, genetics and environmental influences (Chovatiya & Silverberg, 2019). Emerging research continues to recognize the role of Th2 cells in AD, and Th1 and T Helper Cell 17 (Th17) in psoriasis, and their effects on the inflammatory response. Although both skin disorders share similarities, their presentation can differ in appearance and location. AD commonly presents on parts of the body that bend, such as elbows and behind the knees (Nutten 2015). While psoriasis may also present in these areas, it can also be found on the scalp or face region, lower back and palms or soles of the feet (Armstrong & Read, 2020). Additionally, psoriasis may be thicker and more inflamed than AD.

These similarities and associations observed between skin disorders and SvP suggest that a change in CE proteins can lead to an immune response triggered by a potential defect in epithelial barrier function. In further support of this idea, we found two unbiased studies in the literature that globally compared gene expression in SvP. Loricrin was among the most profoundly decreased genes: there was a 7-fold decrease in loricrin in SvP patients compared to healthy controls (Guzeldeimir-Akcakanat *et al*., 2015). In the second study, loricrin gene expression was decreased by 25% in SvP patients compared to chronic periodontal disease patients (Nowak *et al*., 2013). In both studies, filaggrin was also downregulated, but to a lesser extent. Since loricrin is the most abundant protein in the cornified epithelial layer, we considered that its expression in the oral cavity, and more specifically the gingiva, might be important to the functionality of the cornified epithelium. In line with the new WWDC classification, which recognizes periodontitis as a spectrum disorder (Caton *et al*., 2018), we would also consider that when there is more of a decrease in CE proteins such as loricrin and filaggrin, then a larger barrier defect would result, manifesting as a worse disease state. What is even more compelling is that when there is a periodontal disease pathogen present, such as *Pg*, studies suggest it can mediate down-regulation of loricrin gene transcription, thereby playing a role in contributing to the barrier defect (Bao *et al*., 2017; Kim *et al*., 2008).

1.5 Th2 immune response in skin disorders and SvP

As mentioned previously, AD is known to predominately be a disease of Th2 imbalance (Garlet *et al*., 2003; Bartova *et al*., 2000; Lappin *et al*., 2001; Sehra *et al*., 2016). This is because all stages of AD are most strongly influenced by Th2 cell activity, as evidenced by increased expression of cytokines such as IL-4, IL-5, IL-10, IL-13, IL-31 and CC chemokine ligand 5 (CCL5) (Chovatiya & Silverberg, 2019). It is known that this group of mediators is involved in

impairment of terminal keratinocyte differentiation through inhibition of filaggrin, loricrin and involucrin, and downregulation of antimicrobial peptides, which leads to permeability of pathogens. As for psoriasis, the pathogenetic mechanism is still under investigation. Until recently, interferon-gamma (IFN-γ) producing Th1 cells were thought to be the main T helper cell response driving psoriasis susceptibility. Recent investigations have discovered an association between psoriasis and the IL-4/IL-13 gene locus, the site of IL-1 and IL-13 production in the Th2 cell response and predominately implicated in the pathogenesis of AD (Hahn & Goreschi, 2017).

Similar to these skin disorders, SvP cell immune response remains unclear, however, there is significant evidence that suggests an association with a Th2 immune response (Manhart *et al*., 1994; Pan *et al*., 2019; Yamazaki *et al*., 1994). Studies have shown that Th2 cells exert complex effects that can lead to tissue destruction in periodontitis, secreting cytokines such as IL-4, IL-5, IL-6, IL-9, IL-10 and IL-13. There is reason to believe that Th2 cells contribute to the progressive lesion phase of periodontitis due to the predominately large number of B lymphocytes (produced by Th2 cytokines) found in periodontitis (Bartova *et al*., 2000; Pan *et al*., 2019; Seymour *et al*., 1993; Zein *et al*., 2017). The Th2 immune response is known to produce cytokines for B cell activation and production of B cell IL-1, a well-established necessity for stimulation of bone destruction in periodontal disease.

1.6 Mechanism of loricrin downregulation

Studies have shown that individuals who suffer from AD have a downregulation of loricrin caused by Th2 cytokines via the Signal Transducer and Activator of Transcription (Stat) 6 pathway (Bao *et al*., 2017; Kim *et al*., 2008). This was shown to be the case at the protein and

gene level in both affected and non-affected AD sites (Kim *et al*., 2008). Th2 cytokines, specifically IL-4, have been shown to activate Stat6 via Janus kinase (Jak); this is a major signaling pathway in keratinocytes for cell proliferation, differentiation, migration and apoptosis (Bruns *et al*., 2003; Hou *et al*., 1994; Kim *et al*., 2008; Kotanides & Reich, 1993).

1.6.1 Jak-Stat pathway

The Jak-Stat pathway is activated when IL-4 binds to its cell-surface receptor causing dimerization and recruitment of Jak2 (Bao *et al*., 2017; Kim *et al*., 2008). Jak2 phosphorylates specific receptor tyrosine residues, which allow for Stat6 proteins to bind. The Stat6 proteins are then phosphorylated by Jak2 to form a dimer, which triggers translocation to the cell nucleus, DNA binding and transcription of target genes (Bao *et al*., 2017; Kim *et al*., 2008).

1.6.2 Increased Th2 response

As previously mentioned, IL-4 plays a key role in loricrin downregulation in patients with AD (Bao *et al*., 2003; Bruns *et al*., 2003; Hou et al., 1994; Kim *et al*., 2008; Kotanides & Reich, 1993). In keratinocytes, loricrin transcription requires a co-activator called p300/CBP, which is the same co-activator necessary for IL-4 activated Stat6 transcription (Bao *et al*., 2017). Therefore, when there is an increased Th2 response, IL-4 from T-cells stimulates the keratinocyte IL-4 receptor-Jak2-Stat6 pathway. This competes with the loricrin transcription complex for limited levels of the common co-activator, thus suppressing its transcription. This mechanism has been well recognized in AD studies and has only recently been investigated in the field of periodontal research, in which IL-4 was found to play a role in SvP patients. These studies revealed that a polymorphism in the IL-4 promoter leads to both elevated IL-4 and Stat6 expression in SvP patients (Gonzales *et al*., 2017; Gonzales *et al*., 2019).

1.7 Animal model consideration

In studying the role of loricrin downregulation, Th2 cytokines and Stat6, there are a number of mouse models worth considering. A loricrin knockout (KO) mouse was created in the past but interestingly, did not present with barrier dysfunction in the epithelium (Jarnik *et al*., 2002; Koch *et al*., 2000; Rice *et al*., 2016). This was primarily due to the compensatory upregulation of other cell envelope proteins, an occurrence that can be observed when a protein is eliminated early in embryogenesis, as is the case with KO mice. AD researchers have since developed other mouse models, including the Stat6VT transgenic and IL-4 transgenic to further their research.

1.7.1 Stat6VT transgenic mouse model

The Stat6VT transgenic mouse model has been used for over a decade to research the role of the Th2 response in AD (Bruns *et al*., 2003; DaSilva-Arnold *et al*., 2018; Kaplan *et al*., 2007; Sehra *et al*., 2008). These mice develop skin lesions with similarities to human disease over a relatively short period of time. Stat6VT was named as such because valine and threonine residues in the Stat6 protein are replaced with alanine. When these 2 residues are changed, it leads to a constitutive activation of the Stat6 protein, which bypasses the need for receptors to bind to IL-4 entirely (Bruns *et al*., 2003). As a result of constitutive activation of Stat6, the downstream genes are transcribed, which leads to increased production of cytokines that continually activate a Th2 response, ultimately leading to decreased loricrin expression (Bruns *et al*., 2003). The Stat6VT transgenic has approximately 2x less loricrin gene expression compared to wild-type and a decreased expression at the protein level in the CE as well (Kim *et al*., 2008). Interestingly, the oral epithelium of this mouse model has never been studied.

1.8 Hypothesis, research question and objective

Available literature suggests that the concept of barrier dysfunction as an etiology for SvP is plausible but has not been investigated to date. There is support for genetic predisposition and a role for specific pathogens, however the mechanism for SvP still remains unclear. We hypothesize that pathogen-mediated loricrin downregulation could result in an impaired oral epithelial barrier and lead to a heightened inflammatory response in SvP patients, that may explain the resulting pathology observed.

The objective of our study is to determine if the periodontal health of Stat6VT transgenic mice, with and without periodontal disease pathogen challenge, will be impacted by loricrin deficiency in the oral epithelium. We hypothesize that these mice, due to an impaired epithelial barrier as a result of loricrin deficiency, will develop an exaggerated immune response and much greater bone loss compared with littermate control mice, both in response to normal bacteria in the oral cavity, and even more so in response to a pathogen challenge. In order to address this hypothesis, we have defined 3 Aims:

Aim 1. To determine if there is a reduction in the expression of loricrin in the oral epithelium of Stat6VT mice compared to controls.

Aim2. To investigate Stat6VT mice for alveolar bone loss, histological evidence of inflammation, and changes in tissue structure in the oral epithelium.

Aim 3. To infect Stat6VT and control mice with *Pg* and compare alveolar bone loss, histological evidence of inflammation, and changes in tissue structure in the oral epithelium.

CHAPTER 2: METHODOLOGY

2.1 Ethics

All procedures were prior approved by the Animal Care and Use Committee (ACUC) of the University of Alberta (AUP 00002935).

2.2 Mice

Stat6VT transgenic mice were generously provided by Mark H. Kaplan (Indiana School of Medicine) in the form of sperm for rederivation by the Jackson Laboratory (Bar Harbor, ME). Male and female Stat6VT hemizygous mice were mated with wild-type C57Bl/6 mice in the viral antigen free facility at the University of Alberta and then transferred into conventional or biocontainment facilities. Mice were fed normal chow (4% total fat) and provided water ad libitum. Based on our breeding strategy, all Stat6VT positive offspring were hemizygous. Mice were genotyped and separated into sex matched Stat6VT positive or littermate control groups. Mice between the ages of 6 and 18 weeks of both sexes were utilized for this study.

2.3 Genotyping and gel electrophoresis

All chemicals and plasticware used were from Thermo Fisher Scientific. Mice were ear notched for genotyping and identification purposes. Ear notch samples were digested in 200µl of 0.01M ethylenediaminetetraacetic acid (EDTA), 1% sodium dodecyl sulfate, 0.05M Tris, pH 7.5 containing 200ng/ml of proteinase K in a 55°C water bath overnight. Nucleic acids were separated from protein and other tissue constituents by serial extraction with equal volume of tris saturated phenol and chloroform. DNA was precipitated with 2 volumes of 100% ethanol. The pellet was air dried and resuspended in Tris-EDTA (1M Tris, Ph 8, 0.5M EDTA) containing 4µg/ml of RNAse A.

Polymerase chain reaction (PCR) was performed by the protocol designed by our collaborator, Mark H. Kaplan. DNA oligo primers were purchased from Integrated DNA Technologies. Primers HAA9 (5'- GCC TAC CAT GGT GCC TTC TTA TG – 3') and VT FLAG (5'- TAT GCT TGT CAT CGT CCT TGT AGT CA – 3') targeted the novel FLAG tag to differentiate transgenic from wild-type mice. We used Ready-to-use PCR master mix (2X) (DreamTaq Green, K1082, Thermo Fisher Scientific) to achieve the final master mix. The PCR master mix included DreamTaq DNA polymerase, 2X DreamTaq green buffer, deoxyribose nucleotide triphosphate (dNTPs), and 0.004M magnesium chloride. The final master mix was made in sterile PCR grade water and consisted of 1X PCR master mix and 1μm of each primer (10μl volume reactions were used). The samples were then processed using the protocol as described in Table 1, using a model T100 Thermal Cycler (Bio-Rad).

Table 1. PCR thermocycler protocol

Temperature (°C)	Time
94 (denature)	2 minutes
94 (denature)	30 seconds
54 (anneal)	30 seconds
72 (extension)	60 seconds
Repeat	34x
72 (extension)	10 minutes
4	hold

PCR products were resolved on a 1.5% agarose gel using Tris-borate-EDTA as the running buffer (0.089M Tris, 0.089M boric acid, 0.002M EDTA). A ChemiDoc Imaging system

(model XRS+, Bio-Rad) was used to detect and document the results (ChemiDoc MP Imaging System, version 4.1, Bio-Rad).

2.4 Sample size calculations

In order to determine the number of mice per group, we performed a power calculation. We considered that a 25% difference in bone loss and protein expression would be significant. Additionally, periodontal disease model literature suggests a 20% variability in bone loss. Using the website: https://www.stat.ubc.ca/~rollin/stats/ssize/n2.html, we determined our sample size to be n=9 minimum (per sex at 80% power). Extra mice were included in case of malocclusion or unexpected morbidities/mortalities.

In the longitudinal study, sex and age matched mice were grouped into 3 established time points (6-8, 10-13 and 18 weeks). The *Pg* infected cohort was based on one time point. Using the same power calculation and rationale, a group size of at least 9 of each sex was required. In all cases, given the length of the studies and the potential for morbidity, we asked the ACUC for 3 extra mice/group. Thus 12 mice/group were approved in our protocol.

2.5 Study design

Stat6VT mice have been used extensively for studies on AD and inflammatory skin disorders (Bruns *et al*., 2003; DaSilva-Arnold *et al*., 2018; Kaplan *et al*., 2007; Sehra *et al*., 2008). Because there has been no previous study on the oral cavity of Stat6VT mice, a longitudinal study was conducted in order to best understand oral disease manifestation and ideal timing for *Pg* infection. We based our choice of time points on the development of skin lesions, with the consideration that changes in skin epithelium would also be reflected in the oral cavity. Three time points were chosen based on information from the literature, our experience, and the experience of our collaborator, Mark H. Kaplan (Indiana University School of Medicine). 6-8-

week-old mice were free of disease; this time point was our baseline for each group. Lesion onset occurred at approximately 10-13-weeks, thus, we chose this for our second time point. Lesions worsened until 18 weeks, when euthanasia was performed to prevent further distress, and this was our final time point.

After establishing the time points in the longitudinal study, *Pg* infection of a separate cohort of mice was performed from age 10-13 weeks. After euthanasia, samples were collected for investigation of morphological changes in the oral cavity, loricrin expression, alveolar bone loss, and histological evidence of inflammation and changes in epithelial morphology.

2.6 *Pg* infection

Pg (American Type Culture Collection (ATCC) strain# 33277) bacteria were grown under anaerobic conditions in Schaedler's broth containing vitamin K and hemin (BBL Schaedler Broth with Vitamin K1, L007496, Becton Dickinson). Table 2 describes the components for Scheadler's broth (Becton Dickinson).

Table 2. Scheadler's broth with Vitamin K1

Reagents	Amount
Casein	8.1g
Peptic digest of animal tissue	2.5g
Papaic digest of soybean meal	1.0g
Dextrose	5.82g
Yeast extract	5.0g
Sodium chloride	1.7g
Dipotassium phosphate	0.82g

Hemin	0.01g
Vitamin K1	0.01g
L-cystine	0.4g
TRIS aminomethane	3.0g
Milli-Q water	Up to 1000ml
Autoclaved for 15 minutes at 121°C	

Bacteria were grown in a 2.5L anaerobe jar (AnaeroPack, R685025, Thermo Fisher Scientific) for 24-48 hours (Fang 2020). Cultures grown to saturation were centrifuged at 20,000 x g. Bacteria were resuspended in phosphate-buffered saline (PBS) containing 2% sterile carboxymethylcellulose (9004324, Sigma-Aldrich), which is a thickener used to promote bacterial adherence to teeth and gingiva at a concentration of ~10^9/ml (Fang 2020). 10-13-week-old male and female Sta6VT and littermate control mice were weighed to determine proper dose of ketamine/xylazine for anesthesia given via intraperitoneal (IP) injection (20mg/kg ketamine and 10mg/kg xylazine in a volume of 100ul, IP). After anesthesia, mice were infected by oral lavage with a micro brush every other day for 2 weeks.

2.7 Sample collection and preservation

Mice were euthanized by pentobarbital overdose (200mg/kg, IP). Blood was collected from the heart via cardiac puncture for plasma analyses. We collected gingiva, palate, jaws, head and one femur from each mouse. In order to collect the oral samples, small incisions were made at the commissures of the mouth with a scalpel. Using sterilized scissors and forceps, the palate was peeled back starting from the incisive papilla to the soft palate. With the same tools, keratinized gingival tissues from the buccal left molar region were collected. In order to achieve

optimal accuracy, incisions were made with the aid of a 2.5x magnifying light microscope (model DM2000, Leica Microsystems). Tissues were immediately placed in protease inhibitor solution, which consisted of 0.002M 4-(2-aminoethyl)benzenesulfonyl fluoride hydrochloride (AEBSF), 0.3μM Aprotinin, 130μM Bestatin, 0.001M EDTA, 14μM E-64, and 1μM Leupeptin (S8820, general use SIGMAFAST, Millipore Sigma), then frozen at -80°C. Tissue samples intended for histology were fixed in 10% formaldehyde (28908, Thermo Fisher Scientific). Femurs and the complete head samples were collected and preserved in 50ml conical tubes with the same 10% formaldehyde at 4°C for 48 hours on a rotating platform. After 48 hours, these samples were rinsed with PBS twice and then immersed in PBS in a 50ml conical tube at 4°C until microCT scanning was performed. Once imaged, tissue samples were decalcified for histological preparation.

2.8 Decalcification

Following microCT, the skin was removed, and each head was cut into four sections (upper right, upper left, lower left, lower right) to increase surface area for decalcification (Berlin-Broner 2018). These four sections were immersed in 0.5M EDTA, pH 7.4. Head samples were kept in 10ml of EDTA solution, rotating on a platform in a 15ml conical tube and the solution was changed every other day (Berlin-Broner 2018). The decalcification continued for 8 weeks and following this, samples were deemed to be soft enough to be processed and embedded in paraffin (Berlin-Broner 2018).

2.9 Processing

2-5mm thick tissue samples were placed in histologic cassettes and immersed in 50% ethanol for 2 hours before use of the automated processing cycle (Berlin-Broner 2018). The processing cycle is described in Table 3 (Berlin-Broner 2018).

Table 3. Paraffin embedded tissue processing cycle

Solution	Change(s)	Time (hr)
70% ethanol	2	1
96% ethanol	1	1
100% ethanol	1	1
100% ethanol	1	1
100% ethanol	3	1.5
Xylene	3	1.5
Paraffin wax (58-60°C)	2	2

2.10 Embedding

Embedding was performed using an EG1160, Leica Biosystems Embedding Center. Each hemi-mandible with surrounding tissues was embedded individually in embedding wax (Histoplast Paraffin Wax, 22900700, Thermo Fisher Scientific). In order to maintain consistent orientation of the samples during embedding, the buccal side of each specimen was placed on the bottom and the lingual/palatal side was placed facing up**.** In addition, occlusal surfaces were

placed facing the top side of the histologic cassette. To ensure sectioning was performed parallel to the long axis of the roots as much as possible, the occlusal surfaces of the first molar were orientated 90 degrees perpendicular to the floor. Incisors were kept on all mandibular samples to enhance orientation and landmarking.

2.11 Microtome sectioning

After embedding, samples were sectioned with an automated Leica microtome (model Histocore AUTOCUT, 14051956472, Leica Biosystems) and collected on Superfrost Plus microscope slides (22037246, Thermo Fisher Scientific). Landmarks, such as the apex of the roots and crown of the tooth, were used for orientation purposes to ensure collection was done consistently. Sections were 7μm in thickness.

2.12 Hematoxylin and eosin staining (H&E)

We used a modified protocol taken from Gautier *et al*., (2017) to perform our H&E staining. We first heated the slides to 65°C for 10 minutes to de-paraffinize. This was followed by a xylene rinse, and then graded ethanol washes (100%, 95% and 70%) followed by Milli-Q water to re-hydrate the tissues. Slides were then stained with undiluted hematoxylin (245656, Protocol) for about 4 minutes. Following this, slides were again thoroughly washed with Milli-Q water and placed for 30 seconds in undiluted eosin (245658, Protocol). Finally, the slides were immersed in graded ethanol solutions (95% and 100%) followed by xylene for 6 minutes. A very thin layer of mounting solution (Fisher Chemical Permount, SP15100, Thermo Fisher Scientific) was applied on a glass cover slip (22mm x 60mm). Stained slides were allowed to dry and imaged on a light microscope (model DM2000, Leica Microsystems).

2.13 Immunofluorescence

The immunofluorescence protocol was adapted from the study by Christodoulou *et al*., (2019). Slides were de-paraffinized for 10 minutes at 65°C. Tissues were re-hydrated by performing a xylene wash and a series of ethanol washes (in decreasing concentrations). Slides were then washed in Milli-Q water for 5 minutes before immersing them into antigen retrieval solution (0.006M citric acid, 0.01M trisodium citrate buffer, pH 6.0). The antigen retrieval solution, along with the slides were heated at 90°C for 40 seconds and left immersed for 40 minutes. PBS solution was used to wash the slides on a shaker 3 times for 5 minutes each. Samples on the slide were then marked with an ImmunoPen (ImmEdge Hydrophobic Barrier PAP Pen, H4000, Vector Laboratories).

2.13.1 Blocking and primary antibody

Since blocking is based on the host of the secondary antibody, the blocking serum used for loricrin, cluster of differentiation-45 (CD45), antigen KI-67 (Ki67), cytokeratin-1 (CK1) and cytokeratin-14 (CK14) was goat (ab7481, Abcam). Blocking solution was composed of 10% goat serum (100µl of stock and 900µl of bovine serum albumin (BSA)) and Tris Buffered Saline (TBS) (0.05M Tris, pH 7.6; 0.015M sodium chloride). Samples were blocked for 45 minutes in a humid chamber. After removal, the designated primary antibody was placed onto the tissue sample, incubated at room temperature for 1-2 hours in a humid chamber and then placed at 4°C overnight. Table 4 describes information relevant to the primary antibodies used.

Table 4. Description of primary antibodies used

Primary antibody	Host	Type	Dilution in BSA	Brand
Loricrin	Rabbit	Polyclonal	1:100	Abcam (85679)

Ki67	Rat	Monoclonal	1:300	Invitrogen (SOLA15)
CD45	Rat	Monoclonal	1:400	Santa Cruz (53665)
CK1	Rabbit	Monoclonal	1:500	Abcam (185628)
CK14	Rabbit	Monoclonal	1:500	Abcam (119695)

2.13.2 Secondary antibody

The next day, the primary antibody was removed, and the slides washed 3x in PBS-Tween 1% (PBS-T) for 5 minutes each. The secondary antibody was added, and samples incubated for 2 hours in the dark. The secondary antibody used for loricrin, CK1 and CK14 was DyLight 488 conjugated goat anti-rabbit (A32731, Thermo Fisher Scientific), and the secondary antibody used for Ki67 and CD45 was Alexa Fluor 647 conjugated goat anti-rat (A21247, Thermo Fisher Scientific). After incubation, 3 washes with PBS for 5 minutes each were performed and mounting was then done with SlowFade Gold Antifade Mountant 4',6-diamidino-2-phenylindole, (DAPI, S36938, Thermo Fisher Scientific**)** in a low-lit room. Imaging of the slides was done with an immunofluorescent microscope (model IX73 Inverted microscope equipped with IX3 reflected fluorescence system and X-Cite 120LED, LUMEN Dynamics). The imaging analysis system used was cellSens Dimension (version 1.15, Olympus). Microscopic imaging settings were kept constant for each group to allow for comparison**.**

2.14 MicroCT

2.14.1 Scanning

Complete fixed heads were scanned using a 3-dimensional microCT (model U-SPECT-II/CT, Milabs) at 25µm voxel size resolution prior to use in histology, using the following settings (Table 5):

Table 5. MicroCT Settings

Type	Setting
Exposure	75ms
Voltage	50kV
Current	0.24mA

Scanned images were reconstructed using the microCT's fully integrated MILabs software. Reconstruction involved aligning the sagittal, coronal and axial planes, using the nasal septum and occlusal plane of the first molars as reference. 3D reconstructions were performed using Avizo software (version 9.1, Thermo Fisher Scientific).

2.14.2 Alveolar bone measurements

To measure alveolar bone levels in mice, we incorporated a measurement protocol developed by Dr. Raisa Catunda using Avizo software (version 9.1, Thermo Fisher Scientific). Three landmarks were used to perform periodontal bone height analysis: cementoenamel junction (CEJ), alveolar bone crest (ABC) and root apex (RA). The distance from the CEJ to ABC was measured as a ratio of total root length (TRL) in the first and second mandibular molars on the left side. There were a total of 8 measurements: 2 on the sagittal plane and 6 on the

coronal plane (Figure 1). For sagittal measurements, the first molar was initially oriented in the coronal plane. Sagittal plane measurements were taken using the software's measurement line and ruler to precisely ensure center of the middle pulp chamber and root apex (Figure 2). The landmarks were again CEJ, ABC and RA.

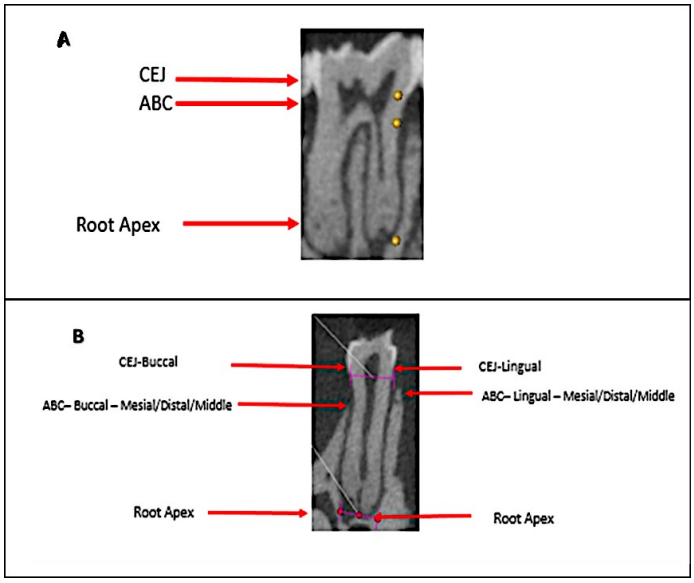

Figure 1. Landmarks used in the protocol. A: Landmarks depicted on the coronal view. B: The 6 standardized measurements as seen on the sagittal view of the tooth.

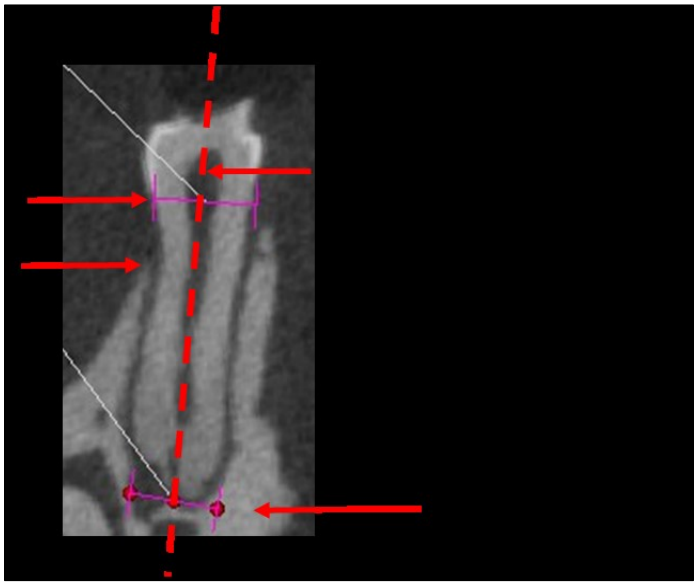

Figure 2. Sagittal plane measurements. Avizo software rulers (as seen in purple) and measurement lines (as seen in the red dash mark), were utilized to ensure plane meets the center point of the tooth.

For coronal measurements, the sagittal plane was used for orientation of the buccal and lingual side (Figure 3). Here, the coronal plane measurement line was precisely aimed at the

middle of the floor of the pulp chamber in the designated root and the middle of the last third of the root. Again, the ruler tool was used here to ensure the center of the root was established.

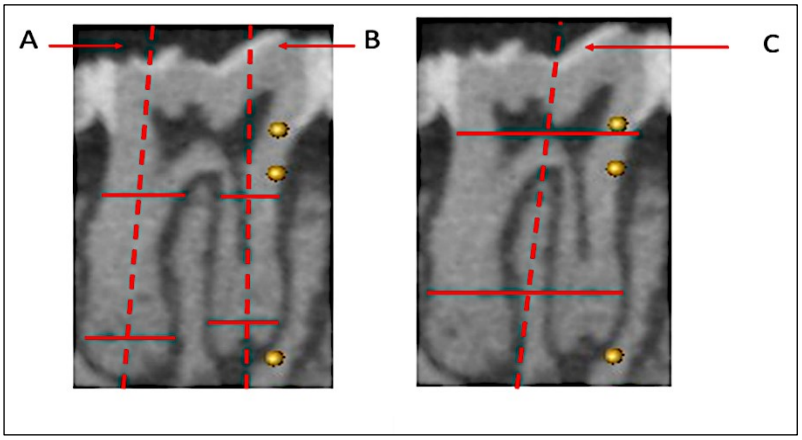

Figure 3. Coronal view of the tooth with sagittal plane placement. A: Orientation plane for lingual and buccal coronal distal measurements. B: Orientation plane for lingual and buccal coronal mesial measurements. C: Orientation plane for lingual and buccal coronal middle measurements.

For the mid-buccal and mid-lingual measurements, the plane was defined as the center of the pulp chamber and the middle distance between the last third of the two roots. Once all planes were established, measurements and statistical analyses were performed.

2.14.3 Statistical analysis

All alveolar bone loss measurements were performed by 3 calibrated and blinded examiners. Results were presented as millimeter measurements and as a percentage of TRL (CEJ – ABC / TRL x 100) relative to wild-type. Using the Euclidean distance formula (Jambu, M., 1991), we gathered data for statistical interpretation using Prism Software (version 9.0.2, GraphPad). The formula illustrated in Figure 4 was utilized for data collection.

Figure 4. Formula that measures the crown/root ratio as a percentage of vertical bone height and percentage of vertical bone loss relative to the wild-type animals.

$$CEJ - ABC\ to\ TRL\ \% = \frac{(CEJ\ to\ ABC)}{TRL} \times 100$$

$$Bone\ loss = (CEJ - ABC\ to\ TRL\%\ of\ pg - induced\ group) - (CEJ - ABC\ to\ TRL\%\ control\ group)$$

In order to calculate data that was of non-normal distribution, Shapiro-Wilk test was utilized. Additionally, Mann Whitney-U test was used to compare groups. Measurements were obtained by 3 examiners. Cohen's kappa inter/intra reliability test was performed, and the average error accepted was ≤ 3% or 0.2mm.

2.15 Faxitron

Bone mineral content (BMC) and bone mineral density (BMD) of the femurs were measured via Faxitron (model DXA UltraFocus, Hologic). dual energy x-ray absorptiometry (DXA). Vision Software (version 3.65, Hologic) was used for analysis. Femur samples and detection tray were placed at the setting of "position 2" and scanned.

2.16 ELISA

2.16.1 Mouse sample preparation

The enzyme-linked immunosorbent assay (ELISA) kit used in this study was by Cloud Clone Corp and specific for mouse loricrin (SEC568Mu, Cloud Clone Corp). Gingival samples were collected and kept frozen at -80°C with proteinase inhibitor. Gingival tissue samples from 3 mice within the same group were weighed and homogenized with a tissue grinder, then suspended in 500µl of lysis buffer that was included in the kit. Samples were stored in -4°C to be used within the same week.

2.16.2 Protein content detection

In order to quantify the amount of protein in each sample, the Pierce Bicinchoninic Acid Kit (BCA) was used (23227, Thermo Fisher Scientific). The assay measures the amount of reduced cuprous ions and their reaction to BCA and the amount reduced is proportional to the amount of protein present in the solution. Purified BSA was used to create standards, which were serially diluted (2000-25μg) to generate a standard curve.

Equal volume (10μl) of samples and standards were loaded into wells in duplicate. 200μl of the working reagent was added into the wells and the plate was mixed thoroughly for 30 seconds then left to incubate at 37°C for 30 minutes. The plate was then cooled to room temperature and using a spectrophotometric microplate reader (model Synergy H1, Multi-Mode Microplate Reader, BioTek), it was read at wavelength 562 nm. The sample concentrations were calculated from the standard curve and the protein concentration was used to normalize our results from the ELISA.

2.16.3 ELISA procedure

A standard curve was created by serial dilution of loricrin in duplicate. A 40ng stock was provided by the manufacturer and diluted from 10-0ng. The kit contained a 96 well plate that was pre-coated with a loricrin capture antibody. In addition, the manufacturer provided diluent solution for the blank and to dilute samples if necessary. Samples were assayed in duplicate (100μl/sample or standard). As per the manufacturer's instructions, the plate was sealed and incubated for 1 hour at 37°C. The contents of the wells were removed by pipetting and 100μl of Detection Reagent A, was added and incubated for 1 hour at 37°C. Samples were aspirated and washed with 350μl of wash solution 3 times for 1 minute each. Each wash was removed by

snapping the plate onto absorbent paper. Following this, 100µl of Detection Reagent B was loaded into each well, covered with the plate sealer and incubated for 30 minutes at 37°C. The same aspiration and wash processes were performed as aforementioned but for 5 times. Once this was complete, 90µl of tetramethylbenzidine (TMB) substrate solution was loaded into each well, covered with a new plate sealer, protected from light, and incubated for 20 minutes at 37°C. By the end of the incubation period, 50µl of stop solution (provided by the kit) was added to each well. The plate was cleaned on the sides and the bottom for fingerprints, debris and liquid. Bubbles were eliminated from within the wells prior to running through the microplate reader.

2.16.4 ELISA data interpretation

The 96-well plate was read with a microplate reader (model Synergy H1, Multi-Mode Microplate Reader, BioTek). As per the manufacturer's instructions, absorbance was set at 450nm in order to read the yellow color produced by the stop solution. The standard curve was created using the mean optical density and concentration from each standard which then formulated a linear line-of-best-fit. The results were averaged between duplicate wells and the mean optical density of the blank was subtracted from the standard, control and sample wells. The data collected from the microplate reader was then analyzed statistically using Prism Software (version 9.0.2, GraphPad).

2.17 Cytokine array

Plasma cytokine array was performed on plasma from the 10-13-week male *Pg*-infected Stat6VT versus control and uninfected Stat6VT versus control mice. For the *Pg*-infected Stat6VT and control experiment, an 8-well tray cytokine array kit was used to perform cytokine profiling (AB193659, Abcam**)**. For the uninfected Stat6VT and control experiment, a 16-well

tray cytokine array kit was used (QAM-INF-1, RayBiotech) and performed entirely by Sara Moradipoor, a research assistant in Dr. Febbraio's lab. Sara followed the manufacturer's instructions as provided by the kit. She prepared the standards and blocked the array surfaces with the material included in the kit. Then, incubation with samples and standards was performed. Following this, another incubation with biotinylated detection antibody cocktail and streptavidin-conjugated fluor was performed.

In the *Pg*-infected cytokine profiling kit, the membranes were provided and blocked by incubating with 2ml blocking buffer at room temperature for 30 minutes; blocking buffer was then aspirated from the tray. 1ml of undiluted plasma samples drawn from 5 mice from the same group were used to perform the experiment. The samples were then incubated for 2 hours at room temperature on a shaker. Samples were then aspirated and 2ml of wash buffer I (provided by the manufacturer). The samples were incubated in this wash buffer for 5 minutes on a shaker and then aspirated and reloaded with fresh wash buffer for a total of 3 times. These steps were repeated with wash buffer II twice. 1ml of biotinylated antibody cocktail, provided by the manufacturer, were loaded into the trays and incubated for 2 hours at room temperature on a shaker. After the cocktail was aspirated, washes were performed the same way as previously. The membranes were then transferred onto a sheet of chromatography paper and any excess wash buffer was removed by blotting the membrane's edges with the chromatography paper. The membranes were then transferred onto a plastic sheet and 500µl of chemiluminescence detection buffer (250µg of detection buffer C and 250µg of detection buffer D), provided by the manufacturer, was loaded onto the membranes. Another plastic sheet was placed directly on top of the membranes and transferred to the ChemiDoc (model XRS+, Bio-Rad) for imaging, where the exposure was set between 1 to 10 second intervals.

Data analysis was performed according to the manufacturer's instructions. The intensity of signal was expressed into pixels and the data was exported into Microsoft Excel. Cytokine expression levels were compared by adjusting the pixel densities on the excel sheet according to the control dots on each membrane. Data was presented as the relative expression, or fold change, of a certain cytokine (Stat6VT over controls) at the specified time point (6-8, 10-13 or 18 weeks). Fold change was calculated as the average signal intensity in the control group subtracted from the average signal intensity in the Stat6VT group, divided by the signal intensity in the control group.

CHAPTER 3: LONGITUDINAL STUDY RESULTS

3.1 Breeding and genotyping of Stat6VT mice and littermate controls

Stat6VT mice (congenic to C57Bl/6j) were rederived by Jackson Laboratories from sperm generously provided by the laboratory of Mark H. Kaplan (Indiana University School of Medicine). Briefly, sperm from Stat6VT hemizygous males were used to fertilize eggs from C57Bl/6j females. 12 offspring resulted and were shipped to the University of Alberta where they were housed in a specific pathogen-free facility with ad libitum access to food (normal chow, 4% fat content) and water. Breeding resulted in a total of 32 males and 47 females that were Stat6VT and 45 males and 49 females that were littermate controls.

Each Stat6VT mouse (male or female) was bred to a C57Bl/6j wild-type control mouse to ensure that all mice were hemizygous for Stat6VT. Therefore, there is a single exogenous DNA insert that exists in one of the homologous chromosomes for each integration of the Stat6VT transgene (Howell, *et al*., 2011). Stat6VT mice were good breeders, and litters displayed the expected Mendelian ratio of Stat6VT:control and males:females. One female died prior to giving birth to any litters. Mice were tracked by breeder. Littermates that did not have the Stat6VT allele were used as controls, such that there would be no differences in strain background.

The Stat6VT transgene contains the human CD2 locus control region upstream of a human Stat6 cDNA, with valine (V) 547 and threonine(T) 548 codons mutated to encode alanine (Turner *et al*., 2014). The CD2 locus control region is a strong specific enhancer (Turner *et al*., 2014). It functions to restrict the expression of the transgene primarily to B and T lymphocytes (Bruns *et al*., 2003). To genotype mice, we used primers specific to the FLAG-tag (Bruns *et al*., 2003), which was inserted in the C-terminal. A FLAG-tag is a novel 8 amino acid sequence (DYKDDDDK: D=Aspartic acid; K=Lysine; Y=Tyrosine; 1012.9 dalton or roughly 1 kDa),

often placed at either end of a protein to distinguish it from the endogenous form, both by PCR and Western blot. Figure 5 shows a representative image of a 1.5% agarose gel of PCR products from a genotyping experiment. Our final results showed 92% concordance between genotyping results and later lesion development. No Stat6VT mouse that did not develop lesions was included in the final results.

Figure 5. A representative 1.5% agarose gel of PCR products used to determine genotype. Lane 1 shows molecular weight markers with 100 basepairs (bp), 500bp, and 1200bp labeled for reference. Lanes 2-9 are samples from newly bred mice. Lanes 10 and 11 are water (no DNA) and positive control, respectively. The results show the expected size band (600bp) in lanes 2, 7, 8, 9 and in the positive control lane (11). Absence of a band was interpreted as a control mouse.

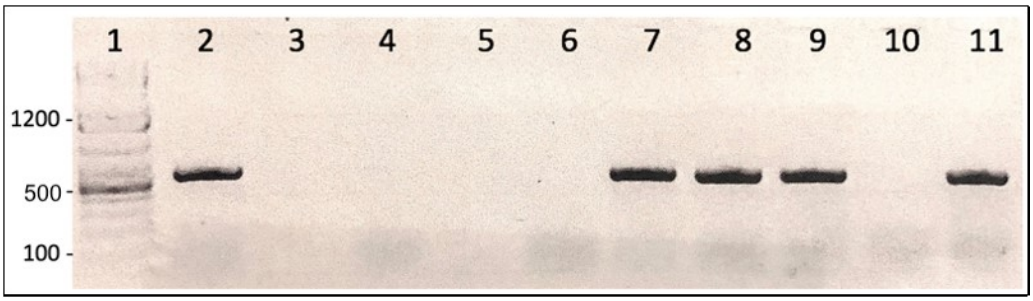

3.2 Longitudinal study confirms timeline of disease in male mice, but female mice show greater variation early

For each time point, observational notes and images were taken to track phenotypical changes of Stat6VT mice in comparison with age and sex-matched littermate controls. As Stat6VT mice presented with skin disease manifestations, notes recorded lesion appearance, location and severity. We also observed any phenotypical changes within the oral cavity.

There were 9-11 male and 9-11 female Stat6VT and control mice for each time point. This was based on our power calculation which called for an n=9 minimum, and the addition of extra mice, in case of malocclusion or other morbidities/mortalities. The time points were: 6-8

weeks old (baseline), 10-13 weeks old (skin disease onset) and 18 weeks old (severe skin disease).

Mice were euthanized by pentobarbital overdose at each time point. Blood was collected from the heart for plasma analyses. We then collected tissue from a consistent, designated location from the gingiva and palate. Femur and the complete head were collected for Faxitron and microCT analyses, respectively. Once imaged, heads were split evenly into quadrants of the upper right, upper left, lower right and lower left. Samples were then decalcified, processed and embedded for histology. All of the aforementioned procedures were assisted by Dr. Catunda.

The 6-8-week time point was our baseline for the longitudinal study. This time point was chosen after reading the prior literature on these mice, which suggested that Stat6VT mice in this age range would not present with skin disease manifestation (Bruns *et al*., 2003; Turner *et al*., 2014). This may also suggest that downregulation of loricrin would not have yet occurred. Upon observation of male 6-8-week-old mice within this time period, we confirmed that there were no phenotypical skin changes nor intraoral disease manifestations. The female 6-8-week-old group, however, did show some disease symptoms. Although most presented with no atypical findings, 5/11 presented with some degree of lesions. More specifically, 4/5 presented with mild edema around the borders of the eyes. The edema around the eyes has been diagnosed as blepharitis by those in the AD field (Turner *et al*., 2014). Briefly, blepharitis is a reaction to bacteria on the eyelids and eyelashes (Turner *et al*., 2014). This can progress to redness due to inflammation and later, scabbing due to scratching. Out of the five animals that presented lesions, one female had early onset of several atypical findings, including blepharitis and scaly borders of the eyes, as well as reddening of the hind feet. The five animals (4 females and 1 male) came from different Stat6VT breeders. These were the only pups from their litter at this age that presented with early

progressive findings. These sex-based differences in the phenotypical presentation may suggest that disease manifestations occur earlier in females than in male mice. This appears to be a novel finding for our mice. This may be due to the hormonal or physiological differences in female Stat6VT breeders compared to male Stat6VT breeders. (We spoke with the graduate student in the lab of our collaborator, and interestingly, he said they did not use female mice as the Stat6VT carrier for breeding because the stress of pregnancy made their disease worse). Figure 6 shows a female 8-week-old Stat6VT mouse that had no atypical findings compared with a control and Figure 7 shows a male 8-week-old Stat6VT mouse compared with a control.

Figure 6. 8-week-old female A: Stat6VT and B: control mice. Both mice demonstrated no atypical findings. The skin around the eyes, ears, snout and mouth area was smooth. The notch on the ear was for identification purposes.

A. 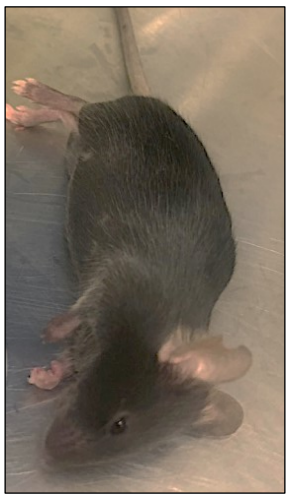

B. 

Figure 7. 8-week-old male A: Stat6VT and B: control mice. All male mice in the 6-8-week-old group showed no atypical findings, as evidenced by the smooth borders of the eyes, the fur around the ears, snout and mouth area. The notch on the ear was for identification purposes.

A.  B. 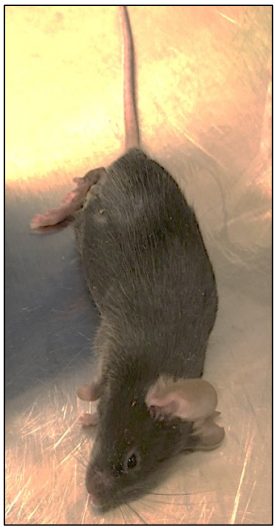

At 10-13 weeks of age, we expected skin lesion onset in both female and male Stat6VT groups compared to their control counterparts, based on the information in the literature and our collaborator's experience (Sehra *et al*., 2008; Bruns *et al*., 2003). All 10-13-week-old Stat6VT female and male mice demonstrated varying degrees of atypical phenotypic findings. Mild to severe scaly edema around the borders of the eyes, and erythema on the ears as a result of scratching due to pruritus were noted. In addition, there was scaling and erythema on the tails due to biting as a result of pruritis. We also noted a loss of fur behind the ears. However, at the gross, phenotypic level, the oral cavity did not show any atypical findings. These findings assert that this time period is appropriate for the expectation of skin lesion onset. We considered this to be an ideal time point for further investigation of the correlation between skin lesions and potential disease manifestations within the oral cavity. Figure 8 is an example of a female 12-week-old Stat6VT mouse with atypical findings compared to control and Figure 9 shows an example of a male 12-week-old Stat6VT mouse with atypical findings compared to control.

Figure 8. 12-week-old female A: Stat6VT and B: control mice. The Stat6VT demonstrated atypical findings, which included edema (white) and scaling (irregular border) around the eye

(blepharitis). Additionally, the ears presented with inflammation, erythema, laceration, and a loss of fur. The snout and lower chin presented with mild loss of fur. In comparison, the female 12-week-old control is seen with no atypical findings. The skin around the face, body, ears and eyes is intact, smooth and within normal conditions.

A. 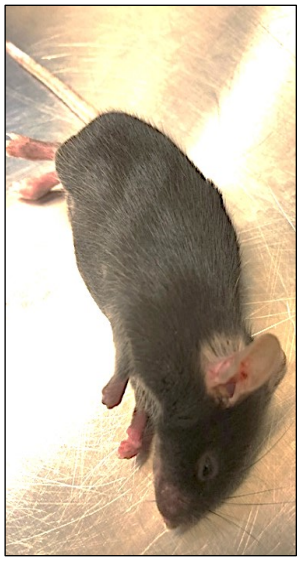 B. 

Figure 9. 12-week-old male A: Stat6VT and B: control mice. The male 12-week-old Stat6VT mouse demonstrated marked edema (white) and scaling (irregular border) around the eye (blepharitis), snout and mouth region. There was mild inflammation (redness) of the inner ear and on the front paws. The ear was notched for identification purposes but does not show any erythema or inflammation. For comparison, a male 12-week-old control mouse is shown. Note the smooth skin around the face, mouth and body. The eyes were not inflamed and were within normal conditions.

A. 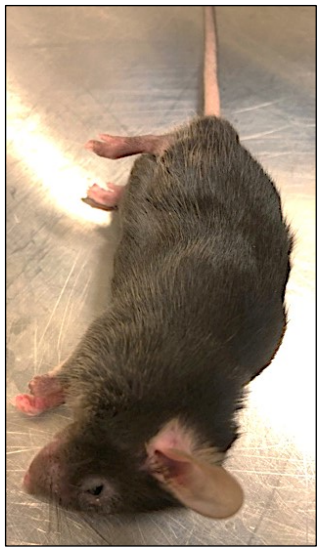 B. 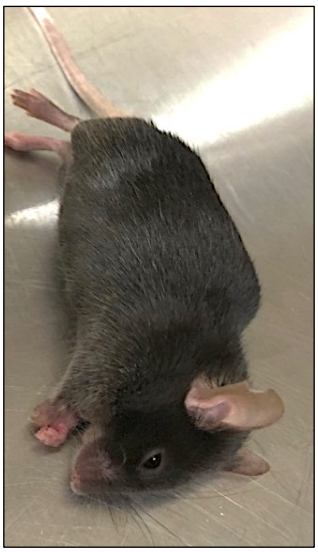

At 18-weeks of age, all Stat6VT males and females demonstrated moderate to severe progression of lesions, including scaly edema around the borders of the eyes, and scaly erythema of the ears, often with traces of dried blood. Loss of fur and scaly, erythematous lesions were observed around the snout, abdomen, lower neck and behind the ears in some mice. This age group also presented with redness and lacerations on the commissures of the mouth and ears in some cases. These findings were most likely caused by excessive scratching due to pruritus. The intraoral examination did not show any atypical findings. Figure 10 is an example of a female 18-week-old Stat6VT mouse compared to control and Figure 11 is an example of a male 18-week-old Stat6VT mouse compared to control.

Figure 10. 18-week-old female A: Stat6VT and B: control mice. The female 18-week Stat6VT demonstrated severe, lacerated, scaly and erythematic lesions of and behind the ears and snout, as well as edema around the eyes. Additionally, there was a loss of hair around the face and mouth region. In comparison, the female 18-week-old control mouse was seen with no atypical

findings. The fur and skin were intact around the face and body. The ears, eyes and snout were normal (the ear was notched for identification purposes).

A. 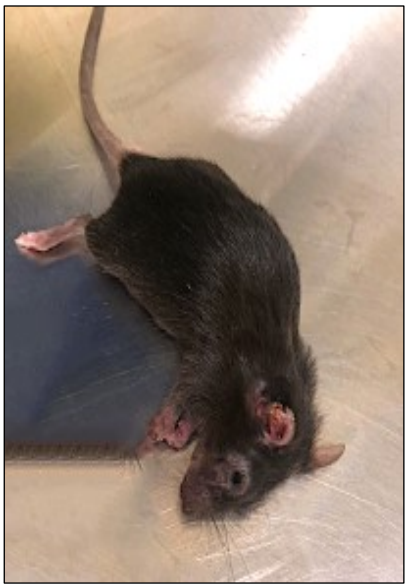 B. 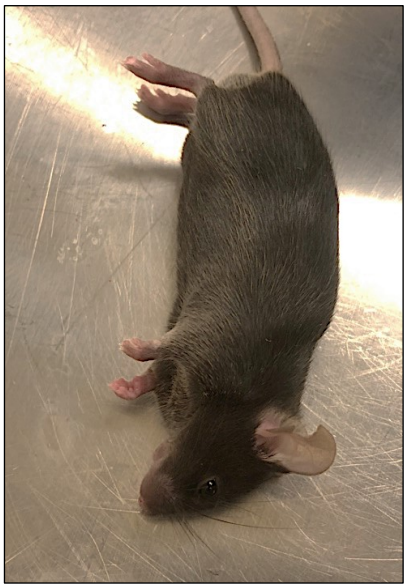

Figure 11. 18-week-old male A: Stat6VT and B: control mice. The male Stat6VT mouse had severe erythema, scabbing, hair loss and inflammation around the ears, eyes, snout and mouth region. The epidermis of the ears was thickened and lacerated. Additionally, dried blood was found around the ears and lower chin area. Whereas the male 18-week-old control mouse had no atypical findings. The skin and fur were smooth with no lesions or inflammation noted. The face and body were within normal conditions.

A. 

B. 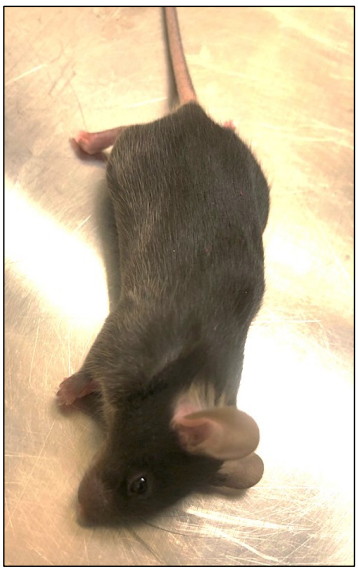

3.3 Femur bone density and mineralization reveal that male Stat6VT mice are not significantly different from controls at 10-13 weeks of age

The left femur of all mice was collected and preserved in 10% formaldehyde at 4°C prior to Faxitron analysis. Collection and analysis were assisted by Dr. Catunda. Faxitron is a DXA system that measures BMC and BMD. BMC is determined at a specific site and measured in grams, while BMD is the measurement of the amount of bone mineral per area of bone (in this case, the femur), measured in milligrams per centimeter^2 (Deng *et al*., 2002). Therefore, while two mice may share the same BMC value, the mouse with the shorter femur would have a higher BMD. Clinically, BMD and BMC measurements are used in humans as indicators of how likely an osteoporotic fracture is to occur (Deng *et al*., 2002). Additionally, they may suggest the effects of certain bone diseases or the impact of certain foods or medicines on the skeletal system (Deng *et al*., 2002). In the Stat6VT mouse model, systemic changes in bone may potentially occur as a result of constitutive activation of Stat6. As a result of this activation, downstream genes are transcribed, which lead to increased production of cytokines that continually activate a Th2 immune response. This Th2 immune response may impact bone composition because

upregulation of Th2 cytokines can induce Receptor Activator of Nuclear Factor Kappa Betta Ligand (RANKL)-mediated osteoclastogenesis through effects on B lymphocytes, as they also express RANKL (Figueredo *et al*., 2019). Continuous B-cell activation may result in increased production of IL-1, which can lead to tissue destruction (Figueredo *et al*., 2019). Th2 cytokines can also upregulate pro-inflammatory factors such as IL-19, IL-20, IL-25, IL-27, IL-12Rβ2, IL-31RA, and nitric oxide synthase 2 (NOS2) (Kim *et al*., 2017; Jeong *et al*., 2019). Therefore, assessing BMC and BMD levels can provide us with insight into the bone condition of this mouse model. This is of fundamental importance as we are investigating the effects of a potential downregulation of an epithelial protein on the oral cavity of these animals, and if, for example, they present with an intrinsic bone condition such as osteoporosis, this could potentially skew our results. Femurs were calibrated using the DXA system "auto object detection" setting. Faxitron analysis was done on femurs from males and females at all time points.

3.3.1 Results for females

Across all time points, femurs from female control mice compared to Stat6VT mice demonstrated significantly more BMC (6-8-weeks old: 0.02294 ± 0.0007378g vs. 0.01828 ± 0.001040g, p=0.0012; 10-13-weeks old: 0.02549 ± 0.0008137g vs. 0.02263 ± 0.0007299g, p=0.0122; 18-weeks old: 0.03098 ± 0.0004485g vs. 0.02114 ± 0.001284g, p<0.0001) (Figure 12). Additionally, at 18-weeks of age, BMD was significantly greater in femurs from control compared to Stat6VT mice (88.25 ± 2.198mg/cm^2 vs. 71.26 ± 3.004mg/cm^2, p=0.0001). However, at 6-8-weeks and 10-13-weeks of age there were no significant differences found between Stat6VT and control mice (Figure 13).

3.3.2 Results for males

At 6-8-weeks and 18-weeks of age, femurs from male control mice compared to Stat6VT demonstrated significantly more BMC (6-8-weeks old: 0.02706 ± 0.001127g vs. 0.01776 ± 0.0009552g, $p<0.0001$; 18-weeks old: 0.03508 ± 0.001188g vs. 0.01910 ± 0.001738g, $p<0.0001$) and BMD (6-8-weeks old: 76.48 ± 1.970 mg/cm^2 vs. 66.05 ± 1.724 mg/cm^2, $p=0.0011$; 18-weeks old: 94.56 ± 2.609 mg/cm^2 vs. 75.75 ± 2.674 mg/cm^2, $p<0.0001$). However, at 10-13-weeks of age, there were no significant difference in both BMC and BMD found between Stat6VT and control. Figure 14 demonstrates the BMC findings for the male control versus Stat6VT group across all ages and Figure 15 demonstrates the BMD findings.

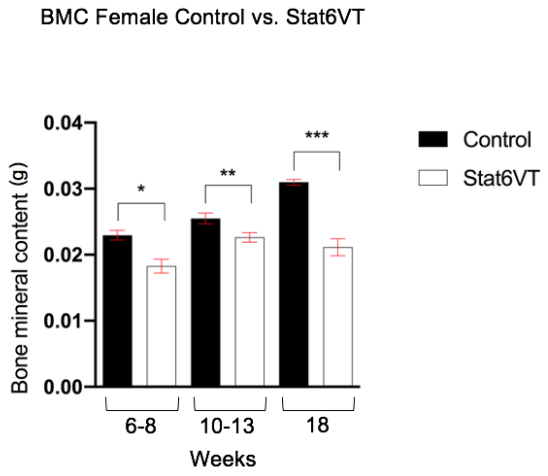

Figure 12. BMC in female control and Stat6VT groups across all ages. *p=0.0012, **p=0.0122, ***p <0.0001.

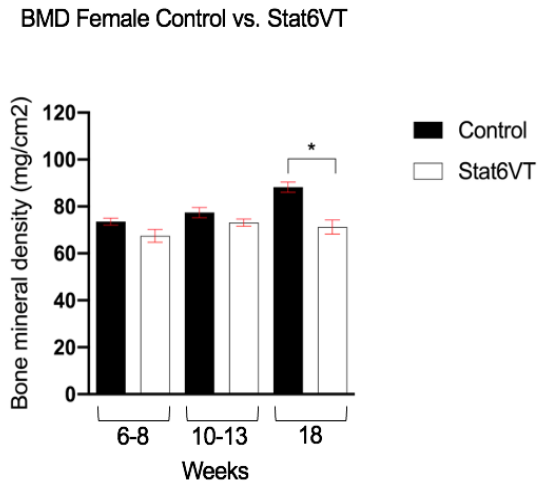

Figure 13. BMD in female control and Stat6VT groups across all ages. *p=0.0001.

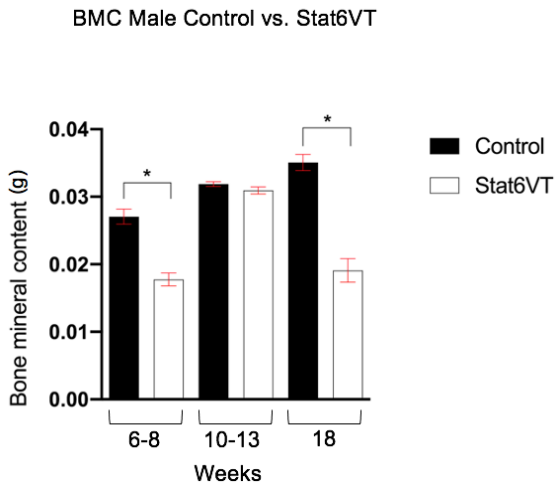

Figure 14. BMC in male control and Stat6VT groups across all ages. *p<0.0001.

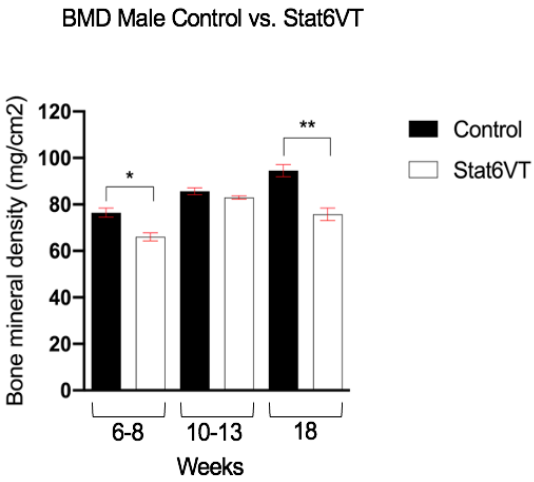

Figure 15. BMD in male control and Stat6VT groups across all ages. *p=0.0011, **p<0.0001.

3.4 MicroCT analysis revealed that Stat6VT mice have significantly lower alveolar bone levels compared to controls

3.4.1 Utilization of a two-plane microCT approach

The first and second molars of the lower left region of female and male mice in all age groups were used for alveolar bone measurements. To measure alveolar bone levels in mice, we utilized the Avizo Software (version 9.1, Thermo Fisher Scientific) and a protocol developed by Dr. Catunda. Furthermore, Dr. Catunda and Shrushti Patel (lab member) assisted in data collection, microCT analysis and formulation of all microCT graphs. Dr. Maria Alexiou

performed the reconstruction of all the mice heads. As a reminder, three landmarks were identified in each image to perform periodontal bone height analysis: cementoenamel junction (CEJ), alveolar bone crest (ABC) and root apex (RA). The distance from the CEJ to the ABC was measured as a ratio of total root length (TRL). There was a total of 8 measurements: two in the sagittal plane and 6 in the coronal plane. For sagittal measurements, the first molar was initially orientated in the coronal plane.

To appropriately represent these measurements, data were expressed according to the plane and and orientation of the tooth (Figure 16).

Figure 16. Mesial, distal and mid-buccal aspects of the molar surface in the coronal plane. A: Coronal view of the first and second molars. B: coronal view of the first and second molars with the sagittal plane splicing the teeth into equal halves. C: Aerial view of the buccal and lingual aspects of the first and second molars. D: Coronal view of the first molar. E: Coronal view of the first molar with the sagittal plane splicing the tooth in half, demonstrating the mesial, mid-buccal and distal aspects.

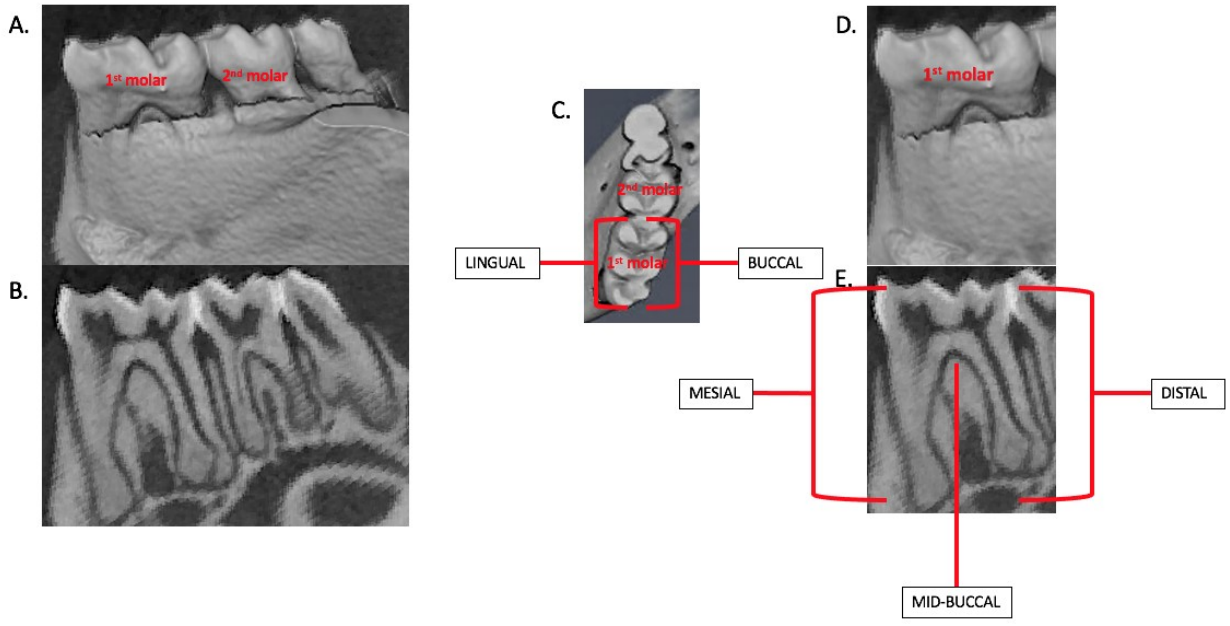

As previously mentioned, we took 6 measurements from the coronal plane, which were as follows:

- Mesial CEJ (CEJM) to ABC on the buccal aspect (CEJM-ABCB) and mesial CEJ to ABC on the lingual aspect (CEJM-ABCL) (Figure 17).
- Mid-buccal CEJ (CEJMid) to ABC on the buccal aspect (CEJMid-ABCB) and mid-lingual CEJ (CEJMid) to ABC on the lingual aspect (CEJMid-ABCL) (Figure 18).
- Distal CEJ (CEJD) to ABC on the buccal aspect (CEJD-ABCB) and distal CEJ to ABC on the lingual aspect (CEJD-ABCL) (Figure 19.)

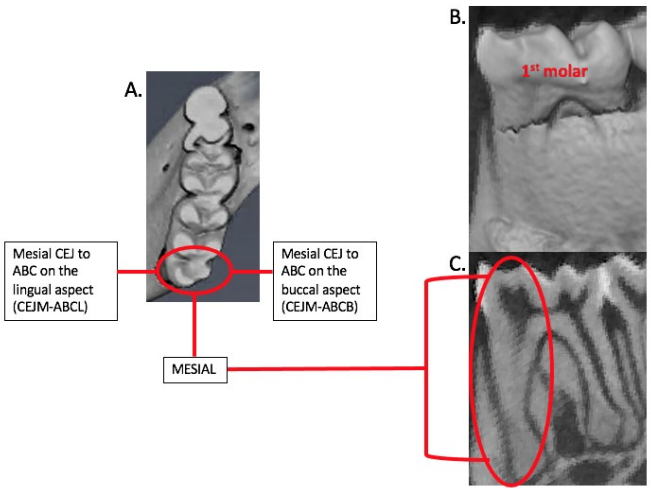

Figure 17. Coronal plane mesial measurements. A: CEJM-ABCB and CEJM-ABCL aspects of the tooth are shown in an aerial view. B: Coronal view of the first molar. C: Coronal view of the first molar with the sagittal plane splicing the tooth in half, demonstrating the mesial aspect.

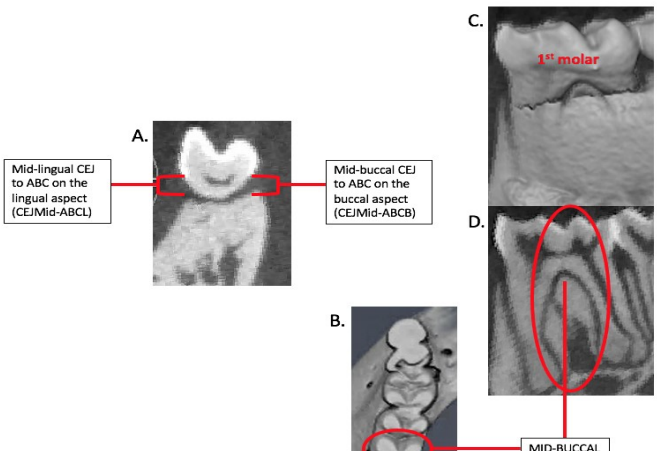

Figure 18. Coronal plane middle measurements. CEJMid-ABCB and CEJMid-ABCL of the first molar shown in A: sagittal, B: aerial, C: coronal views. D: Sagittal plane splicing the tooth in half, demonstrating the mid-buccal aspect.

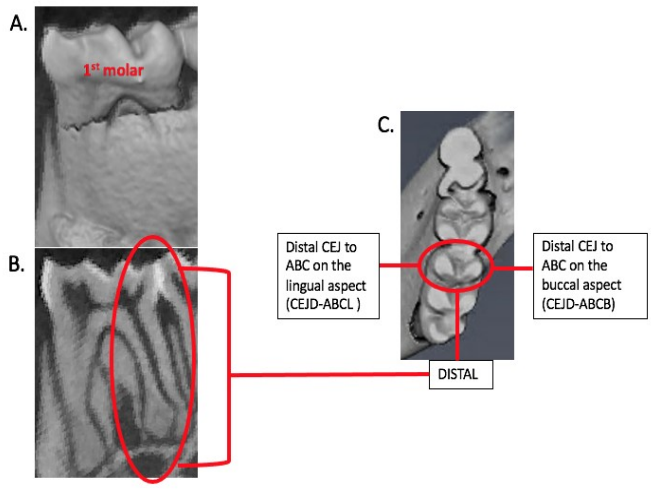

Figure 19. Coronal plane distal measurements. A: Coronal view of the first molar and B: coronal view of the first molar with the sagittal plane splicing the tooth in half, demonstrating the distal aspect. C: Aerial view of the first molar CEJD-ABCB and CEJD-ABCL.

Two measurements were taken from the sagittal plane:

- Mesial CEJ to ABC (CEJM-ABC) (Figure 20)
- Distal CEJ to ABC (CEJD-ABC) (Figure 21).

Once all 8 measurements were collected, alveolar bone levels (ABC-CEJ in mm) and the vertical alveolar bone height (total amount of vertical loss in %) were compared for age and sex matched Stat6VT mice and littermate controls.

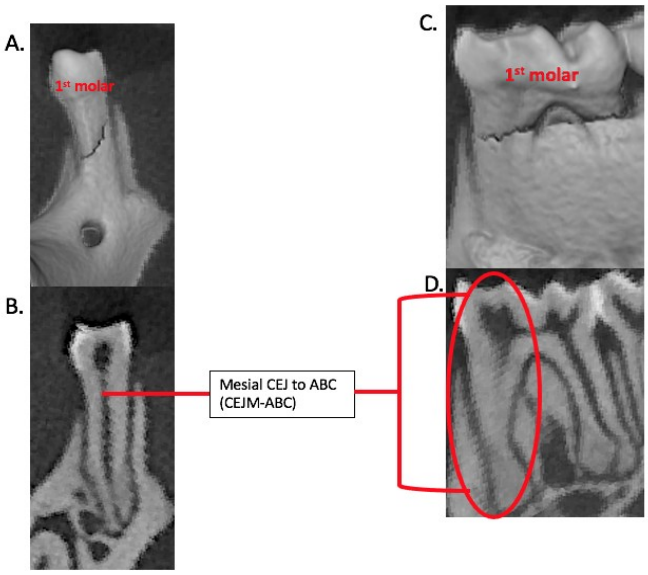

Figure 20. Sagittal plane mesial measurement. A: Sagittal view of the first molar and B: sagittal view of the first molar with the coronal plane splicing the tooth in half, demonstrating CEJM-ABC. C: Coronal view of the first molar. D: Coronal view of the first molar with the sagittal plane splicing tooth in half, demonstrating CEJM-ABC.

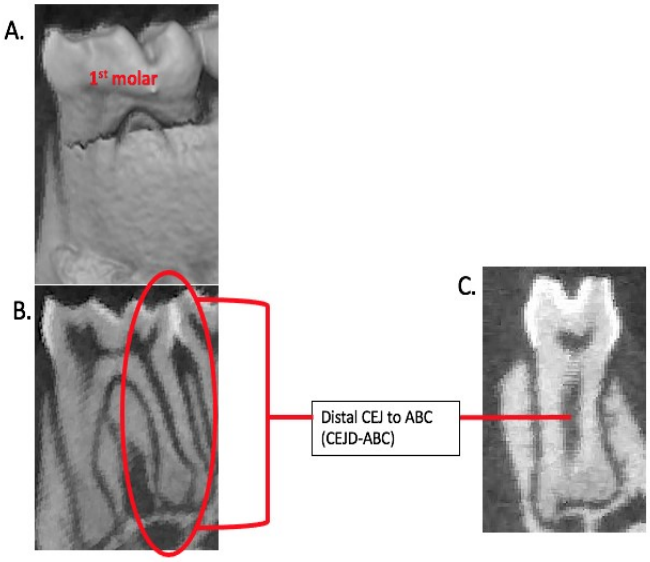

Figure 21. Sagittal plane distal measurement. A: Coronal view of the first molar and B: coronal view of the first molar with the sagittal plane splicing the tooth in half, demonstrating CEJD-ABC. C: Sagittal view of the first molar and D: sagittal view of the first molar with the coronal plane splicing the tooth in half, demonstrating CEJD-ABC.

3.4.2 Results for females

At 6-8 weeks, the female mice demonstrated 3 sites that had greater CEJ-ABC measurements in the Stat6VT when compared to control (Figures 22 and 24). 2 of the sites were located on the first molar (Figures 22A and 24A), which were as follows: CEJD-ABCB (0.0 ±0.0 vs. 0.06288 ± 0.01593, p=0.0043) and CEJM-ABC (0.3155± 0.02219 vs. 0.1993 ± 0.02019,

p=0.0047). The last site was on the second molar (Figure 22B), which was the CEJD-ABCB (0.04092 ± 0.02509 vs. 0.01052 ± 0.009864, p=0.0443). Furthermore, there were 3 sites located on the first molar that demonstrated a significantly greater loss of alveolar bone height measurement in the Stat6VT mice when compared to the controls (Figures 22C, 23C and 24C). The sites were as follows: CEJD-ABCB (0.0 ± 0.0 vs. 4.206 ± 1.070, p=0.0044), CEJM-ABCL (23.32 ± 1.587 vs. 18.10 ± 1.350, p=0.0367) and CEJM-ABC (20.18 ± 2.091 vs. 12.66 ± 1.028, p=0.0120).

At 10-13 weeks, 2 sites on the second molar demonstrated a greater CEJ-ABC measurement in the Stat6VT when compared to controls (Figures 25B and 27B). The sites were as follows: CEJM-ABCB (0.1414 ± 0.009319 vs. 0.1111 ± 0.006231, p=0.0267) and CEJM-ABC (0.2462 ± 0.01060 vs. 0.2071 ± 0.01260, p=0.0449). Additionally, second molar CEJMid-ABCB of the Stat6VT mice also demonstrated a greater loss of alveolar bone height when compared to control mice (12.22 ± 0.8097 vs. 9.250 ± 0.5871, p=0.0178) (Figure 25D). Measurements taken on the lingual aspect of the coronal plane at this time point did not demonstrate any significant differences between Stat6VT and control mice (Figure 26).

At 18 weeks, 3 sites on the second molar demonstrated greater CEJ-ABC measurements in the Stat6VT mice compared to the control mice (Figures 28, 29, 30). These sites were: CEJM-ABCB (0.1151 ± 0.01016 vs. 0.1582 ± 0.008768, p=0.0124), CEJM-ABCL (0.1892 ± 0.004536 vs. 0.2259 ± 0.01075, p=0.0138) and CEJD-ABC (0.2529 ± 0.009459 vs. 0.3238 ± 0.02460, p=0.0274). There was 1 site on the second molar that demonstrated a greater loss of alveolar bone height in the Stat6VT mice compare to control mice (Figure 28), which was CEJM-ABCB (0.2529 ± 0.009459 vs. 0.3238 ± 0.02460, p=0.0274).

Overall, female Stat6VT mice when compared to controls demonstrated various sites of greater CEJ-ABC measurement readings and loss of alveolar bone height. However, the sites were not consistently the same across each time point. When we take into account the inconsistencies observed in the phenotypical lesion onset and BMC/BMD readings of the female mice, the microCT results reflect a similar deviation from our original expectations.

Figure 22. MicroCT measurements of the 6-8-week-old female Stat6VT and control mice on the buccal aspect of the coronal plane. CEJ-ABC measurements of the A: first molar and B: second molar taken on the coronal plane (buccal aspect), and the alveolar bone height of the C: first molar and D: second molar taken on the coronal plane (buccal aspect). *p<0.05.

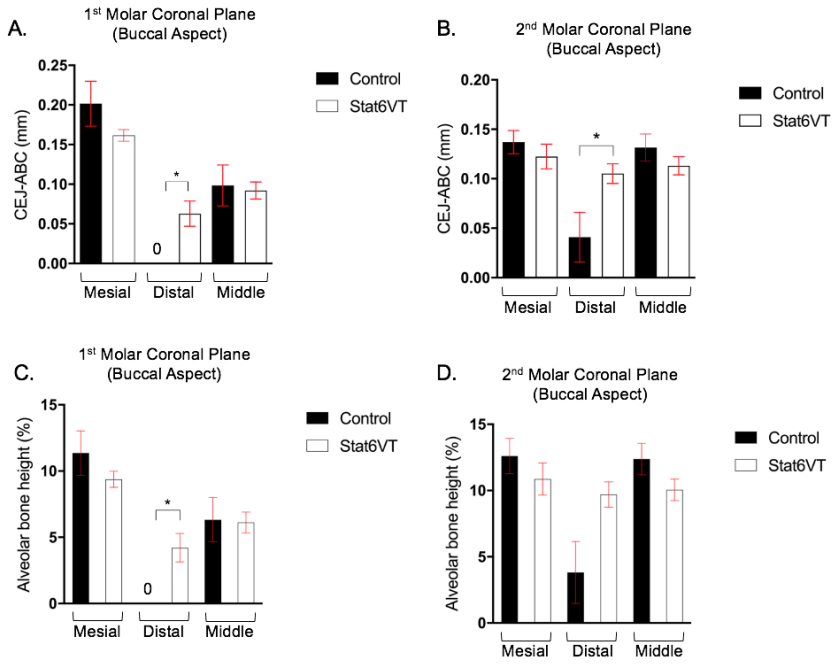

Figure 23. MicroCT measurements of the 6-8-week-old female Stat6VT and control mice on the lingual aspect of the coronal plane. CEJ-ABC measurements of the A: first molar and B: second molar taken on the coronal plane (lingual aspect), and the alveolar bone height of the C: first molar and D: second molar taken on the coronal plane (lingual aspect). *p<0.05.

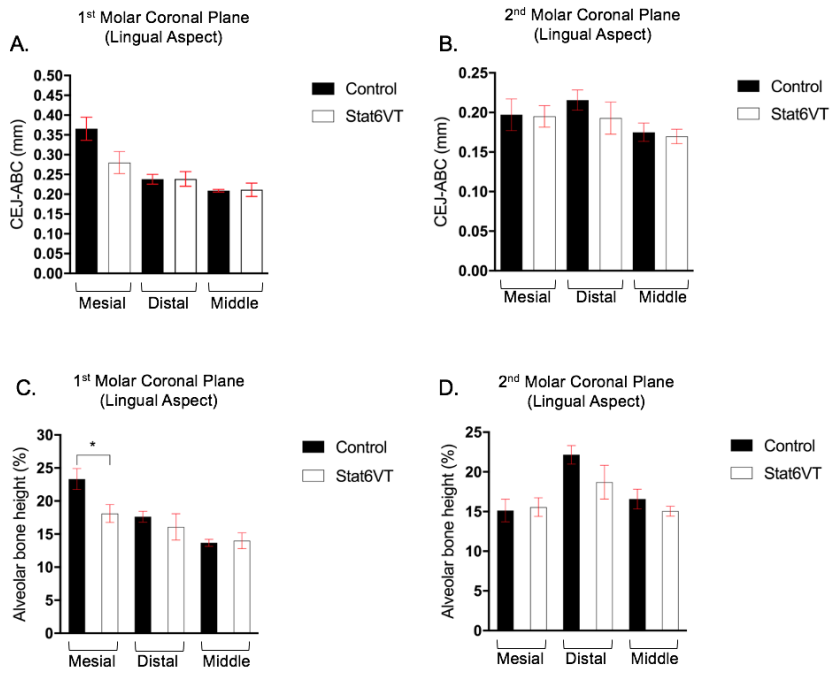

Figure 24. MicroCT measurements of the 6-8-week-old female Stat6VT and control mice on the sagittal plane. CEJ-ABC measurements of the A: first molar and B: second molar taken on the sagittal plane, and the alveolar bone height of the C: first molar and D: second molar taken on the sagittal plane. *p<0.05.

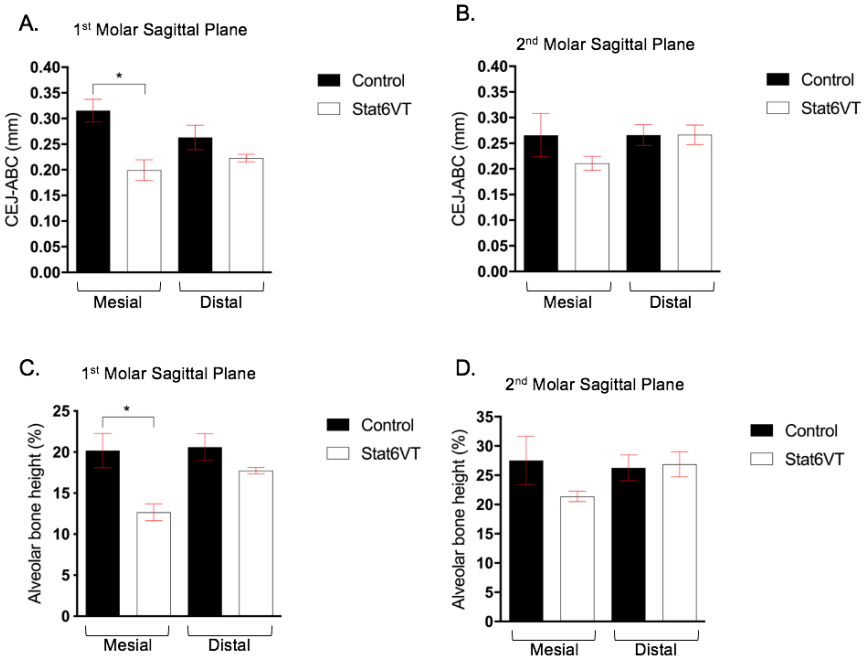

Figure 25. MicroCT measurements of the 10-13-week-old female Stat6VT and control mice on the buccal aspect of the coronal plane. CEJ-ABC measurements of the A: first molar and B: second molar taken on the coronal plane (buccal aspect), and the alveolar bone height of the C: first molar and D: second molar taken on the coronal plane (buccal aspect). *p<0.05.

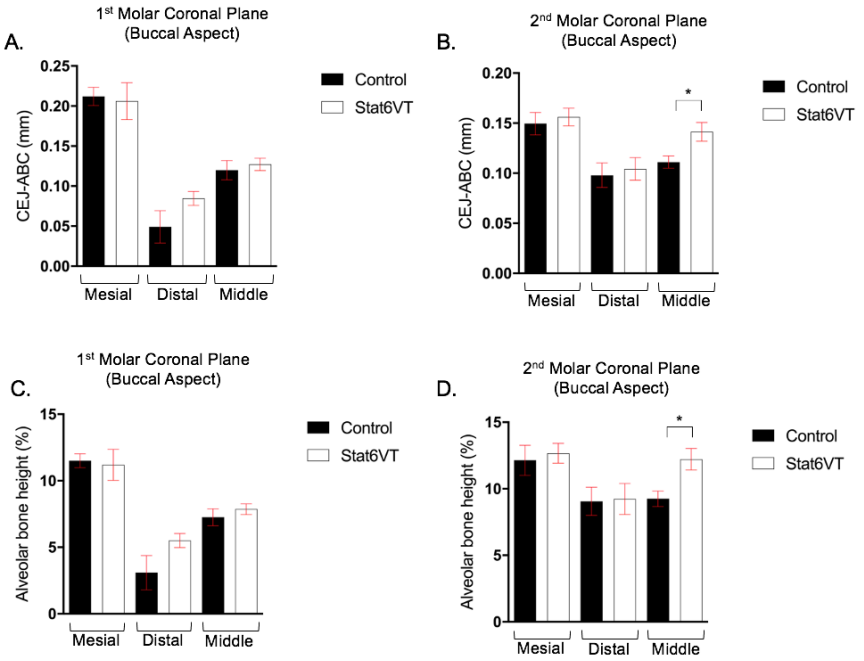

Figure 26. MicroCT measurements of the 10-13-week-old female Stat6VT and control mice on the lingual aspect of the coronal plane. CEJ-ABC measurements of the A: first molar and B: second molar taken on the coronal plane (lingual aspect), and the alveolar bone height of the C: first molar and D: second molar taken on the coronal plane (lingual aspect).

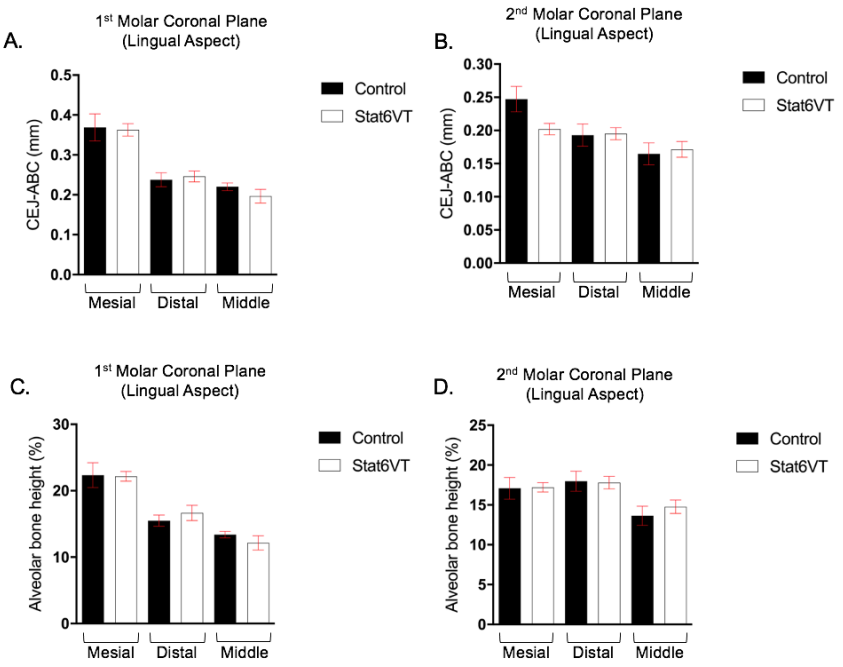

Figure 27. MicroCT measurements of the 10-13-week-old female Stat6VT and control mice on the sagittal plane. CEJ-ABC measurements of the A: first molar and B: second molar taken on the sagittal plane, and the alveolar bone height of the C: first molar and D: second molar taken on the sagittal plane. *p<0.05.

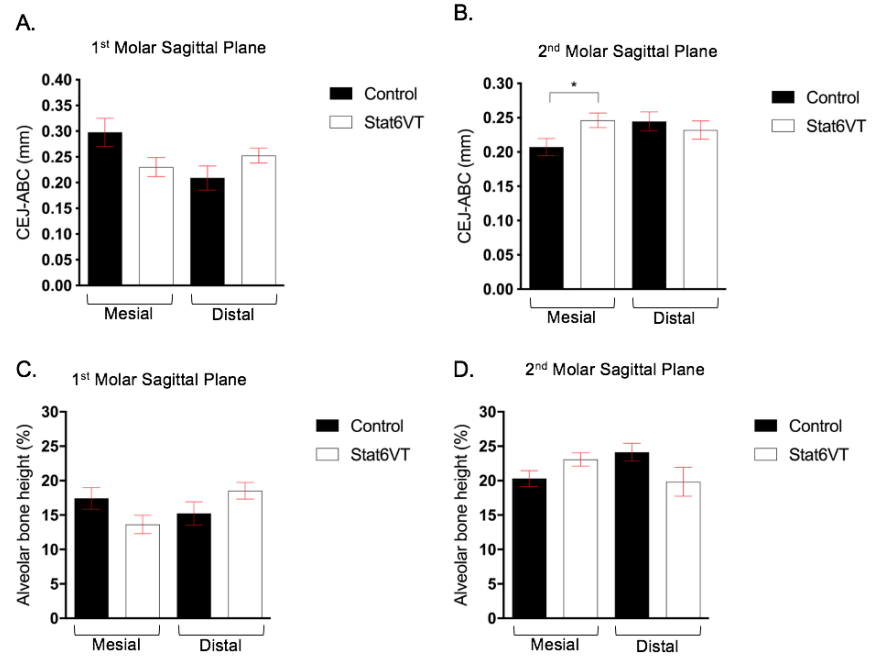

Figure 28. MicroCT measurements of the 18-week-old female Stat6VT and control mice on the buccal aspect of the coronal plane. CEJ-ABC measurements of the A: first molar and B: second molar taken on the coronal plane (buccal aspect), and the alveolar bone height of the C: first molar and D: second molar taken on the coronal plane (buccal aspect). *p<0.05.

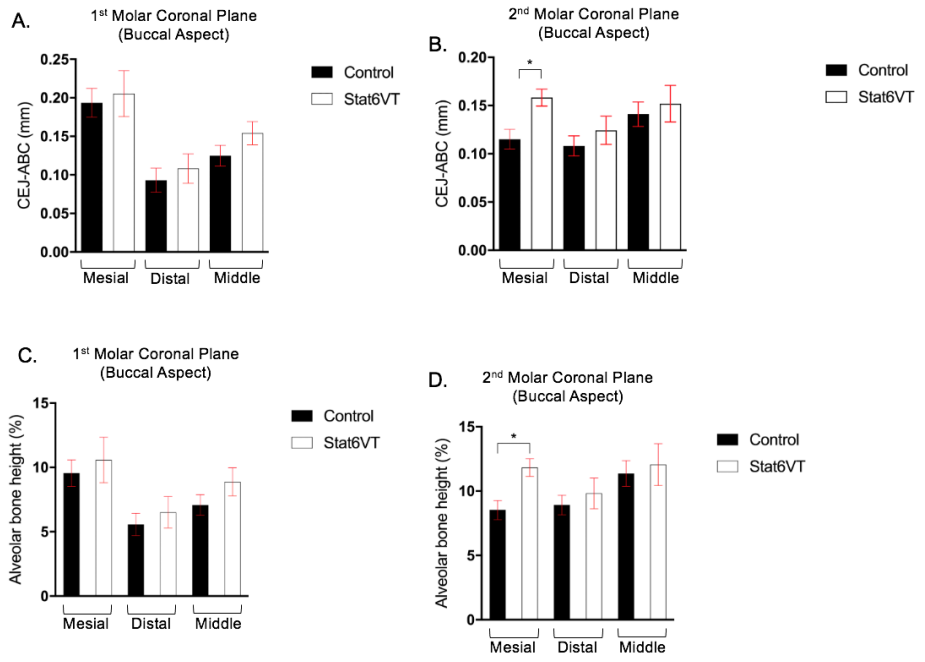

Figure 29. MicroCT measurements of the 18-week-old female Stat6VT and control mice on the lingual aspect of the coronal plane. CEJ-ABC measurements of the A: first molar and B: second molar taken on the coronal plane (lingual aspect), and the alveolar bone height of the C: first molar and D: second molar taken on the coronal plane (lingual aspect). *p<0.05.

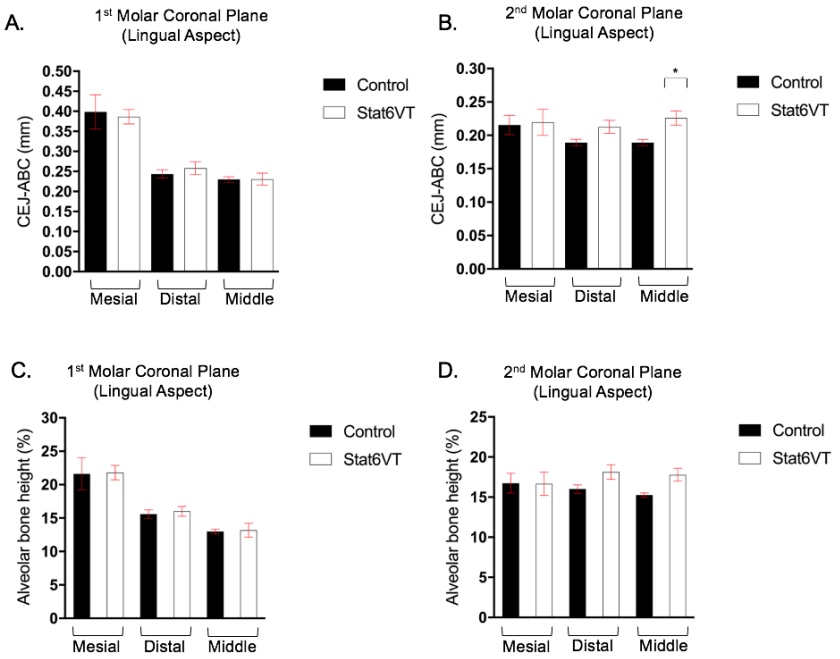

Figure 30. MicroCT measurements of the 18-week-old female Stat6VT and control mice on the sagittal plane. CEJ-ABC measurements of the A: first molar and B: second molar taken on the sagittal plane, and the alveolar bone height of the C: first molar and D: second molar taken on the sagittal plane. *p<0.05.

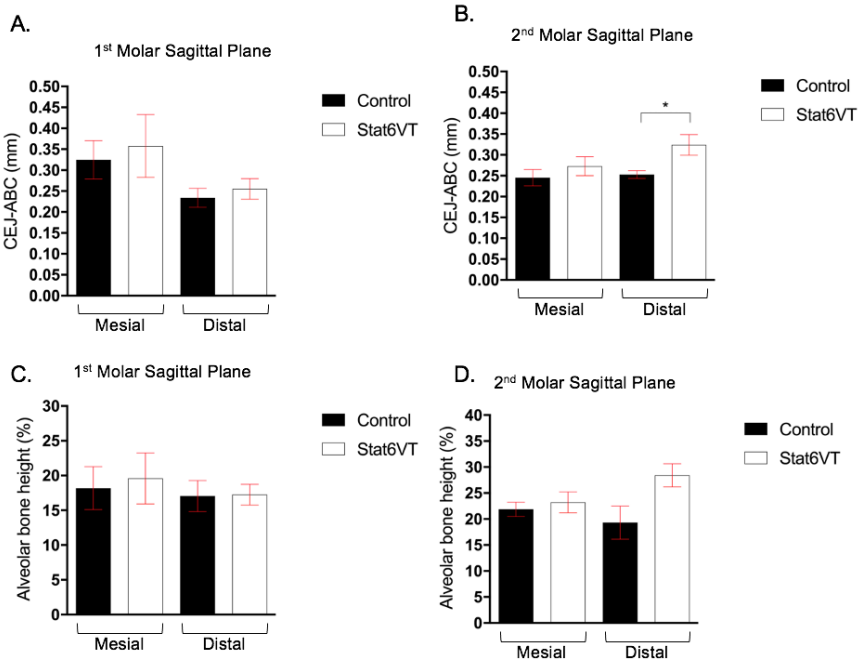

3.4.3 Results for males

At 6-8 weeks, male Stat6VT demonstrated significantly greater CEJ-ABC measurements than control mice across 5 different sites for each tooth (Figures 31A, 31B, 32A, 32B, 33A and 33B). The first molar sites were as follows: CEJMid-ABCB (0.08098 ± 0.004335 vs. 0.1408 ± 0.01077, p= 0.0009), CEJD-ABCL (0.1648 ± 0.007548 vs. 0.2183 ± 0.01593, p=0.0162), CEJMid-ABCL (0.1571 ± 0.007785 vs. 0.2013 ± 0.006296, p=0.022), CEJM-ABC (0.1799 ± 0.008253 vs. 0.2292 ± 0.02306, p=0.0264) and CEJD-ABC (0.1562 ± 0.003573 vs. 0.2418 ± 0.009594, p<0.0001). The second molar sites were: CEJM-ABCB (0.09678 ± 0.004580 vs. 0.1319 ± 0.007082, p=0.0032), CEJMid-ABCB (0.04610 ± 0.005164 vs. 0.09399 ± 0.01212, p=0066), CEJM-ABCL (0.1397 ± 0.005034 vs. 0.1938 ± 0.009595, p<0.0001), CEJM-ABC (0.1206 ± 0.005760 vs. 0.1855 ± 0.01072, p=0.0007) and CEJD-ABC (0.1670 ± 0.03215 vs. 0.2533 ± 0.01335, p=0.0382). Furthermore, there were 3 sites on the first molar (Figure 31C and 32C) and 1 site on the second molar (Figure 33D) that demonstrated greater loss of alveolar bone height in Stat6VT compared to the control mice. The 3 sites on the first molar were CEJMid-ABCB (6.692 ± 0.6885 vs. 9.750 ± 0.6572, p=0.0124), CEJD-ABCL (12.71 ± 0.7620 vs. 17.49 ± 1.241, p=0.0111) and CEJMid-ABCL (11.11 ± 0.9319 vs. 13.97 ± 0.4641, p=0.0251). The 1 site on the second molar was CEJD-ABC 7.19 ± 3.149 vs. 27.19 ± 1.333, p=0.0192) (Figure 33D).

At 10-13 weeks, male Stat6VT when compared to controls demonstrated greater CEJ-ABC measurements in 1 site on the first molar and 4 sites on the second molar (Figures 34B, 35A, 35B, 36B.). The site on the first molar was CEJMid-ABCL (0.1738 ± 0.01006 vs. 0.2373 ± 0.005542, p=0.0006). The 4 sites on the second molar were as follows: CEJMid-ABCB (0.05913 ± 0.02441 vs. 0.1339 ± 0.01036, p=0.0225), CEJM-ABCL (0.1626 ± 0.007351 vs. 0.2172 ± 0.01738, p=0.0201), CEJD-ABCL (0.1419 ± 0.01138 vs. 0.2101 ± 0.006898, p=0.0009), and

CEJM-ABC (0.1278 ± 0.01949 vs. 0.2218 ± 0.02051, p=0.0105). Furthermore, Stat6VT demonstrated a significantly greater loss of alveolar bone height in 1 site on the second molar as compared to the control (Figure 36D), which was on the site CEJM-ABC (12.26 ± 1.848 vs. 20.35 ± 1.842, p=0.0146).

At 18 weeks, there were 2 sites on the first molar that demonstrated greater CEJ-ABC in the Stat6VT mice when compared to control mice (Figures 38A and 39A). The 2 sites were: CEJM-ABCL (0.4100 ± 0.01782 vs. 0.3104 ± 0.03497, p=0.0349) and CEJM-ABC (0.3742 ± 0.03533 vs. 0.2578 ± 0.03250, p=0.0415). Additionally, measurements taken on the lingual aspect of the coronal plane at this time point did not demonstrate any significant differences between Stat6VT and control mice (Figure 38).

The male microCT results revealed that across the 3 established time points, there were various sites that consistently demonstrated greater CEJ-ABC measurements in Stat6VT than controls. On the first molar, CEJMid-ABCL demonstrated an increase in CEJ-ABC measurements from the 6-8-week time point to the 10-13-week time point, and CEJM-ABC demonstrated an increase in CEJ-ABC measurements from the 6-8-week time point to the 18-week time point. On the second molar, CEJM-ABCL and CEJM-ABC demonstrated an increase in CEJ-ABC measurements from the 6-8-week time point to the 10-13-week time point. These findings suggest that the distance from the CEJ to the ABC is becoming greater in the Stat6VT mice over time. This follows our hypothesis because we believe that the downregulation of loricrin can lead to an increased inflammatory response in the Stat6VT mice. Furthermore, these findings also aligned with the phenotypical observations, which revealed that lesion onset occurred at the 10-13-week time point and continued to worsen at the 18-week time point. Similar to the phenotypical observations and BMD/BMC findings, the microCT results for the

male mice groups demonstrated consistency in its findings, whereas the female groups did not. This difference between the sexes is a novel finding in our study. Hormonal and physiological aspects of being female may contribute to the differences observed.

Figure 31. MicroCT measurements of the 6-8-week-old male Stat6VT and control mice on the buccal aspect of the coronal plane. CEJ-ABC measurements of the A: first molar and B: second molar taken on the coronal plane (buccal aspect), and the alveolar bone height of the C: first molar and D: second molar taken on the coronal plane (buccal aspect). *p<0.05.

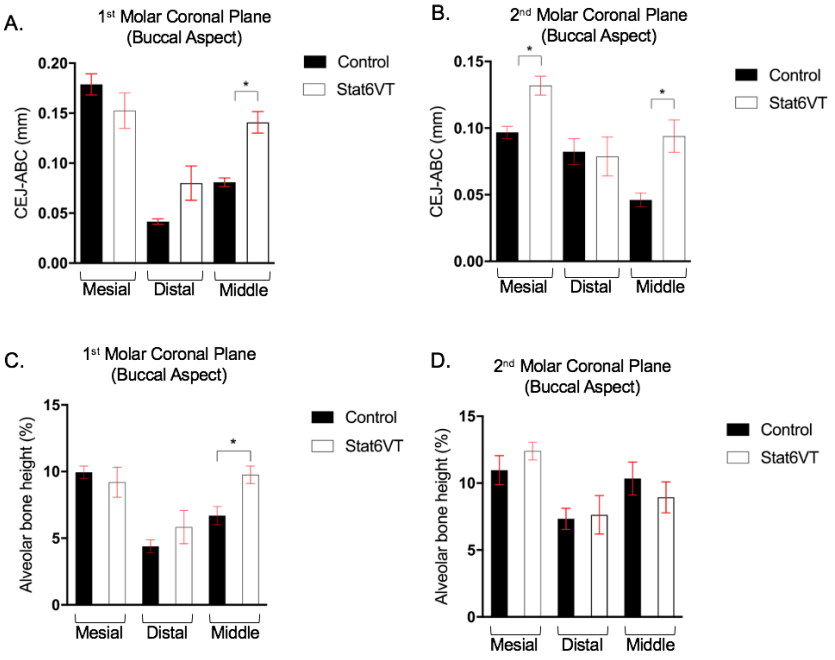

Figure 32. MicroCT measurements of the 6-8-week-old male Stat6VT and control mice on the lingual aspect of the coronal plane. CEJ-ABC measurements of the A: first molar and B: second molar taken on the coronal plane (lingual aspect), and the alveolar bone height of the C: first molar and D: second molar taken on the coronal plane (lingual aspect). *p<0.05.

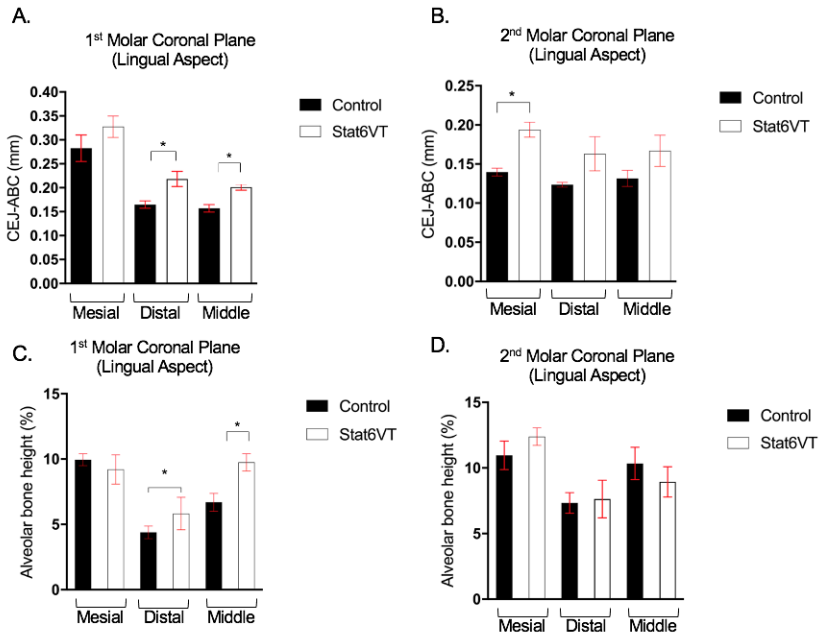

Figure 33. MicroCT measurements of the 6-8-week-old male Stat6VT and control mice on the sagittal plane. CEJ-ABC measurements of the A: first molar and B: second molar taken on the sagittal plane, and the alveolar bone height of the C: first molar and D: second molar taken on the sagittal plane. *p<0.05.

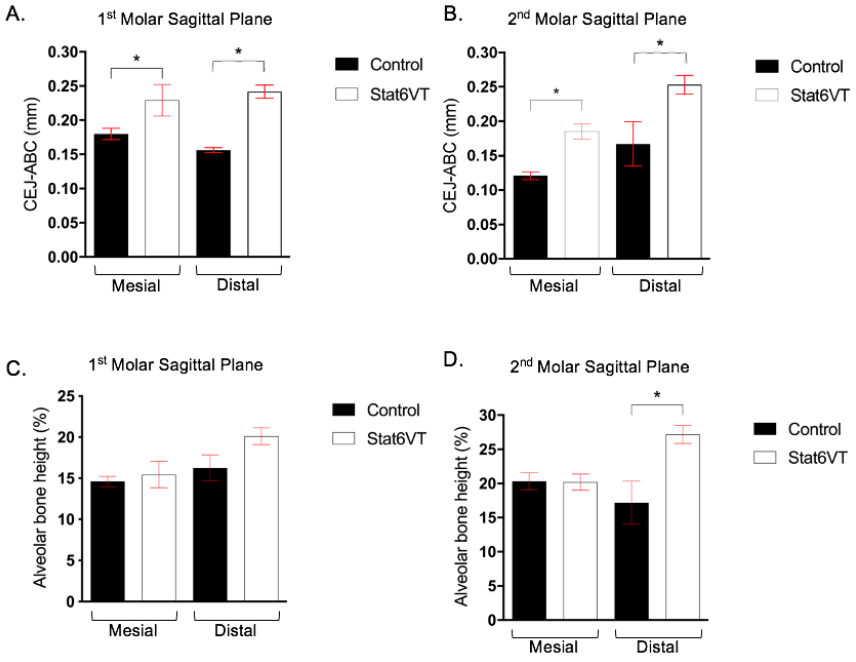

Figure 34. MicroCT measurements of the 10-13-week-old male Stat6VT and control mice on the buccal aspect of the coronal plane. CEJ-ABC measurements of the A: first molar and B: second molar taken on the coronal plane (buccal aspect), and the alveolar bone height of the C: first molar and D: second molar taken on the coronal plane (buccal aspect). *p<0.05.

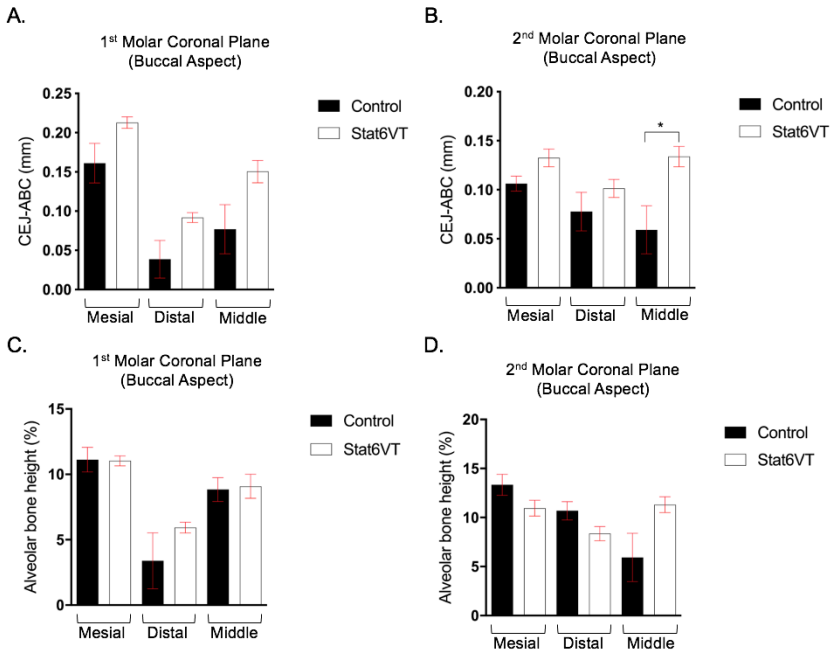

Figure 35. MicroCT measurements of the 10-13-week-old male Stat6VT and control mice on the lingual aspect of the coronal plane. CEJ-ABC measurements of the A: first molar and B: second molar taken on the coronal plane (lingual aspect), and the alveolar bone height of the C: first molar and D: second molar taken on the coronal plane (lingual aspect). *p<0.05.

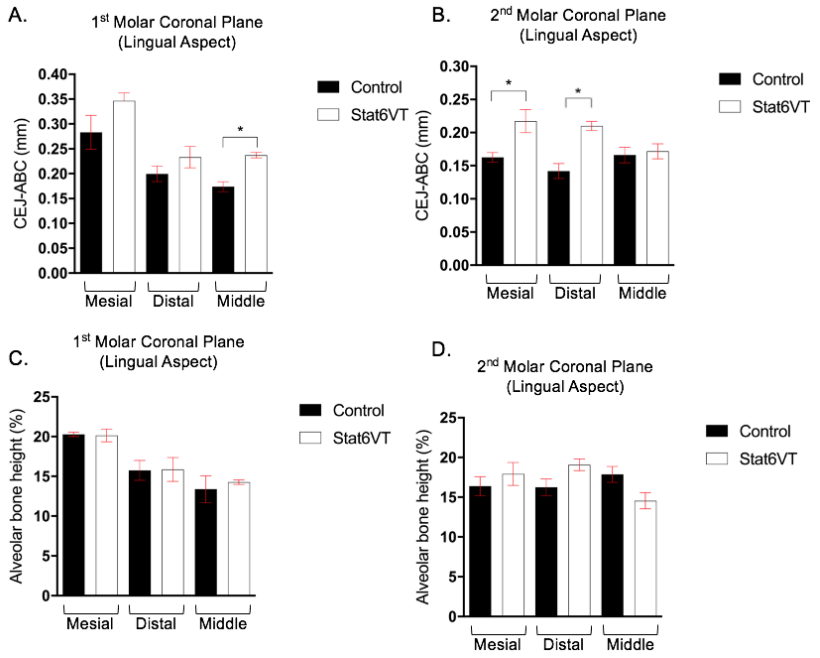

Figure 36. MicroCT measurements of the 10-13-week-old male Stat6VT and control mice on the sagittal plane. CEJ-ABC measurements of the A: first molar and B: second molar taken on the sagittal plane, and the alveolar bone height of the C: first molar and D: second molar taken on the sagittal plane. *p<0.05.

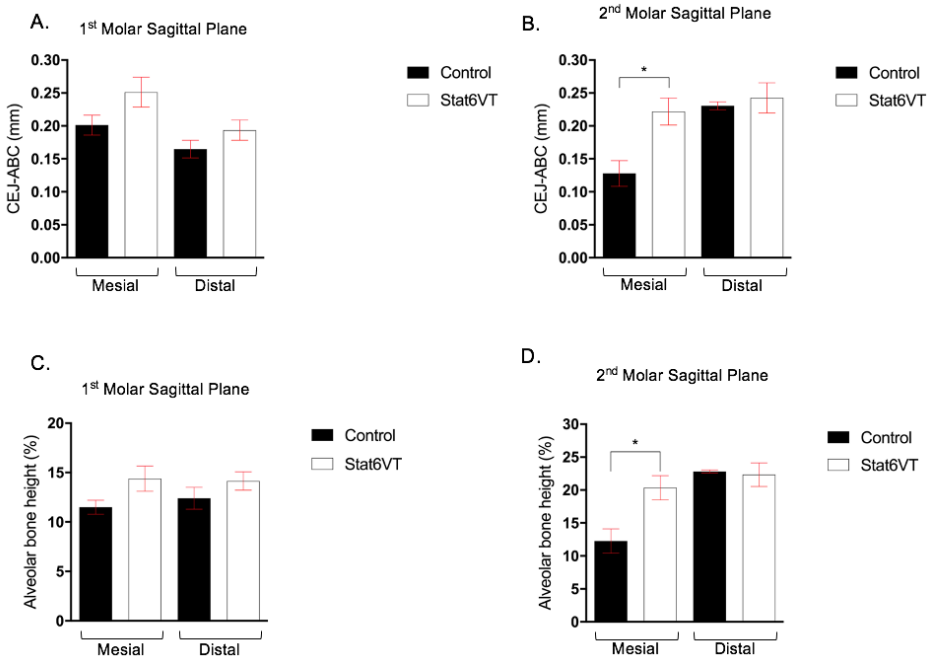

Figure 37. MicroCT measurements of the 18-week-old male Stat6VT and control mice on the buccal aspect of the coronal plane. CEJ-ABC measurements of the A: first molar and B: second molar taken on the coronal plane (buccal aspect), and the alveolar bone height of the C: first molar and D: second molar taken on the coronal plane (buccal aspect).

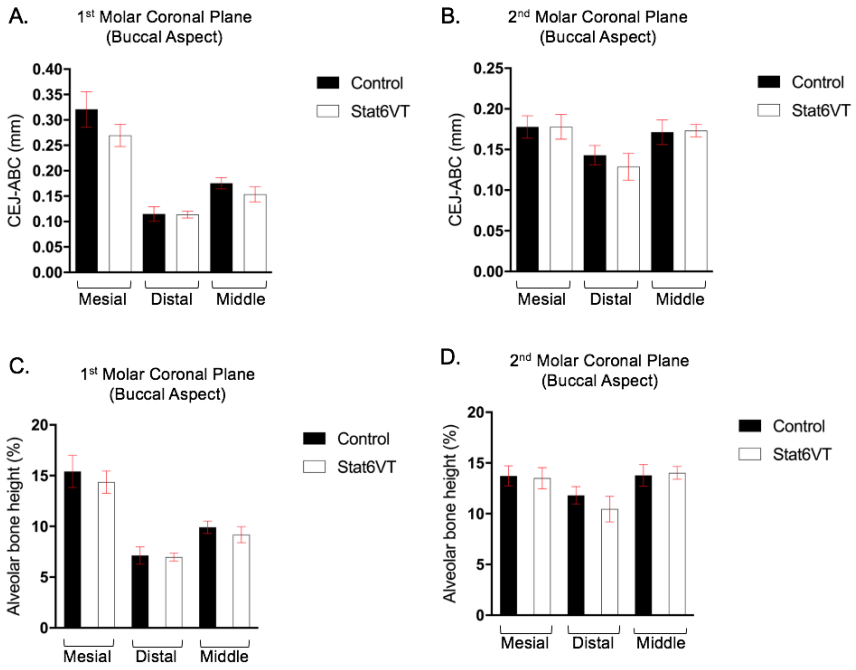

Figure 38. MicroCT measurements of the 18-week-old male Stat6VT and control mice on the lingual aspect of the coronal plane. CEJ-ABC measurements of the A: first molar and B: second molar taken on the coronal plane (lingual aspect), and the alveolar bone height of the C: first molar and D: second molar taken on the coronal plane (lingual aspect). *$p<0.05$.

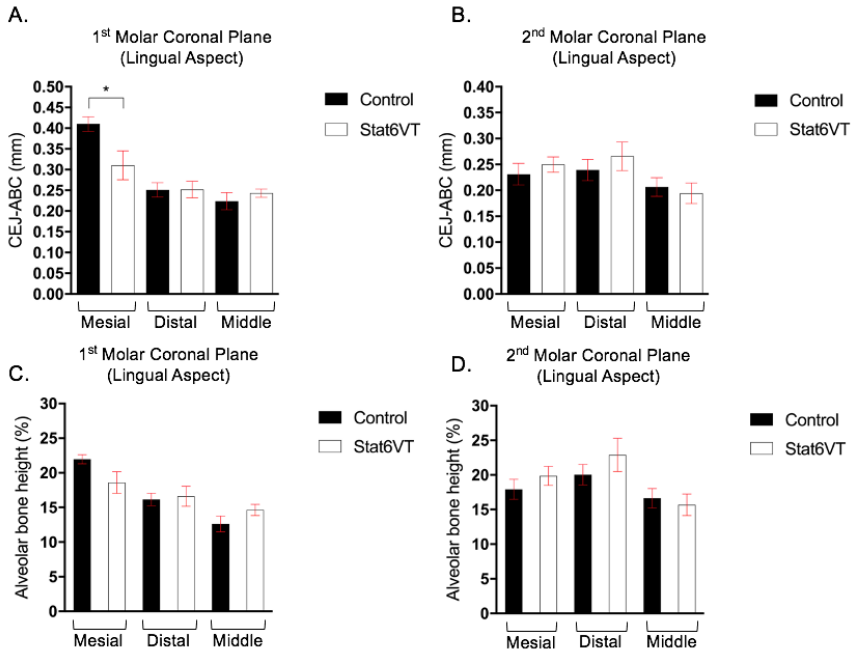

Figure 39. MicroCT measurements of the 18-week-old male Stat6VT and control mice on the sagittal plane. CEJ-ABC measurements of the A: first molar and B: second molar taken on the sagittal plane, and the alveolar bone height of the C: first molar and D: second molar taken on the sagittal plane. *p<0.05.

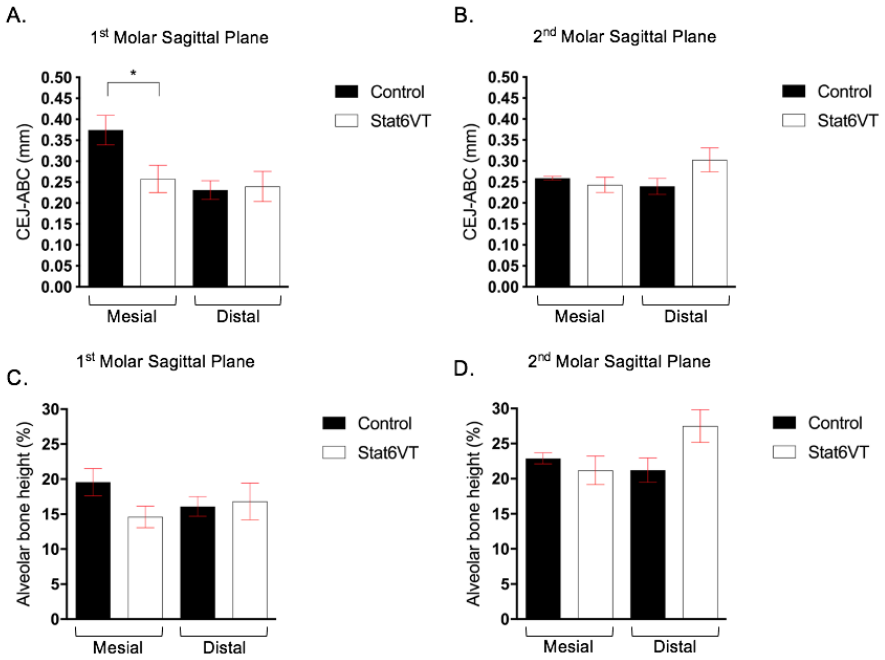

3.5 Histological studies demonstrated epithelial changes and signs of inflammation in Stat6VT mice

3.5.1 The rationale for palates and males

With the assistance of Dr. Catunda and Dr. Bryant Roy (lab mate), the palates of male control and Stat6VT mice at 6-8-, 10-13-, and 18-weeks of age were collected and prepared for histology. Palates are similar to attached gingiva, found near the sulcus of a periodontal pocket, in that they are both classified as masticatory mucosa. Masticatory mucosa includes regions that contain keratinized stratified squamous epithelium, which is of interest in our study since this type of epithelium contains CE proteins, such as loricrin (Kim *et al*., 2008). The palate was ultimately chosen to be used for histological examination in our study because the collection process provided accurate, standardized samples more consistently than any other keratinized site in the oral cavity. Furthermore, the palate was the only keratinized site that could be embedded with a standardized orientation. Histology was performed in the male groups only because the females showed inconsistency in lesion onset (earlier than expected at 6-8 weeks), and they also showed differences in BMC. The early onset of lesions at baseline could indicate that these animals were already undergoing loricrin downregulation.

3.5.2 The rationale for performing histology

We performed H&E and immunofluorescence staining (loricrin, CD45, Ki67, CK1 and CK14) on samples from 3 mice per group. There were 2 investigators that examined all the histology images. Consultation with an oral pathologist was sought as needed. All images were taken with the same microscope and software settings (brightness, exposure and gain) to allow for comparison. We specifically chose H&E staining and immunostaining for CK1 and CK14 because in the literature, these are commonly used in murine models to investigate the organization, structure and type of epithelium (Kim *et al*., 2008). Loricrin immunofluorescence

would give us information as to its expression and distribution in the CE, which has been used in studies investigating skin barrier defects. We also chose to perform CD45 and Ki67 immunofluorescence because these markers have been used in the literature to investigate the inflammatory responses in mouse models as well (Hoste *et al*., 2003; Lee *et al*., 2011).

3.5.3 The rationale for markers and expectations

The intent of performing histology in our study was to observe the epithelium at the microscopic level and compare Stat6VT to control mice. The rationale was that the Stat6VT, having a reduced expression of loricrin, would have an impaired barrier function, allowing any minor threat to be perceived by the host as harmful. This could cause a heightened inflammatory response compared to control mice (intact barrier).

In our study, H&E staining was performed to determine any potential structural and morphological changes, and the extent of inflammatory presentation, such as rete pegs (epithelial projections into the underlying connective tissue), clear cells (the appearance of a clear halo around cell nuclei) and inflammatory cell infiltrate (Kantarci *et al*., 2011; Ross 2006). Furthermore, H&E staining would provide us with insight into the type of keratinized epithelium and potential differences in the outer cornified layer. There are two main keratinized epithelial types that can be seen in the oral cavity, ortho- and para-keratinized epithelium (Ross 2006). Although both types of epithelium contain similar layers (basal, spinous, granular and keratin), the main difference is that the outer layer in para-keratinized epithelium retains nuclei whereas this layer is enucleated in the ortho-keratinized epithelium (Ross 2006). In the H&E staining, due to the heightened immune response in Stat6VT mice, we expected to see more clear cells (potentially indicative of inflammatory cells) and nuclei compared to controls (Ross 2006). Additionally, we expected the basal layer in the Stat6VT mice to demonstrate more rete pegs due

to the increased cell proliferation. This is because at early and established stages of periodontitis, the rete pegs tend to invaginate deeper into the connective tissue in order to maintain epithelial integrity and reinforce the barrier to microbial entry (Kayal 2013).

In the literature, the skin lesions of Stat6VT mice have demonstrated reduced loricrin expression in immunohistochemistry (Kim *et al*., 2008), however, loricrin expression of the oral epithelium via immunofluorescence has never been investigated before. To test our hypothesis, it was crucial for us to assess loricrin expression qualitatively (immunostaining). We expected loricrin expression to be decreased in the Stat6VT mice, similar to the reduction that have been observed in their skin. We recognize that there are caveats in making assumptions about expression using immunofluorescence staining; the results are described qualitatively only and conclusions are conservative.

Immunofluorescence for CD45 and Ki67 were quantified via cell count analysis (all counts performed were of at least 3 fields at 400x magnification (similar to what has been done in the literature by Wu *et al*., (2008)). Cell count analyses were assisted by Sara Moradipoor, Ramesh Mahdavifar (lab mate) and Dr. Catunda. CD45 is a protein expressed on all leukocytes and it plays a crucial role in the functionality of leukocytes (Altin & Sloan, 1997). Therefore, a greater expression of CD45 positive cells may be indicative of an increased inflammatory response (Altin & Sloan, 1997). Ki67 antigen is a commonly used proliferation marker, as it plays a crucial role in interphase during mitosis (Reichrath & Holick, 2011). It is commonly used in psoriasis studies as a marker of epidermal proliferation. Ki67 expression increases as the cells prepare to divide (Reichrath & Holick, 2011). Research suggests that in normal oral epithelium, Ki67 positive cells are restricted to the basal layer (Birajdar *et al*., 2014; Kumar *et al*., 2015; Saito *et al*., 1999; Takkem *et al*., 2018). When Ki67 positive cells are located past the basal

layer, such as in the parabasal and spinous layer, this is indicative of oral epithelial dysplasia (Birajdar *et al*., 2014; Takkem *et al*., 2018). Additionally, inflammation leads to cell death and the increase in turnover is reflected in the basal layer of the epithelium, where cell proliferation occurs (Birajdar *et al*., 2014; Takkem *et al*., 2018). Turnover of the epithelium may also occur due to other mechanisms related to changes in loricrin expression that result in cell death (Birajdar *et al*., 2014; Takkem *et al*., 2018). The rationale for performing Ki67 immunofluorescence staining and cell count analysis was to investigate the degree of proliferation in the palate and to relate it to other phenotypic changes observed. We expected to see more CD45 and Ki67 positive cells in the Stat6VT mice compared to controls. We also anticipated seeing a significantly greater cell count of these cells in Stat6VT mice compared to controls in the *Pg* infection study.

The functionality of the epidermis depends on structural proteins, such as keratins (Roth *et al*., 2012). Keratins are members of the intermediate filament family of cytoskeletal fibers (Roth *et al*., 2012). There are two types of intermediate filaments, type I and II (Roth *et al*., 2012. CK1 is a type II keratin due to its relative size and charge (Jacob *et al*., 2018). CK1 plays a crucial role in the maintenance of skin integrity, barrier formation and inflammation control (Jacob *et al*., 2018). It is normally expressed starting from the basal up to the granular layer of the epithelium (Jacob *et al*., 2018). CK1 was included as a marker of interest in our study because it can provide insight into how these cells were expressed in the Stat6VT mice compared to controls. CK1 expression found outside of the designated epithelial layers or absence of CK1 expression within the designated layers in the Stat6VT mice could be indicative of abnormal epithelial growth and development.

CK14 is a type 1 keratin and a marker of dividing basal keratinocytes that helps in the maintenance of epidermal cell shape and structure (Alam *et al*., 2011). Research suggests that decreased expression of CK14 may be associated with skin diseases and malignant transformations (Harnden & Southgate, 1997; Yoshida *et al*., 2015). CK14 is specifically expressed in the basal layer of all stratified epithelium (Harnden & Southgate, 1997; Yoshida *et al*., 2015). Any expression of CK14 outside of the basal layer would be considered abnormal (Harnden & Southgate, 1997; Yoshida *et al*., 2015). Our intent in performing CK14 immunofluorescence was to investigate the expression of these keratins in the Stat6VT mice compared to controls for any atypical observations. An abnormal expression may suggest a change in cell differentiation and proliferation (Alam *et al*., 2011).

3.5.4 H&E staining

6-8-week time point. At 6-8 weeks of age, the palate of Stat6VT male mice seemed to have demonstrated observably more rete pegs and basal cells as compared to controls. Additionally, other observations included fewer nuclei in the upper epithelial layers and a thinner keratinized outer layer in the Stat6VT palate compared to control. In the keratinized layer of Stat6vt mice, we also observed flattened nuclei remnants. Both groups demonstrated few observable clear cells in the spinous layer. We considered that even at baseline, Stat6VT transgenic mice, when compared to controls, could begin to show signs of inflammation. Furthermore, the thinner keratinized and incompletely keratinized layer may suggest a more vulnerable and weaker outer layer; however, this was not a consistent finding. Images of H&E staining of control and Stat6VT palate at 6-8 weeks are shown in Figure 40.

Figure 40. H&E-stained palates from 6-8-week-old male A: control and B: Stat6VT mice. Layers of the epithelium, clear cells and rete pegs are marked. Scale bar 20µm.

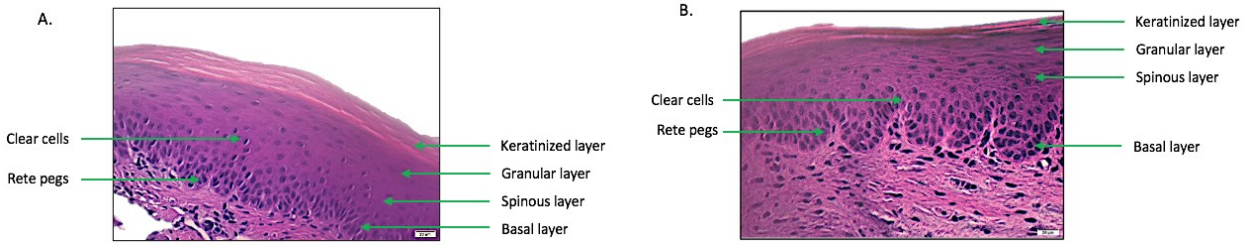

10-13-week time point. At 10-13 weeks of age, the palate of Stat6VT mice demonstrated suggestively more rete pegs than controls, which had a uniformly straight basal layer with minimal to no rete pegs. Control mice qualitatively had few clear cells compared to Stat6VT mice, which seemed to have more clear cells. Additionally, there appeared to have been an increase in proliferation around the basal layer due to rete peg formation, which may be indicative of increased cellular turnover and connective tissue invagination (a protective mechanism). These differences in rete pegs, clear cells and expansion of the basal layer are signs of inflammation (Kantarci *et al*., 2011; Ross 2006). The differences observed between control and Stat6VT mice at 10-13 weeks of age were in line with our hypothesis and the development of skin lesions, although no overt lesions were noted in the oral cavity. Figure 41 shows H&E-stained control and Stat6VT mouse palates at 10-13 weeks of age.

Figure 41. H&E-stained palates from 10-13-week-old male A: control and B: Stat6VT mice. Clear cells and rete pegs are marked. Scale bar 20µm.

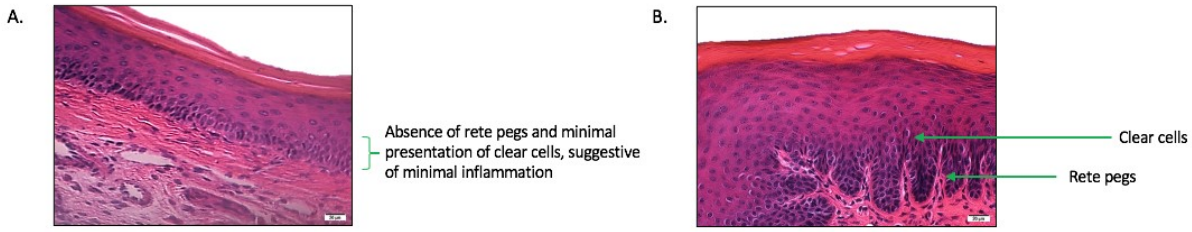

18-week time point. At 18-weeks of age, the palate of Stat6VT mice consistently demonstrated a non-uniform and detached outer keratinized layer compared to controls. Both groups had a greater number of clear cells at this time point compared to 6-8- and 10-13- weeks of age, but Stat6VT mice still seemed to present more. Additionally, when the basal layer up to the spinous layer is compared, nuclei are significantly more clustered and disorderly in the epithelium of Stat6VT mice compared to control. The connective tissue below the epithelium in the Stat6VT and control palate demonstrated clustering of cells, that may have been suggestive of inflammation. In addition, these sites were observed to suggestively be more intense in Stat6VT than control, as evidenced by more nuclei clustering along the basal layer and connective tissue layer. These observations align with our hypothesis, as we believed that the mice would show increased inflammation as they age, and due to the heightened Th2 immune response in the Stat6VT mice, they would demonstrate greater inflammation than the controls. Figure 42 demonstrates the palates of control and Stat6VT mice at 18-weeks of age.

Figure 42. H&E-stained palates from 18-week-old male A: control and B: Stat6VT mice. Clear cells, sites indicative of inflammation and keratinized layer are labeled for identification purposes. Scale bar 20µm.

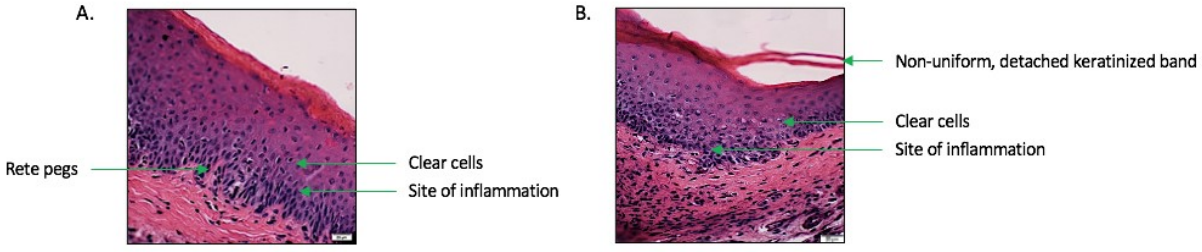

3.5.5 Loricrin immunofluorescence

6-8-week time point. At 6-8-weeks of age, male Stat6VT and control mice demonstrated many similarities in loricrin expression in the palate (Figure 43). The intensity of expression was

comparable, as observed by the similarity in brightness, and the distribution of loricrin expression in control and Stat6VT was localized to the granular layer, with approximately the same width. Interestingly, the control group had a few cells below the granular layer that demonstrated positive loricrin expression, which was not seen in the Stat6VT group. Loricrin expression in control and Stat6VT mice at 6-8 weeks of age was in line with our hypothesis, as we believed that at this age, given the absence of skin lesions, the expression would be relatively the same.

Figure 43. Loricrin immunofluorescence in the palate of 6-8-week-old male A: control and B: Stat6VT mice. C: Secondary-antibody alone control to show non-specific staining. The keratinized and granular layers are labeled for identification purposes. The white dashed line demarcates the top of the keratinized layer for landmarking purposes. Scale bar 20μm.

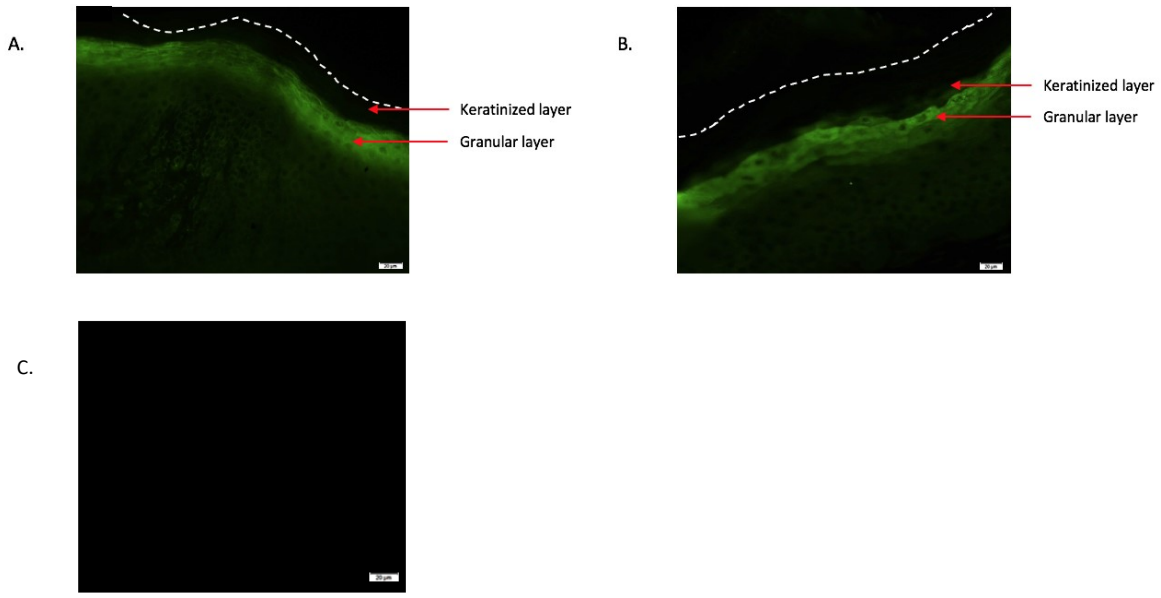

10-13-week time point. At 10-13 weeks of age, expression of loricrin in the palate was evident in control and Stat6VT mice, however, we observed a difference in localization. Loricrin expression was localized to a single row of cells in the granular layer in the control group as

compared to the Stat6VT group, which had an expression that spanned multiple rows of the granular layer, and potentially into the spinous layer (Figure 44). We hypothesized that Stat6VT mice would show loricrin downregulation, as a result of constitutive activation of Stat6. Instead, we observed disruption of loricrin expression, in terms of location. Whether this affects barrier function is not known.

Figure 44. Loricrin immunofluorescence in the palate of male 10-13-week-old A: control and B: Stat6VT mice. C: Secondary-antibody alone control to show non-specific staining. The granular and spinous layers are labeled for identification purposes. Scale bar 20µm.

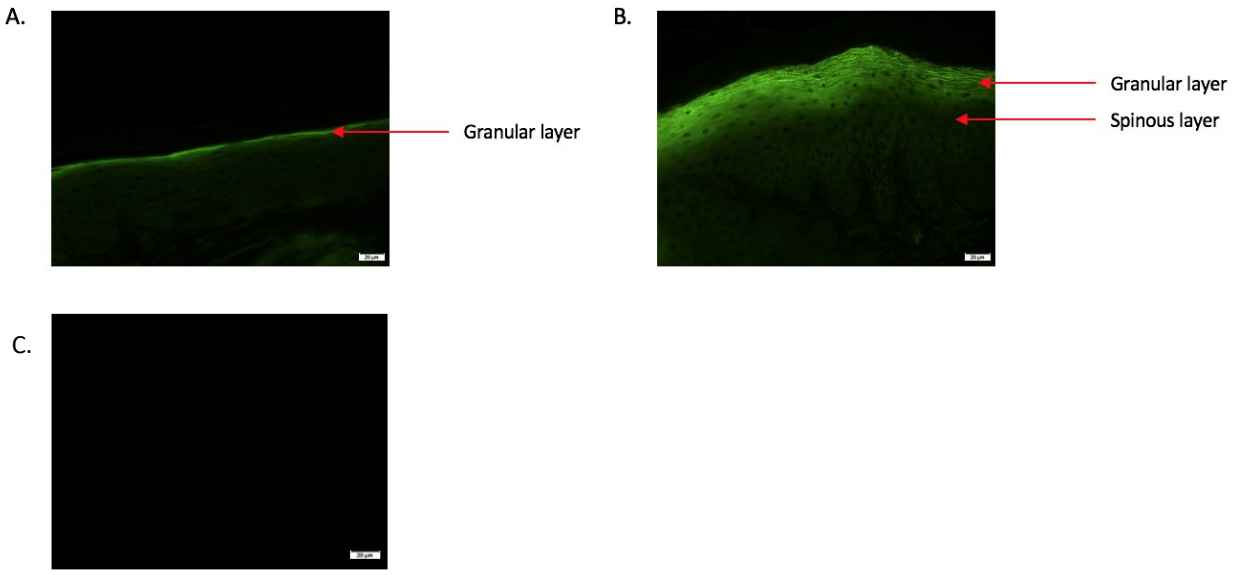

18-week time point. At 18-weeks of age, the immunofluorescent signal for loricrin in the palate of control mice was stronger, suggesting greater expression, in comparison to the Stat6VT group (Figure 45). The control mice also had a very defined expression of loricrin: it was localized to the upper layers of the granular layer. The palate of Stat6VT mice demonstrated a wider distribution of loricrin, but it still appeared to be confined to the granular layer. These observations suggest that loricrin expression is reduced in Stat6VT mice compared to controls, and also disrupted in terms of localization.

Figure 45. Loricrin immunofluorescence in the palate of male 18-week-old A: control and B: Stat6VT mice. C: Secondary-antibody alone control to show non-specific staining. The white dash marks demarcate where the top of the keratinized layer is located for landmarking purposes. Scale bar 20µm.

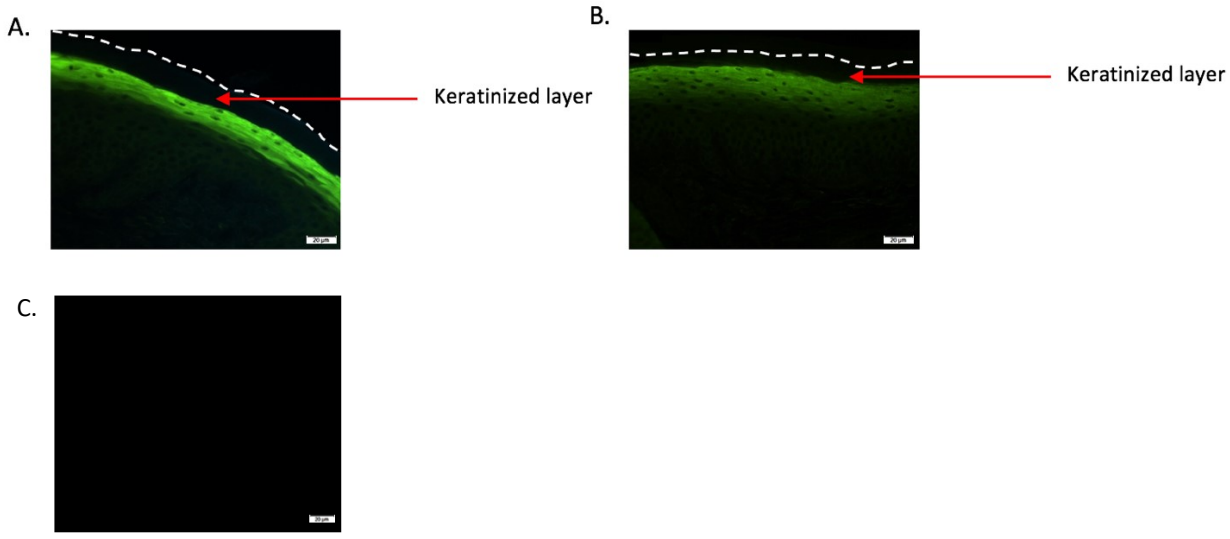

3.5.6 CD45 immunofluorescence

6-8-week time point. We observed CD45 positive cells in the palate of 6-8-week-old male control and Stat6VT mice via immunofluorescence staining. The number of cells appeared to be comparable in both groups (Figure 46). After performing the cell count, we confirmed that there were no significant differences (CD45 positive cells: control: 12.88± 1.641; Stat6VT: 13.4 ± 2.159, n=3/group, p=0.9340) (Figure 47). These findings follow our hypothesis, as we were expecting 6-8 weeks to act as a baseline and demonstrate a similar level of inflammation between both the control and Stat6VT group.

Figure 46. CD45 positive cells in the palate of male 6-8-week-old A. control and B: Stat6VT mice. C: Secondary-antibody alone control to show non-specific staining. The white dashed line demarcates the keratinized layer for landmarking purposes and representative CD45 positive cells are circled. Scale bar 20µm.

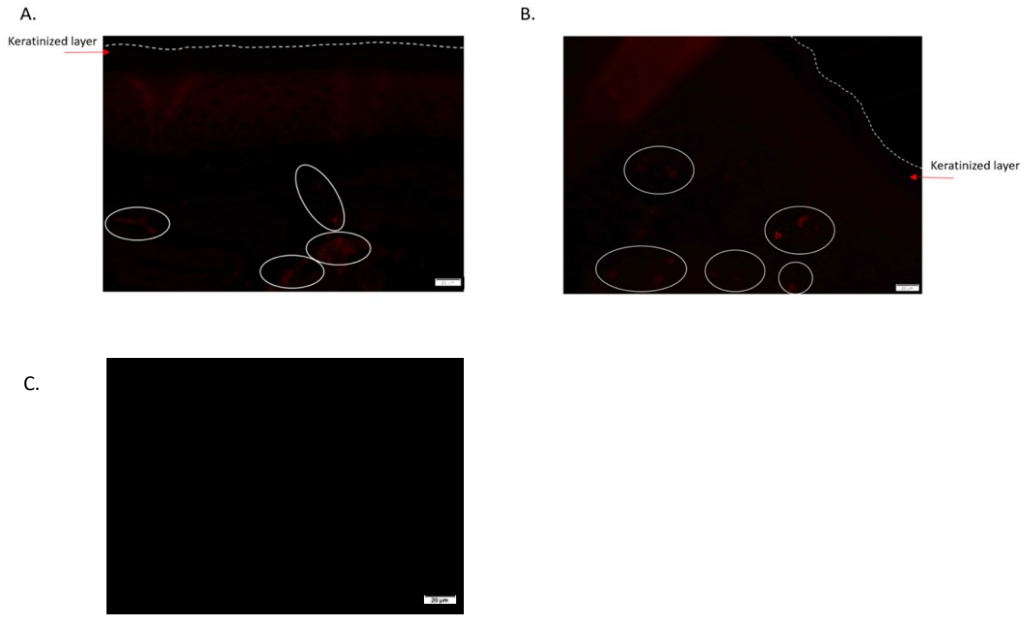

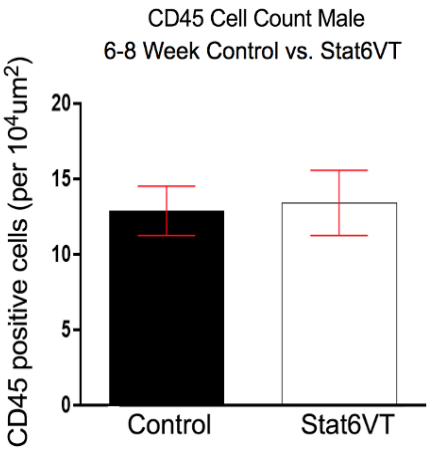

Figure 47. Cell count analysis of CD45 positive cells in the palate of male 6-8-week-old mice.

10-13-week time point. At 10-13-weeks of age, the palate of Stat6VT mice had more CD45 positive cells compared to controls, especially around the basal layer (Figure 48). This was confirmed by cell counts; Stat6VT mice had 19.08 ± 0.7432 CD45 positive cells, compared to the control group, which had 11.08 ± 1.654 CD45 positive cells (n=3/group, p= 0.0012) (Figure 49). These findings support the hypothesis that at disease onset in the skin, there is also increased inflammation in the epithelium of the oral cavity. They also support our H&E findings, in which

we observed increased numbers of rete pegs and clear cells, which are suggestive of inflammation.

Figure 48. CD45 positive cells in the palate of male 10-13-week-old A: control and B: Stat6VT mice. C: Secondary-antibody alone control to show non-specific staining. The white dashed line demarcates the top of the keratinized layer for landmarking purposes. Scale bar 20µm.

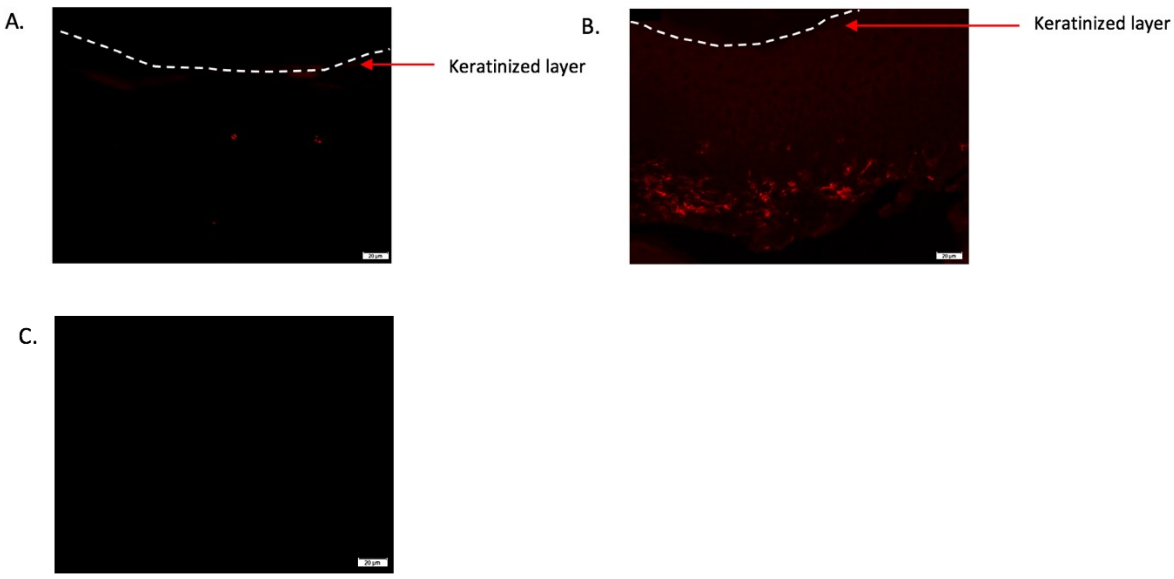

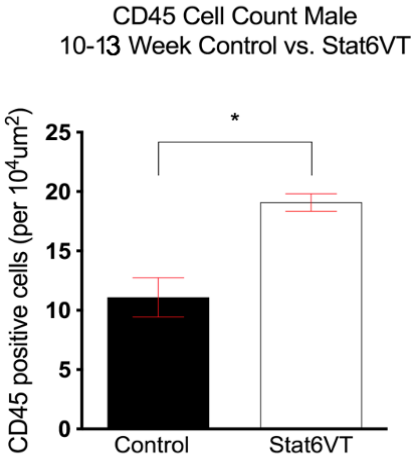

Figure 49. Cell count analysis of CD45 positive cells in male 10-13-week-old control and Stat6VT mice. *p=0.0012.

18-week time point. At 18 weeks of age, CD45 positive cells spanned across the basal, spinous and granular layers in the palates of both Stat6VT and control mice (Figure 50). There

was no significant difference, however, between the groups (CD45 positive cells: Stat6VT: 17.13 ± 2.912; control: 13.5 ± 0.4282, n=3/group, p=0.3096) (Figure 51).

Figure 50. CD45 positive cells in the palate of male 18-week-old A: Control and B: Stat6VT mice. C: Secondary-antibody alone control to show non-specific staining. The white dashed line demarcates the keratinized layer for landmarking purposes. Scale bar 20µm.

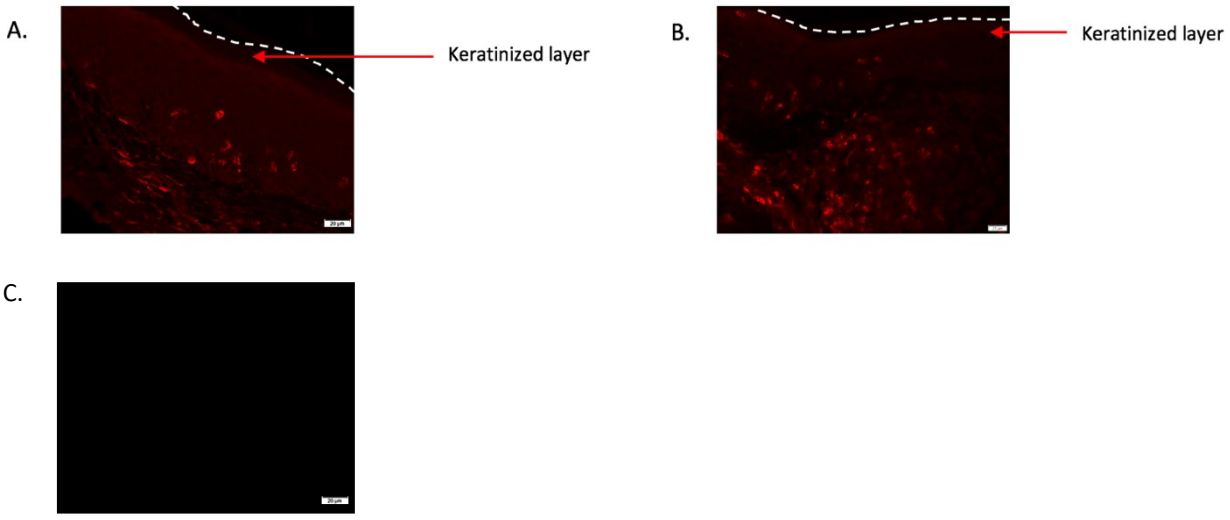

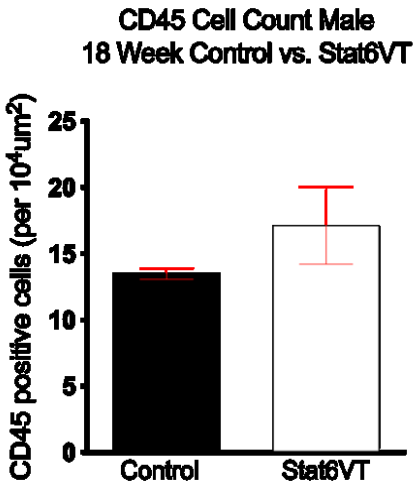

igure 51. Cell count analysis of CD45 positive cells in the alate of 18-week-old control and Stat6VT mice.

3.5.7 Ki67 immunofluorescence

6-8-week time point. The palate of 6-8-week-old male Stat6VT mice demonstrated greater expression of Ki67 compared to controls in the basal layer of the epithelium (Figure 52).

Cell counts confirmed these observations (Ki67 positive cells: control: 6.39 ± 0.4900; Stat6VT: 45.58 ± 5.552, n=3/group, p<0.0001) (Figure 53).

Figure 52. Ki67 positive cells in the palate of 6-8-week-old male A: control and B: Stat6VT mice. C: Secondary-antibody alone control to show non-specific staining. The white dashed line demarcates the basal layer for reference and representative Ki67 positive cells are circled. Scale bar 20µm.

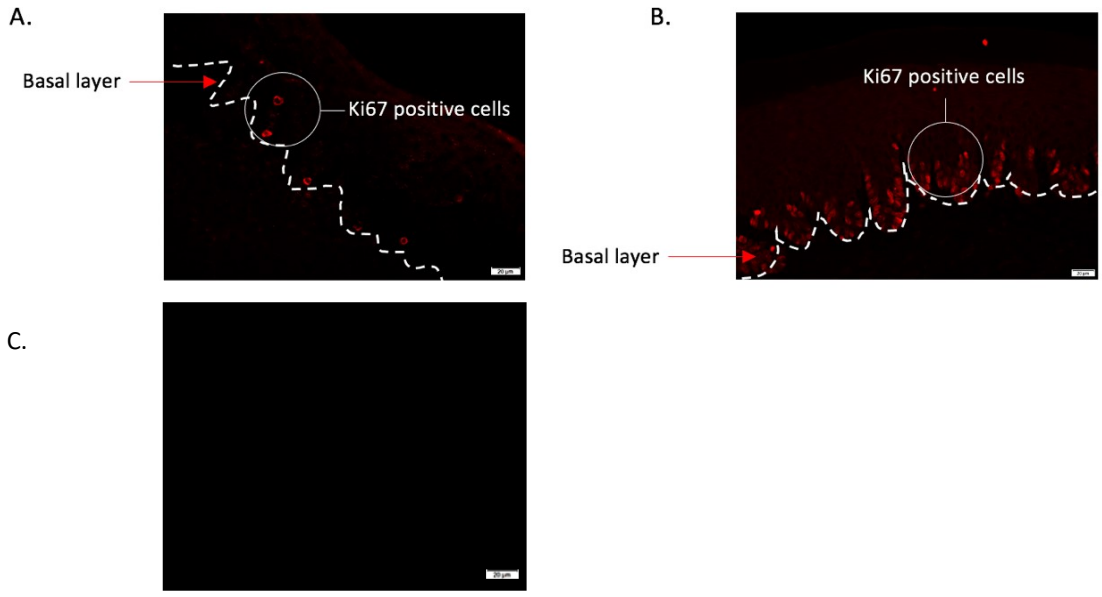

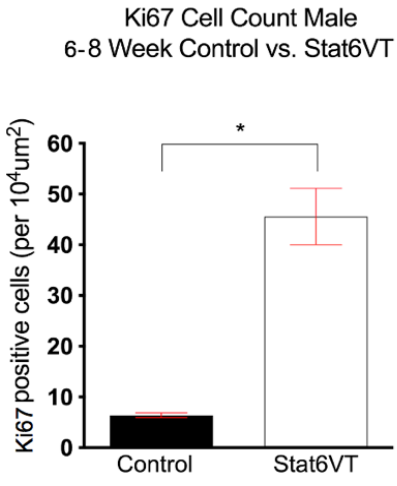

Figure 53. Cell count analysis of Ki67 positive cells in the palate of 6-8-week-old mice. *p<0.0001.

10-13-week time point. At 10-13 weeks of age, the palate of male Stat6VT mice had greater numbers of positive Ki67 cells in the basal layer in comparison to controls (Figure 55). Additionally, we noted greater clustering together of the Ki67 positive cells in the Stat6VT group (Figure 54). The cell count analysis confirmed these findings; there were significantly more Ki67 positive cells in the Stat6VT group compared to control (Ki67 positive cells: control: 29.57 ± 3.416; Stat6VT: 43.86 ± 3.420, n=3/group, p=0.0039). These findings support the H&E analysis, which showed greater numbers of basal cells and rete pegs. They are also in line with our hypothesis, that with (skin) disease onset, there would be increased inflammation.

Figure 54. Ki67 positive cells in the palate of 10-13-week-old male A: control and B: Stat6VT mice. C: Secondary-antibody alone control to show non-specific staining. The white dashed line demarcates the basal layer for reference. Scale bar 20µm.

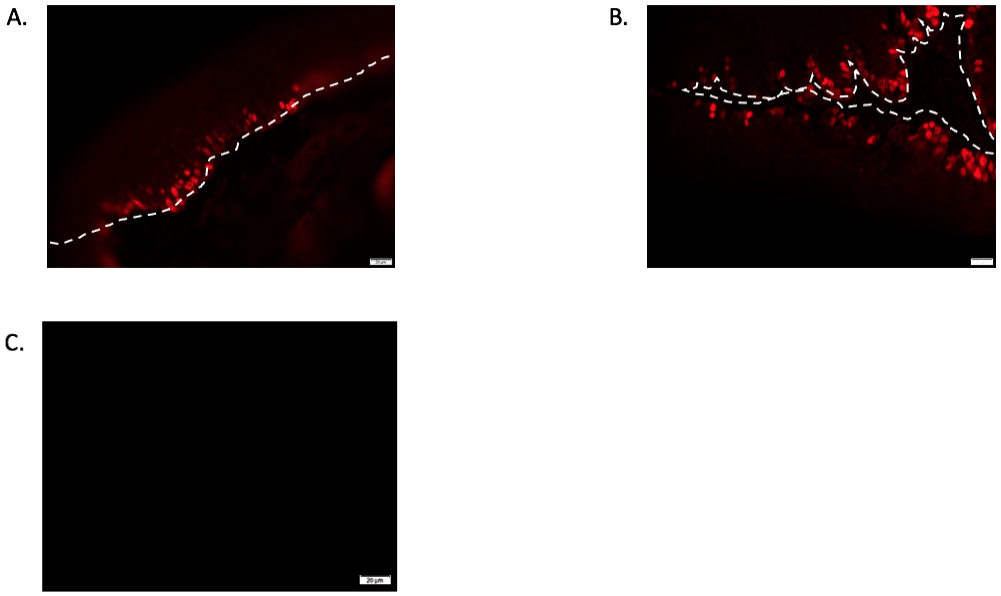

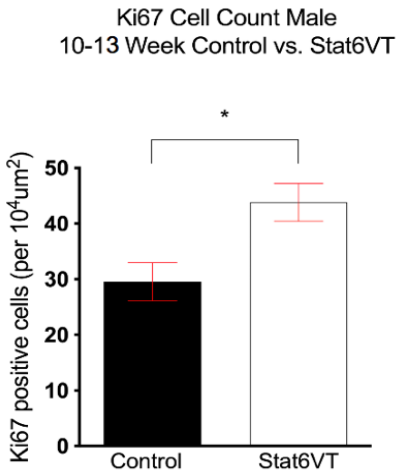

Figure 55. Cell count analysis of Ki67 positive cells in the palate of 10-13-week-old control vs Stat6VT mice. *p=0.0039.

18-week time point. At 18 weeks of age, we detected Ki67 positive cells mainly localized to the basal layer in both groups (Figure 56). Interestingly, we also observed Ki67 positive cells in the spinous layer in the Stat6VT mice. Cell count analysis revealed a significantly greater count of Ki67 positive cells in the Stat6VT group compared to controls (Figure 57). Stat6VT mice had 49.89 ± 2.273 Ki67 positive cells while controls had 32.83 ± 4.137 (n= 3/group, p=0.0189).

Figure 56. Ki67 positive cells in the palate of 18-week-old male A: control and B: Stat6VT mice. C: Secondary-antibody alone control to show non-specific staining. The white dashed line demarcates the basal layer for landmarking. The white circles in B. show Ki67 positive cells located in the spinous layer. Scale bar 20µm.

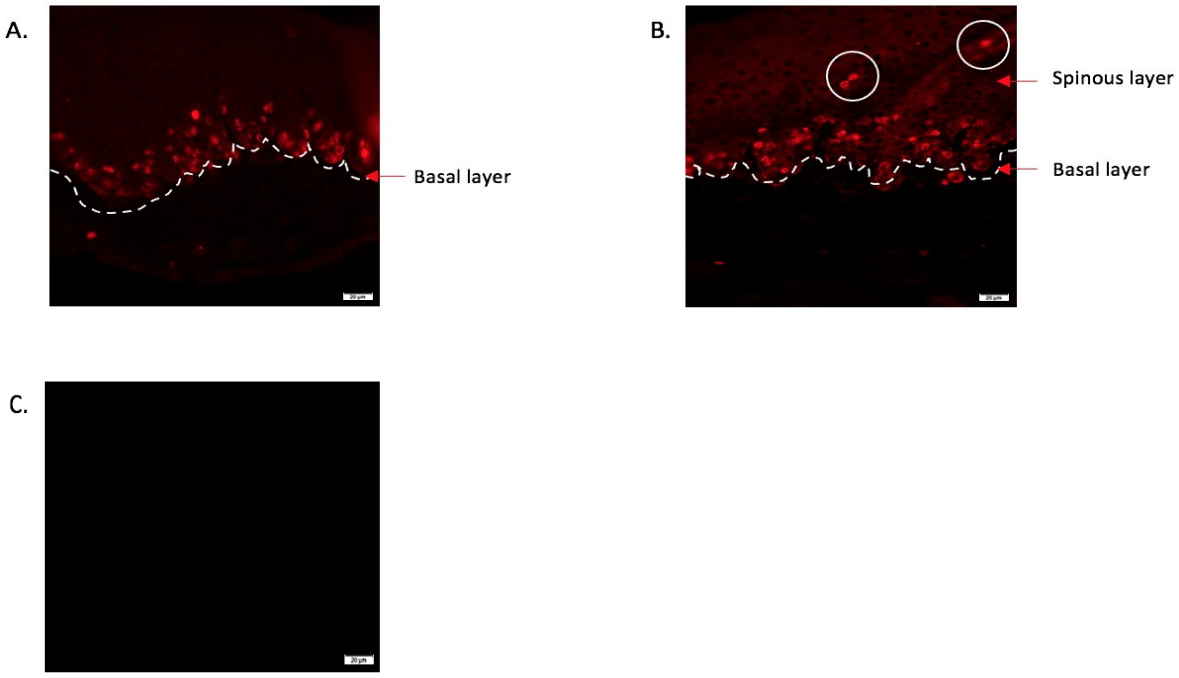

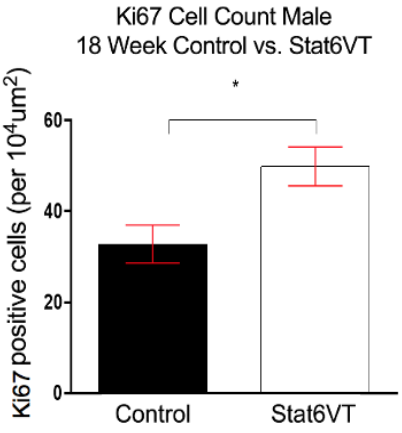

Figure 57. Cell count analysis of Ki67 positive cells in the palate of 18-week-old control and Stat6VT mice. *p= 0.0189.

3.5.8 CK1 immunofluorescence

6-8-week time point. At 6-8 weeks of age, the palate of male control and Stat6VT mice demonstrated similar expression of CK1 and somewhat similar distribution. CK1 positive cells were localized to the basal and granular layers (Figure 58). Expression in the granular layer cells appeared stronger in both groups. CK1 expression in the control group demonstrated a more

uniform appearance, as the positive cells were more evenly spaced across the layers, whereas in the Stat6VT mice, there were areas that appeared negative in the same layers.

Figure 58. CK1 expression in the palates of male 6-8-week-old A: control and B: Stat6VT mice. C: Secondary-antibody alone control to show non-specific staining. The white dashed line demarcates the basal layer for reference. Scale bar 20µm.

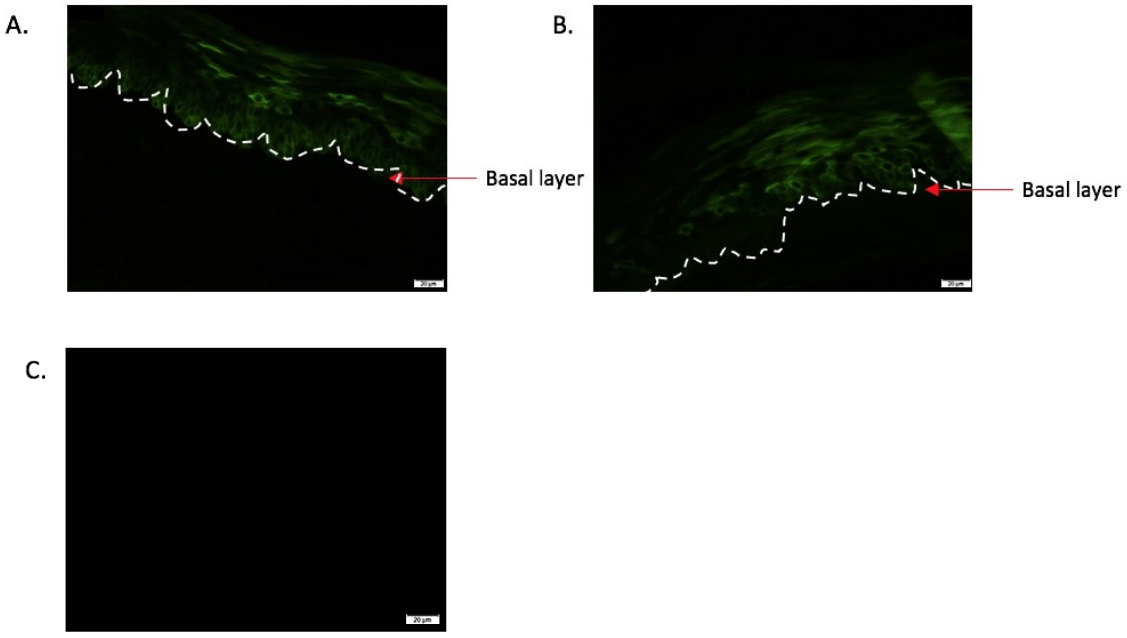

10-13-week time point. At 10-13 weeks of age, CK1 expression appeared to be stronger in the palate of Stat6VT mice compared to controls, as evidenced by the greater number of cells stained and brighter staining (Figure 59). Both groups demonstrated CK1 expression in the basal and granular layers. We found more heterogeneity amongst the samples and we are doing further study to determine if this antigen is more sensitive to fixation time. Nonetheless, Stat6VT mice demonstrated much more pronounced positivity in CK1 expression in the basal layer compared to controls.

Figure 59. CK1 expression in the palates of male 10-13-week-old A: control and B: Stat6VT mice. C: Secondary-antibody alone control to show non-specific staining. The white dashed line demarcates the basal layer for reference. Scale bar 20µm.

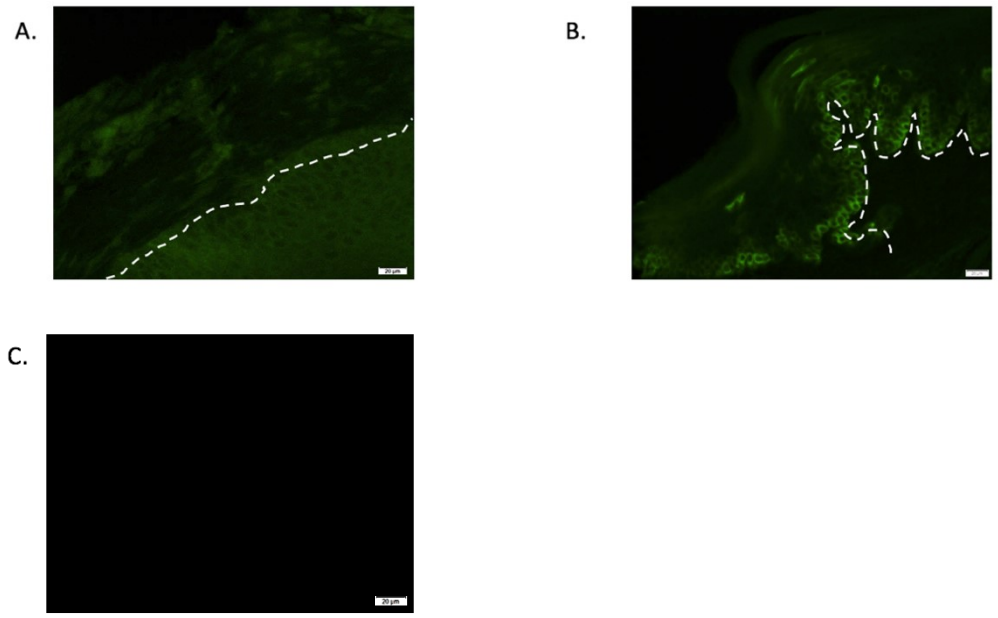

18-week time point. At 18 weeks of age, the palate of control mice showed a greater degree of positive CK1 staining in the granular layer, although the basal layer showed some low-level positivity. In contrast, the palate of the Stat6VT mice had greater fluorescence in the basal layer compared to control, and less intensity in the cells of the granular layer (Figure 60).

Figure 60. CK1 expression in the palates of male 18-week-old A: control and B: Stat6VT mice. C: Secondary-antibody alone control to show non-specific staining. The white dashed line demarcates the keratinized layer for landmarking purposes. Scale bar 20µm.

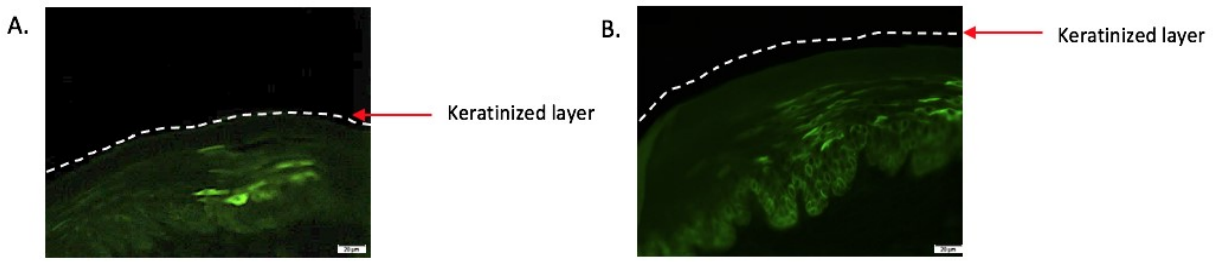

C.

3.5.9 CK14 immunofluorescence

6-8-week time point. At 6-8-weeks of age, control and Stat6VT mice demonstrated comparable CK14 expression localized to the basal layer as we expected for our baseline (Figure 61).

Figure 61. CK14 expression in the palates of 6-8-week-old male A: control and B: Stat6VT mice. C: Secondary-antibody alone control to show non-specific staining. The basal layer is identified for reference. Scale bar 20µm.

A.

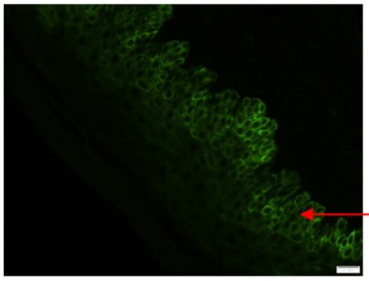

B.

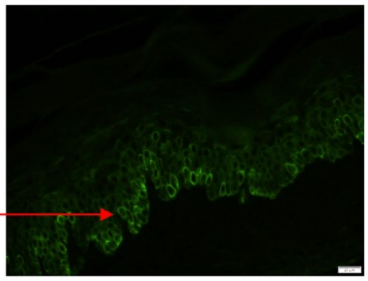

C.

10-13-week time point. At 10-13 weeks of age, CK14 was localized to the basal layer of the palate in both Stat6VT and control mice (Figure 62), and expression was of similar intensity.

However, the Stat6VT group had more layers of basal cells that were CK14 positive. These findings are consistent with the previous observations made for the H&E staining and Ki67 cell counts.

Figure 62. CK14 expression in the palates of 10-13-week-old male A: control and B: Stat6VT mice. C: Secondary-antibody alone control to show non-specific staining. The basal layer is identified for reference. Scale bar 20µm.

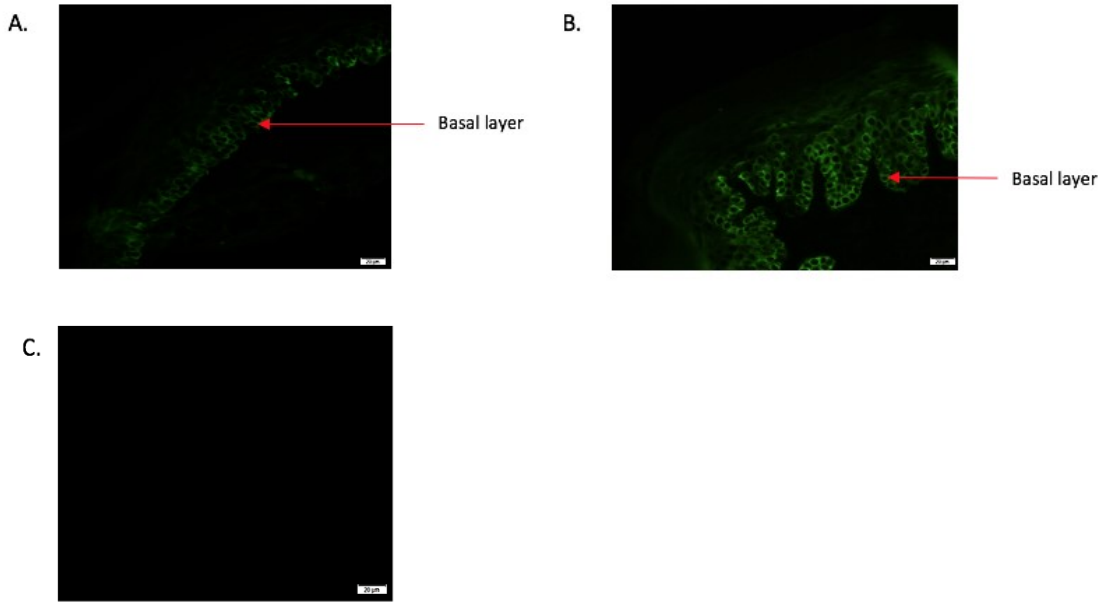

18-week time point. At 18 weeks of age, CK14 was localized to the basal layer of the palate in the control group, however, in the Stat6VT group, CK14 was detected also in cells in the spinous layer (Figure 63). Recall that we observed Ki67 expression in cells of the spinous layer in 18-week-old Stat6VT mice as well. These results suggest that Stat6VT mice may have greater inflammation compared with controls, which potentially may impact the normal differentiation of the oral epithelium.

Figure 63. CK14 expression in the palates of 18-week-old male A: control and B: Stat6VT mice. C: Secondary-antibody alone control to show non-specific staining. The basal and spinous layers are identified. Scale bar 20µm.

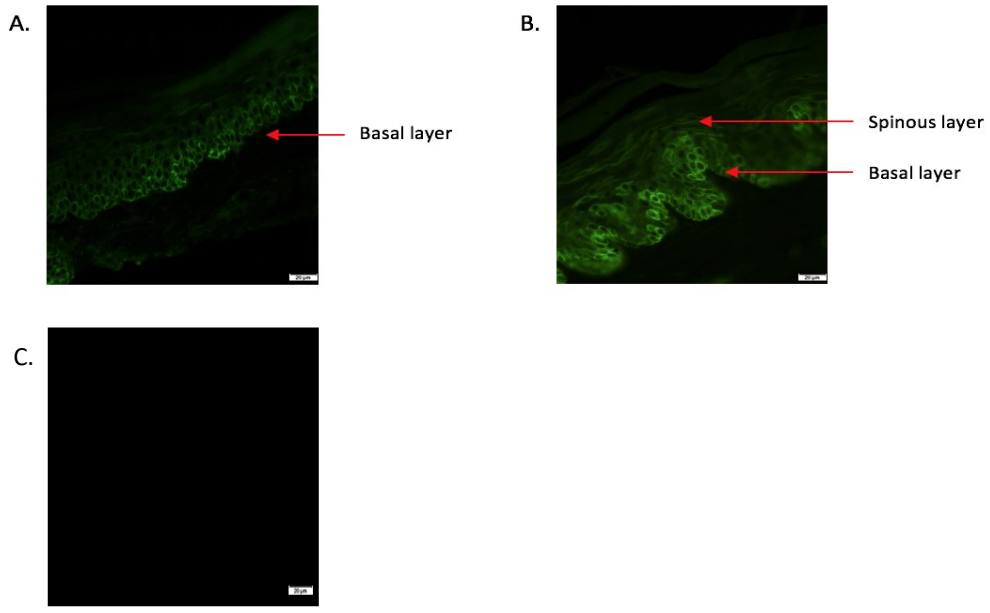

3.6 ELISA did not reveal any differences in mouse loricrin protein content at 10-13- and 18-week

We analyzed gingival samples collected from male Stat6VT and control mice from each age group (6-8 weeks, 10-13 weeks and 18 weeks of age). Gingival tissue samples were pooled from 3 mice within the same group. Once again, Dr. Catunda assisted with the experiment and data analysis. There was no difference in mouse loricrin protein content comparing Stat6VT with control at aged 10-13 weeks or 18 weeks. We found that control mice had greater loricrin protein content at 6-8 weeks of age (control: 0.0006215 ± 0.0001491 vs. Stat6VT: 0.00016 ± 0.00004295 pg loricrin/ug protein; p= 0.0140) (Figure 64), however, this data is inconsistent with our immunofluorescent data. There are several reasons we question the validity of our loricrin ELISA data, which will be discussed in the "Discussion" section of my thesis.

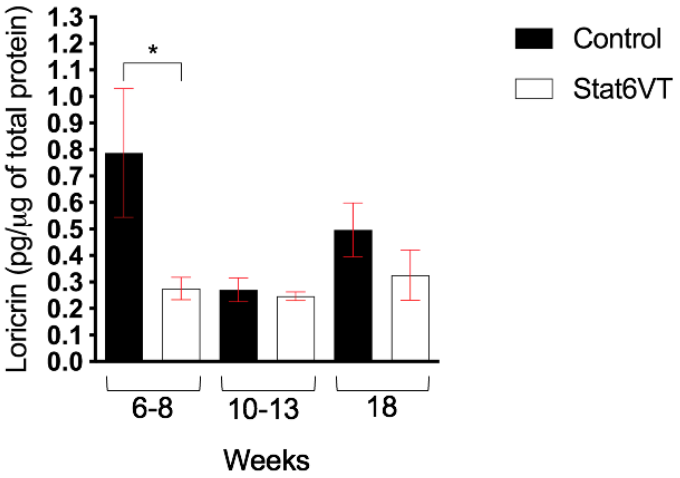

Figure 64. ELISA of male control vs. Stat6VT gingiva across age groups. *p=0.0140.

3.7 Plasma cytokine profiling revealed 5 cytokines significantly increased in 10-13-week-old male Stat6VT mice compared to controls

A cytokine array was performed on plasma collected from 10-13-week-old male Stat6VT and control mice (QAM-INF-1, Mouse Inflammation Array 1, RayBiotech). This experiment was performed by Sara Moradipoor and analyzed by Dr. Maria Febbraio. The following cytokines were found to be significantly increased in the Stat6VT mice compared to controls: Cluster of Differentiation 30 Ligand (CD30L), Eotaxin 2 or also known as C-C Motif Chemokine Ligand 24 (CCL24), Monocyte Chemotactic Protein 5 (MCP5), Monokine Induced Gamma Interferon (MIG) or also known as C-X-C motif Ligand 9 (CXCL9), and B Lymphocyte Chemoattractant (BLC) or also known as C-X-C motif Ligand 13 (CXCL13). Additionally, there were no cytokines that had a decreased expression greater than 1-fold in the 10-13-week male Stat6VT vs. control mice. Table 6 is a table of the cytokines found to have a significant difference, the mean ± SEM and their p-value.

Table 6. Plasma cytokine array results of the 10-13-week male control vs. Stat6VT mice

Cytokine	Control Mean ± SEM	Stat6VT Mean ± SEM	p-value

CD30L	123.8 ± 29.72	324.0 ± 60.33	0.0248
Eotaxin2 (CCL24)	87.64 ± 18.88	398.6 ± 166.3	0.003, Mann-Whitney
MCP5	18.69 ± 3.512	77.41 ± 16.1	0.0031
MIG (CXCL9)	99.26 ± 30.45	363.5 ± 71.83	0.0044
BLC (CXCL13)	214.3 ± 64.36	849.5 ± 250.1	0.0275

CHAPTER 4: PG STUDY RESULTS

4.1 Oral infection with *Pg* was performed on 10-13-week-old male and female mice

In order to create a model of periodontal disease, *Pg* bacteria (ATCC #33277), were used for infection. This strain is commonly used in the literature for periodontal research and is known to have a strong ability to adhere to the host tissue; it is the most common strain isolated from human adults with periodontal disease (Amano *et al*., 1999; Zheng *et al*., 2011). Bacteria were grown by Dr. Catunda and *Pg* infection was assisted by Dr. Febbraio. Mice were orally infected with *Pg* using a micro brush to instill bacteria (~$2x10^9$) around the molars every other day for 2 weeks. These studies were carried out in a level 2 biocontainment facility. Two weeks after the last oral infection of bacteria, mice were euthanized.

We used male and female mice at 10-13-weeks of age for this study because the longitudinal study demonstrated consistent skin lesion onset at this time point. Based on our previous study involving different strains of mice (but all on the C57Bl/6j background), we performed a power calculation to determine group size and enrolled 11 mice/group to obtain 80% power with alpha = 0.05. Due to some complications with injections, the final numbers of mice that completed the study are as follows: Males: 11 control and 7 Stat6VT; Females: 9 control and 8 Stat6VT. When we recalculated power based on bone loss (see microCT results), we found that for males, n=6-11 would provide appropriate power, depending on the site. The females had greater standard deviations, and that means the *Pg* study was underpowered. We show the data from females for the microCT analysis, but omit further data for females from the *Pg* study. That data can be used for the design of subsequent studies.

4.2 *Pg*-infected and control mice did not show phenotypical differences

Similar to the observations noted in the longitudinal study, 10-13-week male and female mice demonstrated varying degrees of atypical findings at the study start and 2 weeks later at study end. All Stat6VT positive mice had mild to moderate scaly edema around the border of the eyes and erythema of the ears as a result of scratching due to pruritus. Some had loss of fur behind the ears from pruritus as well. At the gross phenotypical level, however, the oral cavity did not show any atypical findings before nor after *Pg* infection.

4.3 MicroCT analysis revealed significantly reduced alveolar bone levels in *Pg*-infected Stat6VT mice compared to controls

The same examiners, protocol and approach that was taken to achieve the microCT results in the longitudinal study were repeated in the *Pg* study. Male and female mice after infection were utilized for microCT analysis. Male and female CEJ-ABC and alveolar bone height measurements were analyzed by comparing: *Pg*-infected Stat6VT to *Pg*-infected controls, *Pg*-infected controls to uninfected controls, and *Pg*-infected Stat6VT to uninfected Stat6VT mice.

4.3.1 Results for females

Pg-infected controls versus uninfected controls. There were no significant differences found in any of the planes when *Pg*-infected controls were compared to uninfected controls (Figures 65, 66, 67).

Figure 65. MicroCT measurements of female *Pg*-infected and uninfected controls on the buccal aspect of the coronal plane. CEJ-ABC measurements of the A: first molar and B: second molar taken on the coronal plane (buccal aspect), and the alveolar bone height of the C: first molar and D: second molar taken on the coronal plane (buccal aspect).

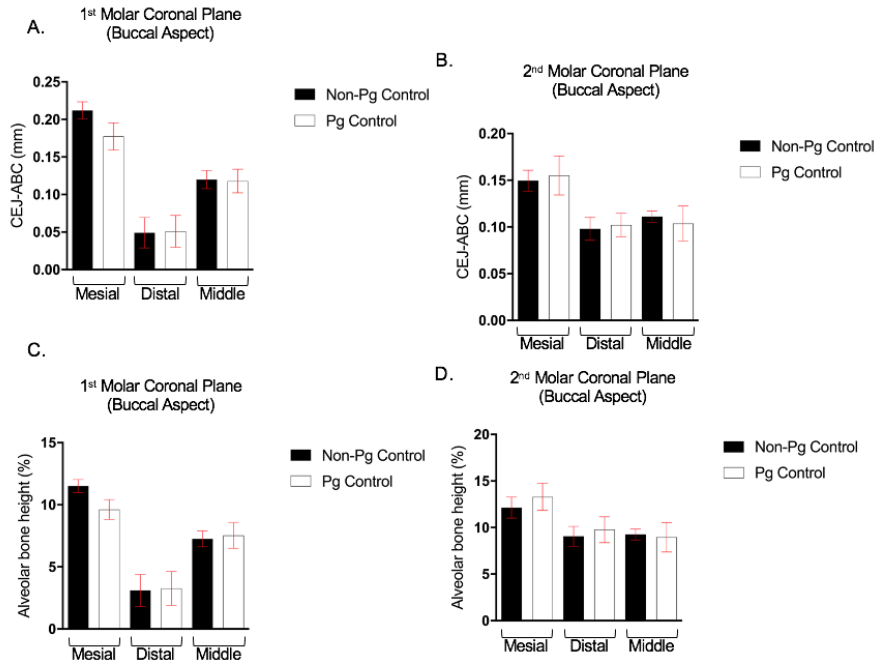

Figure 66. MicroCT measurements of female *Pg*-infected and uninfected controls on the lingual aspect of the coronal plane. CEJ-ABC measurements of the A: first molar and B: second molar taken on the coronal plane (lingual aspect), and the alveolar bone height of the C: first molar and D: second molar taken on the coronal plane (lingual aspect).

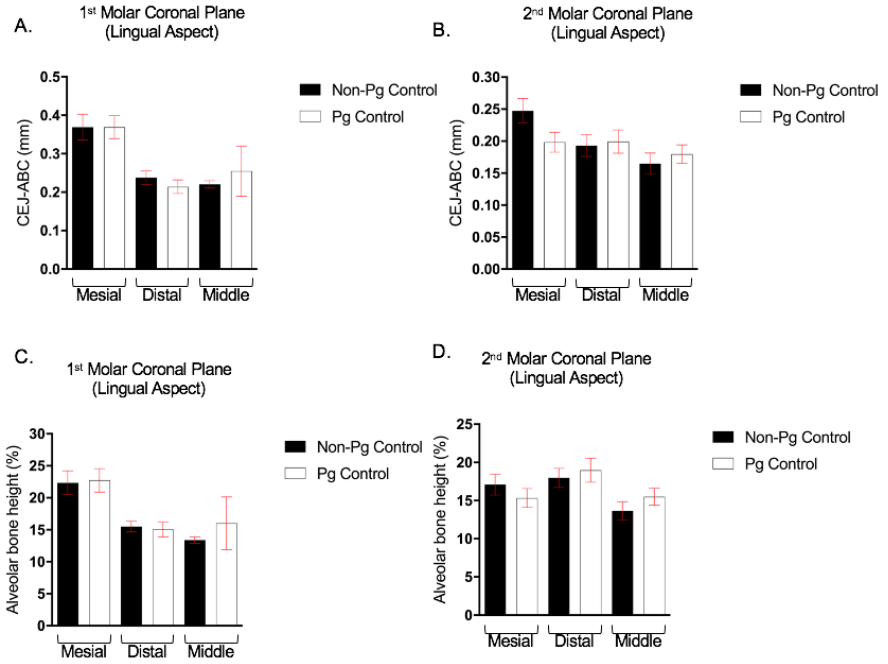

Figure 67. MicroCT measurements of female *Pg*-infected uninfected controls on the sagittal plane. CEJ-ABC measurements of the A: first molar and B: second molar taken on the sagittal plane, and the alveolar bone height of the C: first molar and D: second molar taken on the sagittal plane.

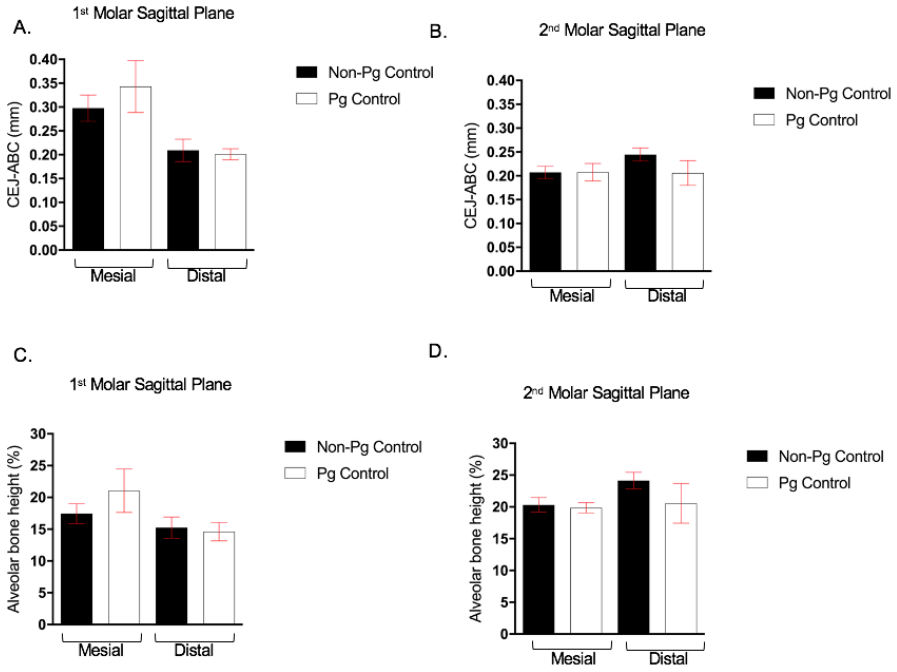

Pg-infected Stat6VT versus Pg-infected controls. Female *Pg*-infected Stat6VT mice when compared to *Pg*-infected controls demonstrated greater CEJ-ABC measurements in 2 sites on the first molar (Figures 69A and 70A) and 1 site on the second molar (Figure 69B). The 2 sites on the first molar were CEJD-ABCL (41 ± 0.01778 vs. 0.2906 ± 0.02152, p=0.0278) and CEJD-ABC (0.2007 ± 0.01165 vs. 0.2579 ± 0.01647, p=0.0224). The site on the second molar was CEJM-ABCL (0.1983 ± 0.01561 vs. 0.2810 ± 0.02902, p=0.0322). Furthermore, 3 sites demonstrated greater reduction of alveolar bone height in the Stat6VT mice compared to controls (Figures 69C, 70C, and 70D). 2 of these sites were found on the first molar, which were CEJD-ABCL (15.05 ± 1.174 vs. 20.88 ± 1.743, p=0.0239) and CEJD-ABC (14.60 ± 1.430 vs. 20.15 ± 1.636, p=0.0375). The last site was found on the second molar CEJM-ABC (19.86 ± 0.7959 vs.

25.82 ± 2.457, p=0.0383). The coronal plane on the buccal aspect did not demonstrate any significant differences for either CEJ-ABC nor alveolar bone height measurements (Figure 68).

Figure 68. MicroCT measurements of female *Pg*-infected Stat6VT and *Pg*-infected controls on the buccal aspect of the coronal plane. CEJ-ABC measurements of the A: first molar and B: second molar taken on the coronal plane (buccal aspect), and the alveolar bone height of the C: first molar and D: second molar taken on the coronal plane (buccal aspect).

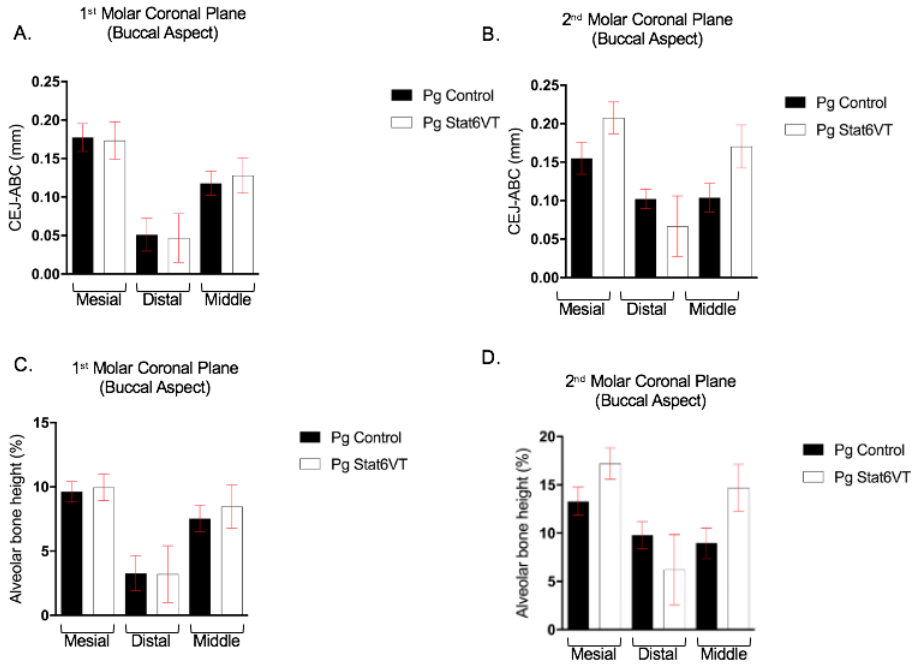

Figure 69. MicroCT measurements of female *Pg*-infected Stat6VT and *Pg*-infected controls on the lingual aspect of the coronal plane. CEJ-ABC measurements of the A: first molar and B: second molar taken on the coronal plane (lingual aspect), and the alveolar bone height of the C: first molar and D: second molar taken on the coronal plane (lingual aspect). *p<0.05.

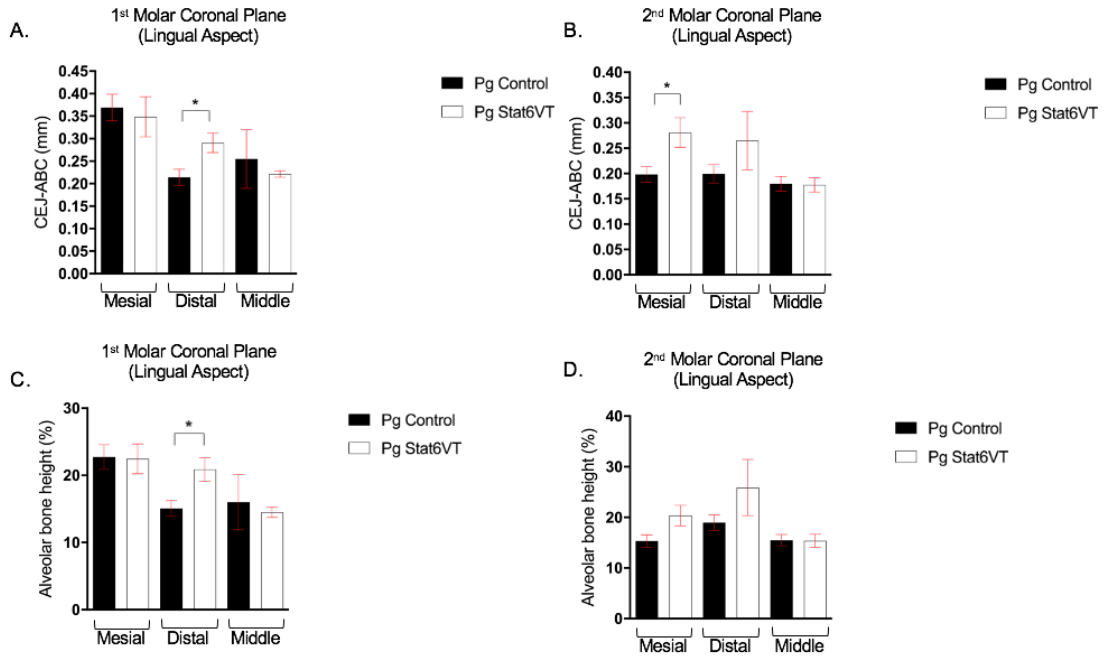

Figure 70. MicroCT measurements of female *Pg*-infected Stat6VT and *Pg*-infected controls on the sagittal plane. CEJ-ABC measurements of the A: first molar and B: second molar taken on the sagittal plane, and the alveolar bone height of the C: first molar and D: second molar taken on the sagittal plane. *p<0.05.

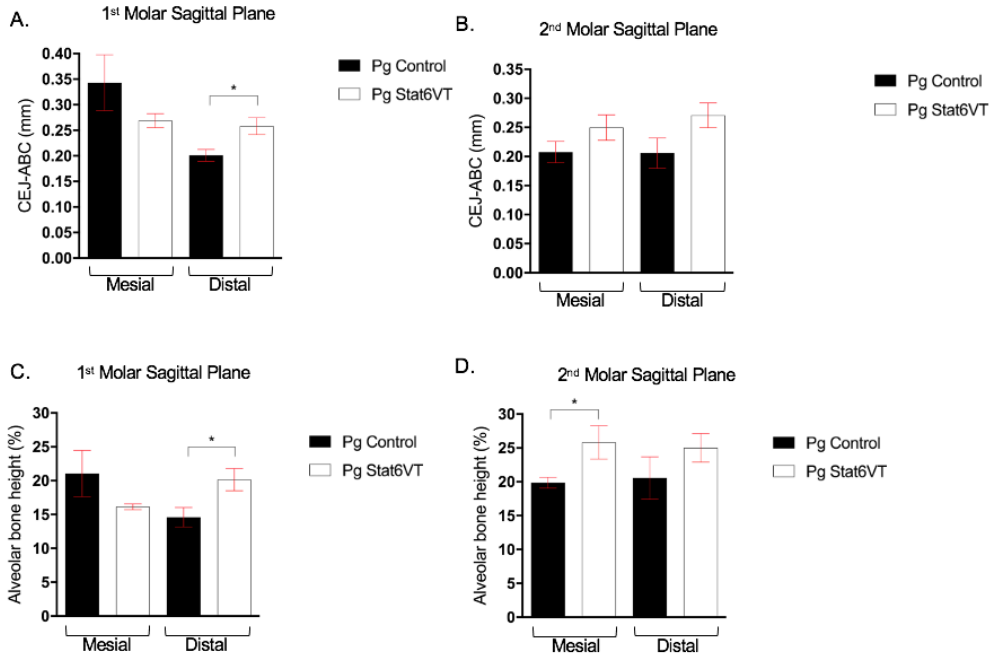

Pg-infected Stat6VT versus uninfected Stat6VT. Female Pg-infected Stat6VT when compared to uninfected Stat6VT had 1 site that demonstrated a significantly greater CEJ-ABC measurement (Figure 72B). This site was the CEJM-ABCL on the first molar (0.2022 ± 0.008553 vs. 0.2704 ± 0.02483, p=0.0317). There were no significant differences found on the buccal aspect of the coronal plane and the sagittal plane for either CEJ-ABC and alveolar bone height measurements (Figures 71 and 73).

These findings seem to align with the findings gathered in the longitudinal study. When 10-13-week uninfected female Stat6VT mice were compared to uninfected female controls, the CEJ-ABC measurements on the lingual aspect of the coronal plane also did not demonstrate any significant findings. The inconsistencies seen in the female group findings as compared to the findings in the male groups may be a result of hormonal and physiological differences.

Figure 71. MicroCT measurements of female *Pg*-infected Stat6VT and uninfected Stat6VT on the buccal aspect of the coronal plane. CEJ-ABC measurements of the A: first molar and B: second molar taken on the coronal plane (buccal aspect), and the alveolar bone height of the C: first molar and D: second molar taken on the coronal plane (buccal aspect).

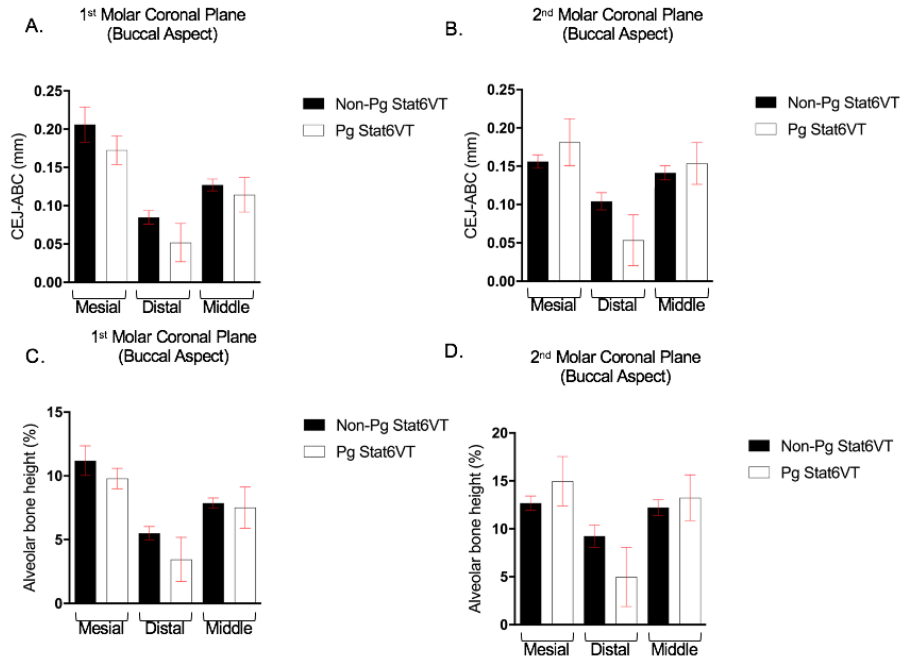

Figure 72. MicroCT measurements of female *Pg*-infected Stat6VT and uninfected Stat6VT on the lingual aspect of the coronal plane. CEJ-ABC measurements of the A: first molar and B: second molar taken on the coronal plane (lingual aspect), and the alveolar bone height of the C: first molar and D: second molar taken on the coronal plane (lingual aspect).

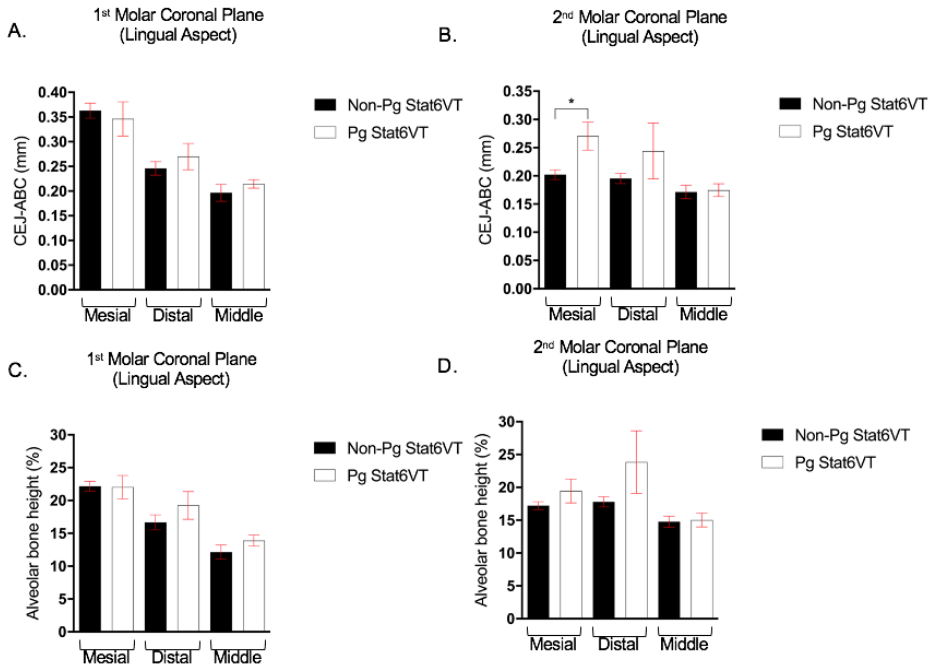

Figure 73. MicroCT measurements of female *Pg*-infected Stat6VT and uninfected Stat6VT on the sagittal plane. CEJ-ABC measurements of the A: first molar and B: second molar taken on the sagittal plane, and the alveolar bone height of the C: first molar and D: second molar taken on the sagittal plane.

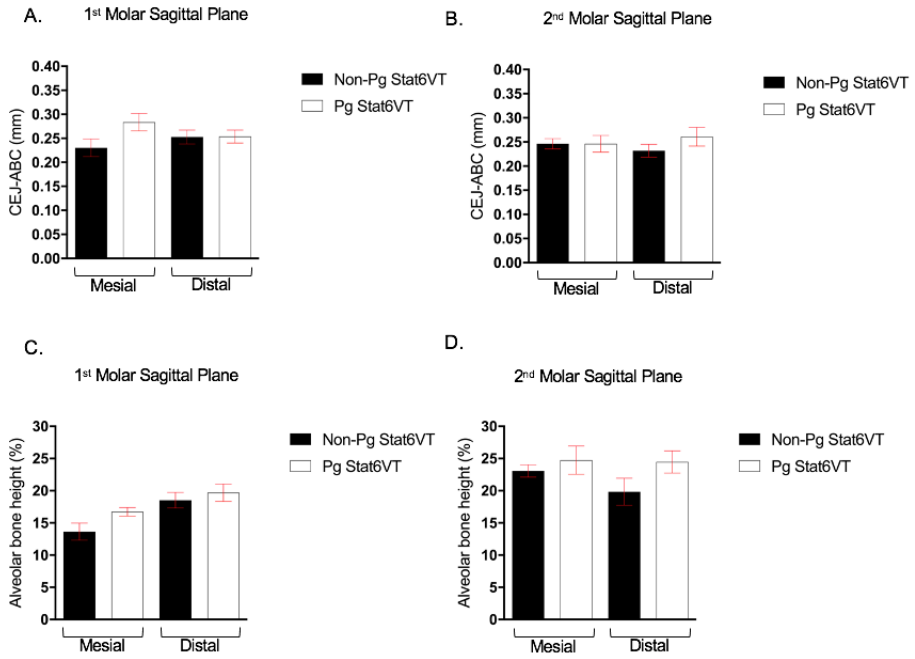

4.3.2 Results for males

Pg-infected controls versus uninfected controls. *Pg*-infected controls when compared to uninfected controls demonstrated 1 site that had a greater CEJ-ABC measurement on each molar (Figures 75A and 75B). The site on both molars was CEJM-ABCL (first molar: 0.2833 ± 0.03406 vs. 0.3034 ± 0.01190, p=0.0130. Second molar: 0.1626 ± 0.007351 vs. 0.2050 ± 0.01645, p=0.0464). Additionally, *Pg*-infected controls compared to uninfected controls demonstrated a greater loss of alveolar bone height in 3 sites on the second molar (Figures 75D and 76D), which were CEJMid-ABCL (17.87 ± 1.005 vs. 13.43 ± 1.385, p=0.0320), CEJM-ABC (12.26 ± 1.848 vs. 19.67 ± 1.995, p=0.0260) and CEJD-ABC (22.82 ± 0.2401 vs. 20.68 ± 1.593, p=0.0147). The buccal aspect of the coronal plane did not show any significant differences for

neither CEJ-ABC nor alveolar bone height readings (Figure 74). Overall, the reduction in alveolar bone levels seen in the *Pg*-infected controls versus the uninfected controls suggests that periodontal infection in male mice was achieved.

Figure 74. MicroCT measurements of male *Pg*-infected and uninfected controls on the buccal aspect of the coronal plane. CEJ-ABC measurements of the A: first molar and B: second molar taken on the coronal plane (buccal aspect), and the alveolar bone height of the C: first molar and D: second molar taken on the coronal plane (buccal aspect).

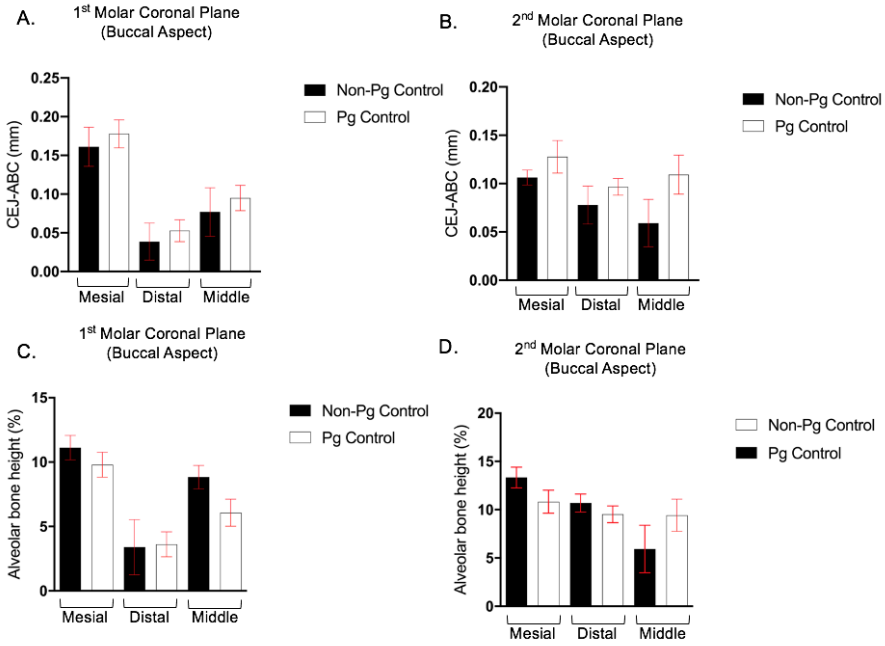

Figure 75. MicroCT measurements of male *Pg*-infected and uninfected controls on the lingual aspect of the coronal plane. CEJ-ABC measurements of the A: first molar and B: second molar taken on the coronal plane (lingual aspect), and the alveolar bone height of the C: first molar and D: second molar taken on the coronal plane (lingual aspect). *$p<0.05$.

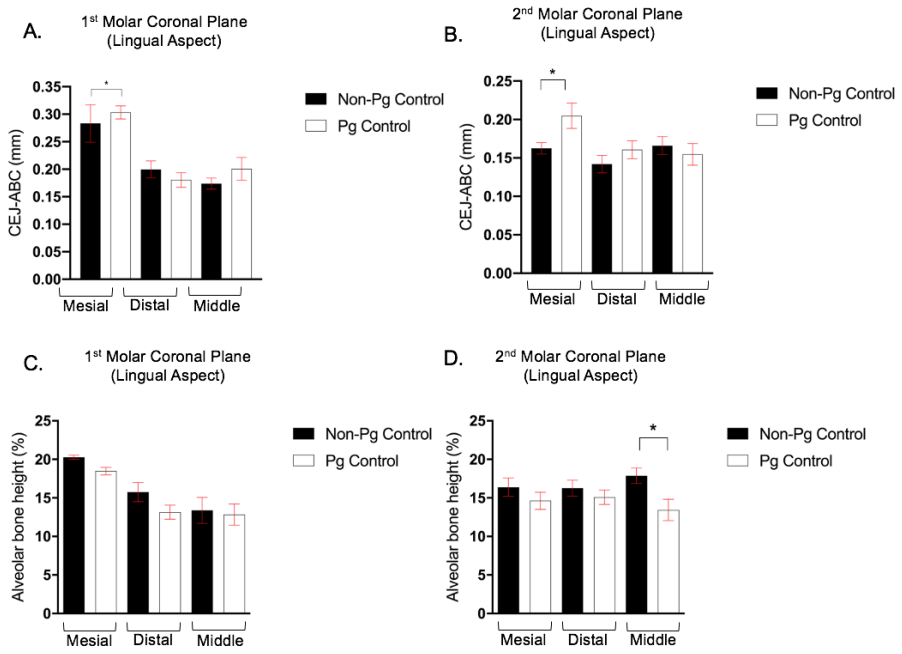

Figure 76. MicroCT measurements of male *Pg*-infected and uninfected controls on the sagittal plane. CEJ-ABC measurements of the A: first molar and B: second molar taken on the sagittal plane, and the alveolar bone height of the C: first molar and D: second molar taken on the sagittal plane. *p<0.05.

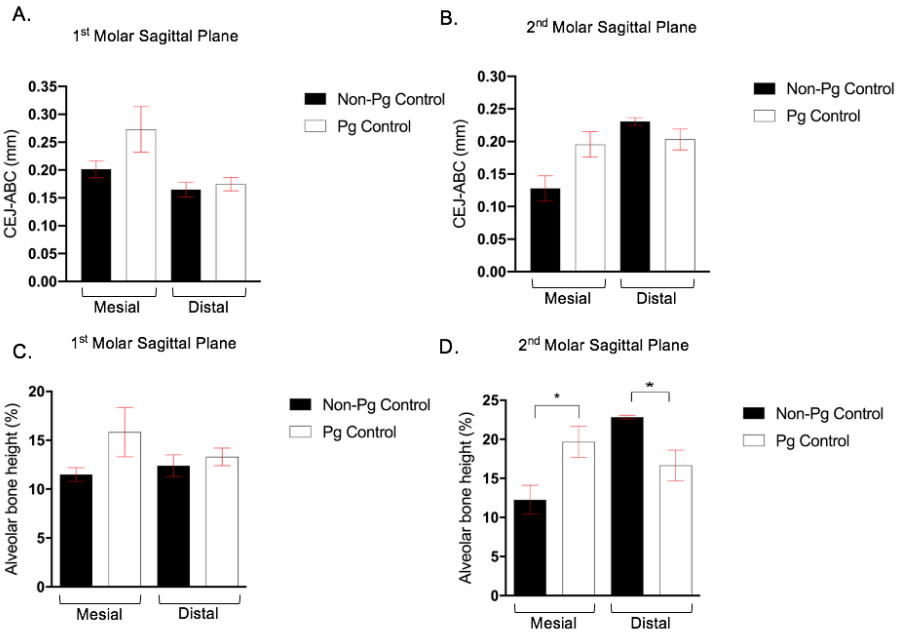

Pg-infected Stat6VT versus Pg-infected controls. *Pg*-infected Stat6VT male mice when compared to *Pg*-infected controls demonstrated 3 sites that had a greater CEJ-ABC measurements on the first molar (Figures 77A, 78A and 79A) and 6 sites that had a greater CEJ-ABC measurements on the second molar (Figures 77B, 78B and 79B). The sites on the first molar were as follows: CEJMid-ABCB (0.09496 ± 0.01630 vs. 0.1661 ± 0.02439, p=0.0145), CEJD-ABCL (0.1806 ± 0.01328 vs. 0.2386 ± 0.01258, p=0.0132), and CEJD-ABC (0.1747 ± 0.01201 vs. 0.2247 ± 0.01638, p=0.0391). The sites on the second molar were: CEJM-ABCB (0.1278 ± 0.01685 vs. 0.1699 ± 0.006931, p=0.0494), CEJD-ABCB (0.09655 ± 0.008621 vs. 0.1395 ± 0.009256, 0.0094), CEJD-ABCL (0.1607 ± 0.01166 vs. 0.2282 ± 0.01048, p=0.0026), CEJMid-ABCL (47 ± 0.01413 vs. 0.1954 ± 0.01026, p=0.0480), CEJM-ABC (0.1954 ± 0.01947 vs. 0.3008 ± 0.05744, p=0.0317, and CEJD-ABC (0.1636 ± 0.02007 vs. 0.2958 ± 0.02889, p=0.0159). Furthermore, *Pg*-infected Stat6VT mice demonstrated a greater loss of alveolar bone height when compared to *Pg*-infected controls in 3 sites on the first molar (Figures 77C and 78C) and 6 sites on the second molar (Figures 77D, 78D and 79D). The sites on the first molar were: CEJMid-ABCB (6.068 ± 1.046 vs. 10.89 ± 1.728, p=0.0439), CEJM-ABCL (18.48 ± 0.4873 vs. 22.84 ± 1.177, p=0.0091) and CEJD-ABCL (13.15 ± 0.9140 vs. 17.83 ± 1.212, p=0.0151). The sites on the second molar were: CEJM-ABCB (10.83 ± 1.194 vs. 14.70 ± 0.7812, p=0.0265), CEJD-ABCB (9.522 ± 0.8637 vs. 13.09 ± 0.9124, p=0.0218), CEJM-ABCL (14.63 ± 1.120 vs. 19.87 ± 1.333, p=0.0169), CEJD-ABCL (15.10 ± 0.9325 vs. 21.82 ± 1.151, p=0.0019), CEJMid-ABCL (13.42 ± 1.385 vs. 17.77 ± 0.6561, p=0.0221), and CEJD-ABC (16.65 ± 1.978 vs. 29.63 ± 2.824, p=0.0055).

Figure 77. MicroCT measurements of male *Pg*-infected Stat6VT and *Pg*-infected controls on the buccal aspect of the coronal plane. CEJ-ABC measurements of the A: first molar and B: second

molar taken on the coronal plane (buccal aspect), and the alveolar bone height of the C: first molar and D: second molar taken on the coronal plane (buccal aspect). *p<0.05.

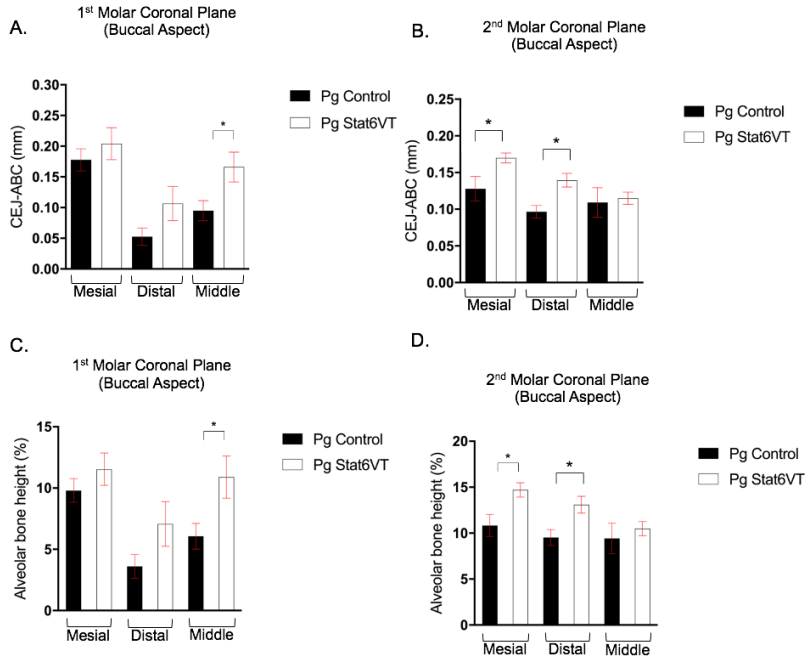

Figure 78. MicroCT measurements of male *Pg*-infected Stat6VT and *Pg*-infected controls on the lingual aspect of the coronal plane. CEJ-ABC measurements of the A: first molar and B: second molar taken on the coronal plane (lingual aspect), and the alveolar bone height of the C: first molar and D: second molar taken on the coronal plane (lingual aspect). *p<0.05.

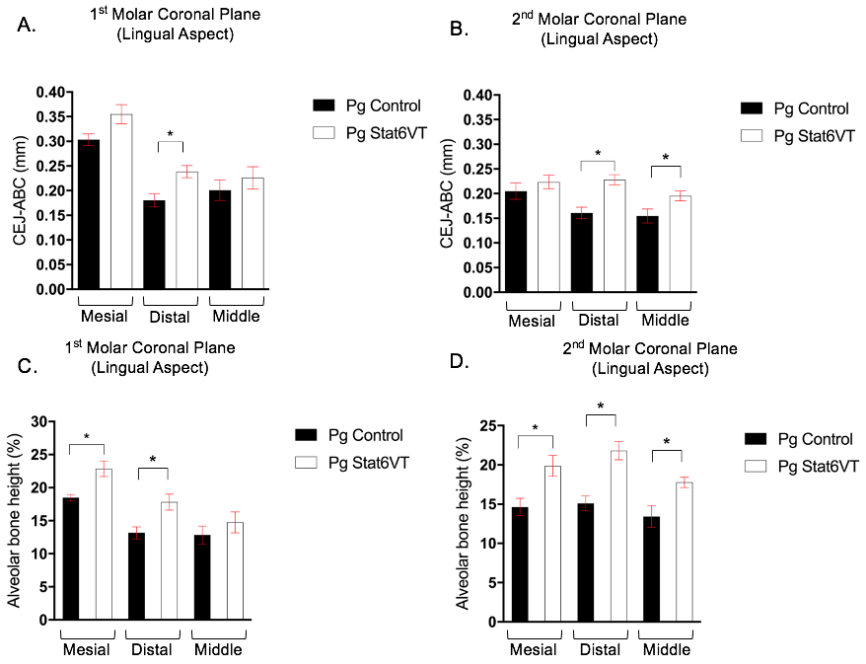

Figure 79. MicroCT measurements of male *Pg*-infected Stat6VT and *Pg*-infected control on the sagittal plane. CEJ-ABC measurements of the A: first molar and B: second molar taken on the sagittal plane, and the alveolar bone height of the C: first molar and D: second molar taken on the sagittal plane. *p<0.05.

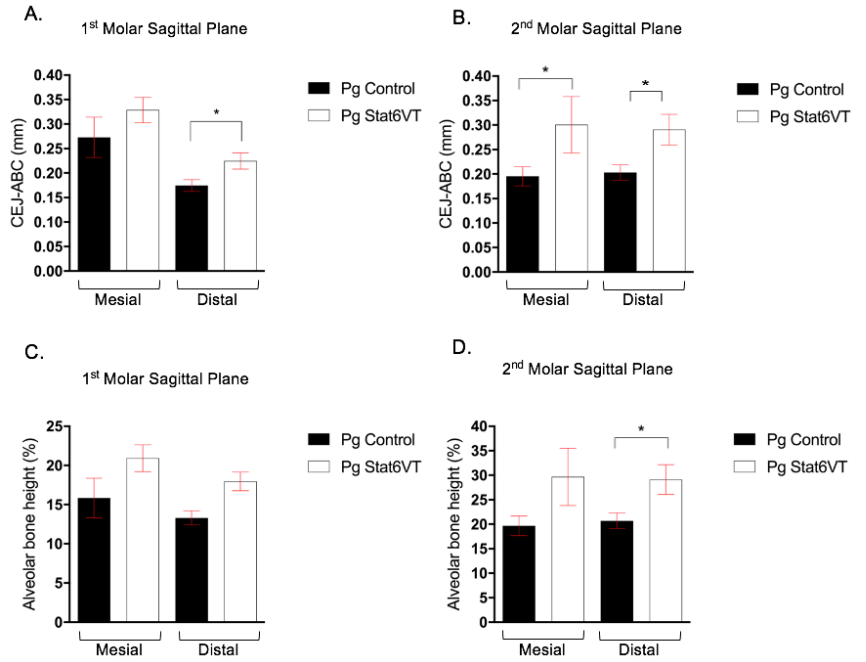

Pg-infected Stat6VT versus uninfected Stat6VT. *Pg*-infected Stat6VT compared to uninfected Stat6VT mice demonstrated greater CEJ-ABC measurements in 2 sites on the second molar (Figure 80B), which were CEJM-ABCB (0.1325 ± 0.009015 vs. 0.1699 ± 0.006931, p=0.0111) and CEJD-ABCB (0.1014 ± 0.009185 vs. 0.1395 ± 0.009256, p=0.0191). Furthermore, *Pg*-infected Stat6VT compared to uninfected Stat6VT mice demonstrated a greater loss of alveolar bone height in 2 sites on the first molar (Figure 82C) and 3 sites on the second molar (Figures 80D and 81D). The sites on the first molar were: CEJM-ABC (14.39 ± 1.276 vs. 20.93 ± 1.711, p=0.0154) and CEJD-ABC (14.14 ± 0.9248 vs. 17.97 ± 1.179, p=0.0340). The site on the second molar were: CEJM-ABCB (10.93 ± 0.8053 vs. 14.70 ± 0.7812, p=0.0099), CEJD-ABCB (8.356 ± 0.7129 vs. 13.09 ± 0.9124, p=0.0035), and CEJMid-ABCL (14.56 ± 1.012 vs. 17.77 ± 0.6561, p=0.0287).

Figure 80. MicroCT measurements of male *Pg*-infected Stat6VT and uninfected Stat6VT on the buccal aspect of the coronal plane. CEJ-ABC measurements of the A: first molar and B: second molar taken on the coronal plane (buccal aspect), and the alveolar bone height of the C: first molar and D: second molar taken on the coronal plane (buccal aspect). *p<0.05.

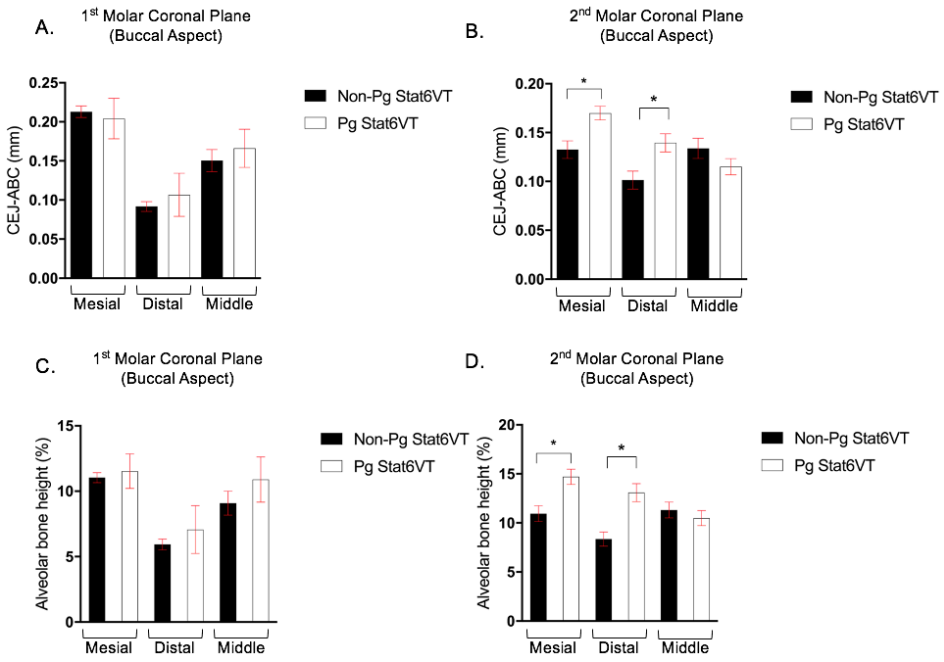

Figure 81. MicroCT measurements of male *Pg*-infected Stat6VT and uninfected Stat6VT on the lingual aspect of the coronal plane. CEJ-ABC measurements of the A: first molar and B: second molar taken on the coronal plane (lingual aspect), and the alveolar bone height of the C: first molar and D: second molar taken on the coronal plane (lingual aspect). *p<0.05.

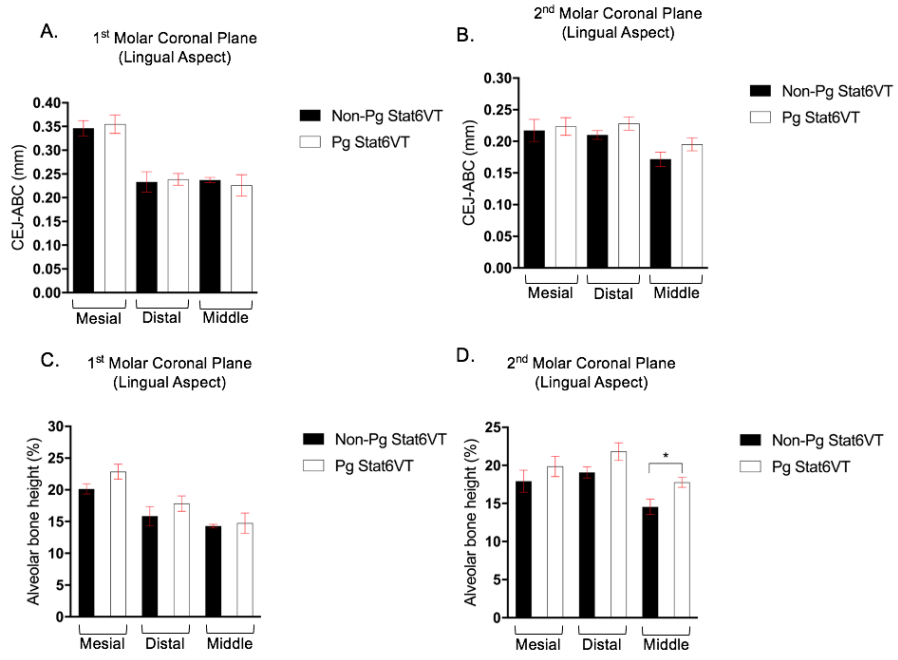

Figure 82. MicroCT measurements of male *Pg*-infected Stat6VT and uninfected Stat6VT on the sagittal plane. CEJ-ABC measurements of the A: first molar and B: second molar taken on the sagittal plane, and the alveolar bone height of the C: first molar and D: second molar taken on the sagittal plane. *p<0.05.

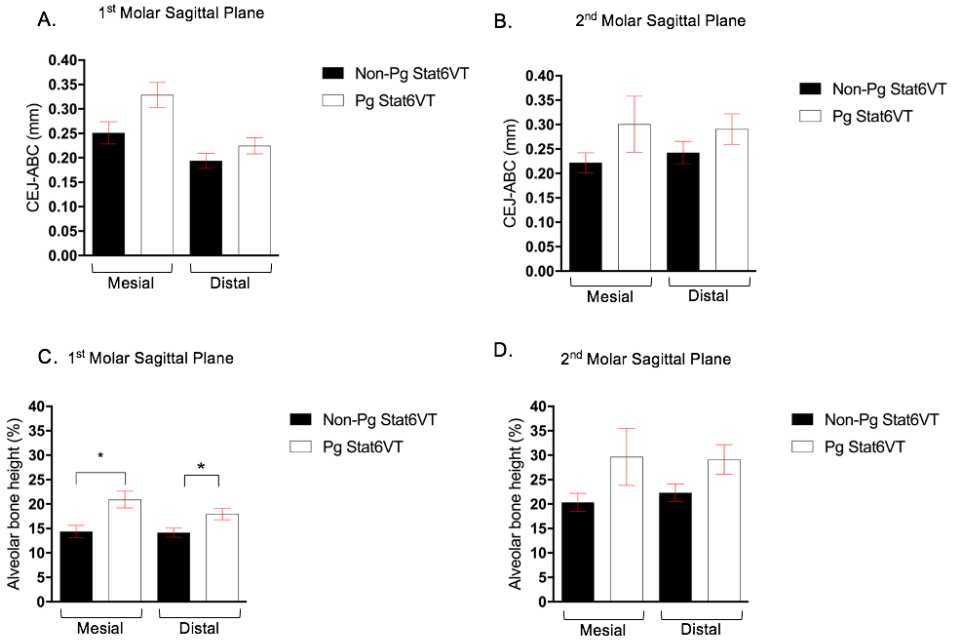

4.4 Histological findings of the soft tissues revealed successful *Pg* infection that caused increased signs of inflammation

2 weeks after the end of the *Pg*-infection protocol, mice were euthanized via pentobarbital overdose, and palates were collected for histology. Ramesh Mahdavifar and Sara Moradipoor assisted with data interpretation and cell count analysis. Dr. Catunda also assisted with the aforementioned procedures, including sample collection and histology. Because our data showed more consistent differences in males, and the female study was underpowered, we focused our efforts on males. Similar to the longitudinal study, we performed H&E staining and immunofluorescence detection for loricrin, CD45, Ki67, CK1, and CK14. CD45 and Ki67 positive cells were counted utilizing the same technique as the longitudinal study. T-tests were

used to calculate any significant differences. Images were examined by the same 2 investigators that examined the histological images in the longitudinal study. Representative images for each group are shown below.

We hypothesized that loricrin would be downregulated both as a result of overexpression of the Stat6VT mutant and effects of *Pg.* We expected Stat6VT transgenic mice to have more inflammation and bone loss compared to controls. Therefore, we anticipated the histological findings to demonstrate a greater extent of inflammation (i.e., more rete pegs, greater number of clear cells and CD45 positive cells, greater inflammatory cell infiltrates) in the Stat6VT mice compared to controls, and even greater when compared to the longitudinal study groups.

4.4.1 H&E staining

Palates from male Stat6VT mice observably demonstrated more clear cells and rete pegs than controls, which showed an absence of rete pegs and few clear cells (Figure 83). Additionally, Stat6VT mice had more nuclei clustered around the basal layer and across the spinous layer, whereas controls had fewer nuclei along the basal layer, and more sporadic nuclei across the layers. Overall, the presentation noted in the H&E-stained palates of Stat6VT mice is suggestive of increased inflammation. These findings support the hypothesis that the combination of constitutively activate Stat6 and *Pg* infection increases inflammation in the oral cavity.

Figure 83. A: H&E-stained palates of male *Pg*-infected A: control and B: Stat6VT mice. Rete pegs and cells suggestive of inflammatory infiltrate are labeled. Scale bar 20μm.

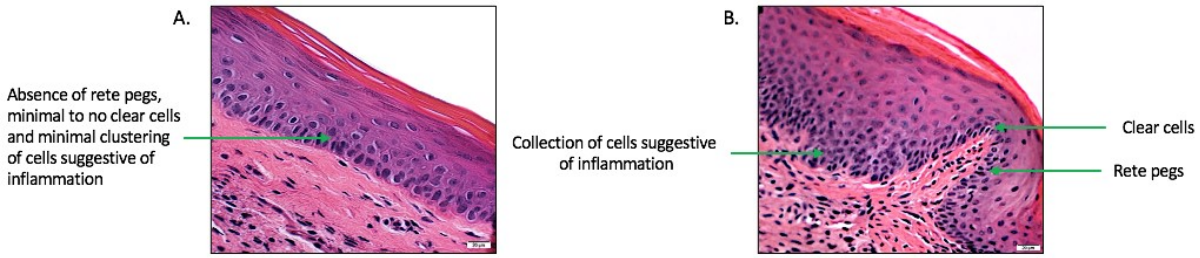

4.4.2 Loricrin immunofluorescence

Control and Stat6VT mice both demonstrated loricrin expression localized to the granular layer of the palate; however, the control group had apparent stronger expression of loricrin, as evidenced by the brighter staining (Figure 84). Interestingly, *Pg*-infected Stat6VT mice demonstrated apparent weaker expression of loricrin compared to uninfected Stat6VT mice at 10-13 weeks of age (compare with Figure 44). These findings support our hypothesis that loricrin expression is down-regulated by both constitutively activated Stat6 and *Pg*-infection.

Figure 84. Loricrin immunofluorescence in the palates of male *Pg*-infected A: control and B: Stat6VT mice. C: Secondary-antibody alone control to show non-specific staining. Loricrin expression in the granular layer is indicated by the arrow. Scale bar 20µm.

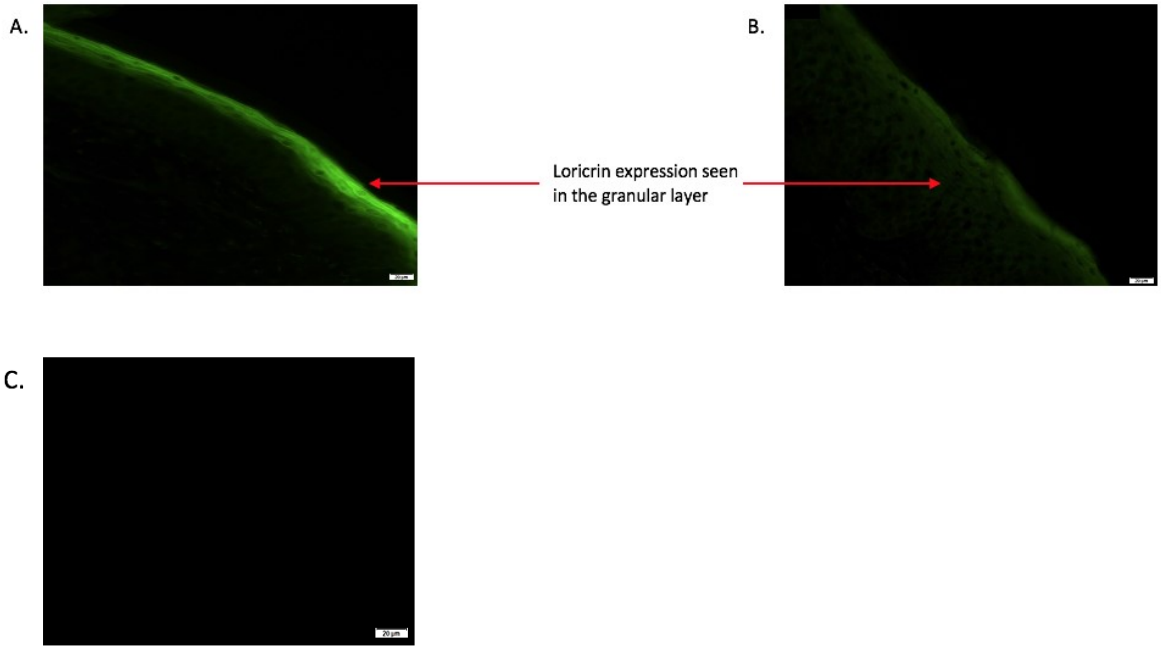

4.4.3 CD45 immunofluorescence

Palates of control mice had CD45 positive cells that were more dispersed throughout all the epithelial layers, whereas the palates of Stat6VT mice had CD45 positive cells that were found in clusters, localized to the basal or spinous layer of the epithelium (Figure 85).

CD45 cell count analysis revealed that Stat6VT and control mice did not significantly differ in the number of CD45 positive cells (Stat6VT: 41.91 ± 8.085 vs. control: 28.07 ± 3.851, n=3/group, p=0.1183) (Figure 86). In comparison to their uninfected counterparts, *Pg*-infected control and Stat6VT mice showed a statistically significant difference in CD45 positive cells (control uninfected: 11.08 ± 1.654 vs. control *Pg*-infected: 28.07 ± 3.851, n=3/group, p=0.0008; Stat6VT uninfected: 19.08 ± 0.7432 vs. Stat6VT *Pg*-infected: 41.92 ± 8.085, n=3/group, p=0.0101) (Figure 87). These findings affirm that our *Pg*-infection protocol successfully caused an increased inflammatory response.

Figure 85. CD45 positive cells in the palates of male *Pg*-infected A: control and B: Stat6VT mice. C: Secondary-antibody alone control to show non-specific staining. The white dashed line demarcates the keratinized layer for reference, and representative CD45 positive cells are circled. Scale bar 20µm.

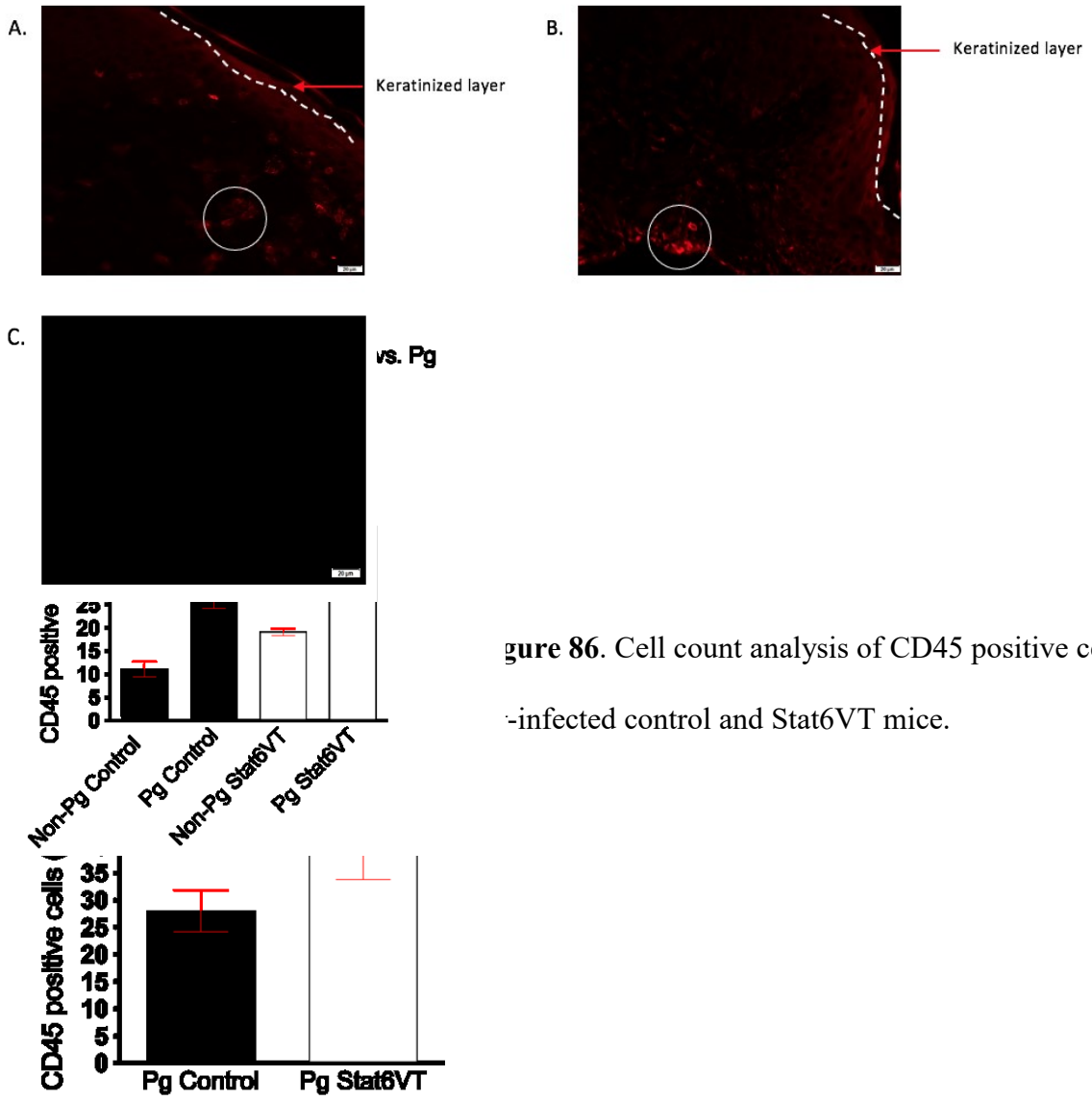

gure 86. Cell count analysis of CD45 positive cells in -infected control and Stat6VT mice.

Figure 87. Cell count analysis of CD45 positive cells, comparing uninfected and *Pg*-infected control and Stat6VT mice. *p=0.0008, **p=0.0101.

4.4.4. Ki67 immunofluorescence

Ki67 was expressed similarly in intensity in the palates of male control and Stat6VT mice; positive cells were located in proximity to the basal layer (Figure 88). Stat6VT, when compared to control, had more clusters of Ki67 positive cells, especially along the basal layer going up the rete pegs.

Ki67 cell count analysis revealed that control mice had significantly more Ki67 cells compared to Stat6VT mice (control: 53.97 ± 3.870 vs. Stat6VT: 38.54 ± 2.637, n=3/group, p=0.0013) (Figure 89). When *Pg*-infected control mice were compared to their uninfected counterparts, the *Pg*-infected controls had more Ki67 positive cells (uninfected control: 29.56 ± 3.416 vs. Pg-infected control: 53.97 ± 3.870, n=3/group, p<0.0001) (Figure 90), which suggests that inflammation from *Pg*-infection increased cell proliferation. Interestingly, when uninfected and *Pg*-infected Stat6VT mice were compared, they did not show any difference in Ki67 cell number.

Figure 88. A: Ki67 positive cells in the palates of male *Pg*-infected A: control and B: Stat6VT mice. C: Secondary-antibody alone control to show non-specific staining. The white dashed line demarcates the basal layer for reference. Scale bar 20μm.

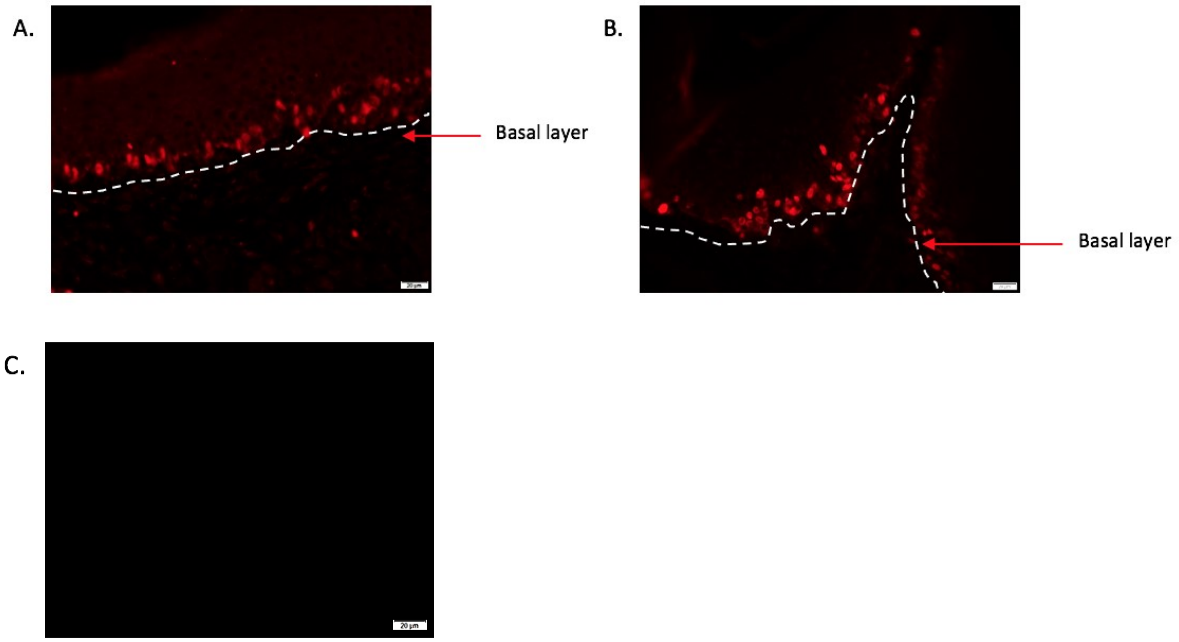

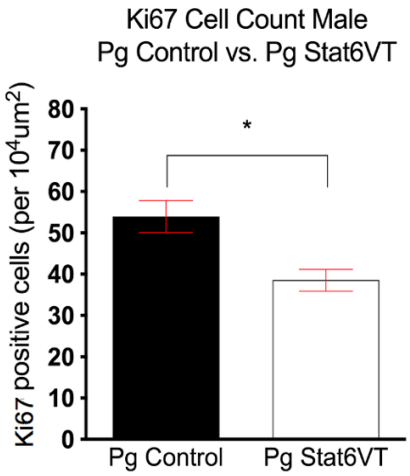

Figure 89. Cell count analysis of Ki67 positive cells in *Pg*-infected control and Stat6VT mice. *p=0.0013.

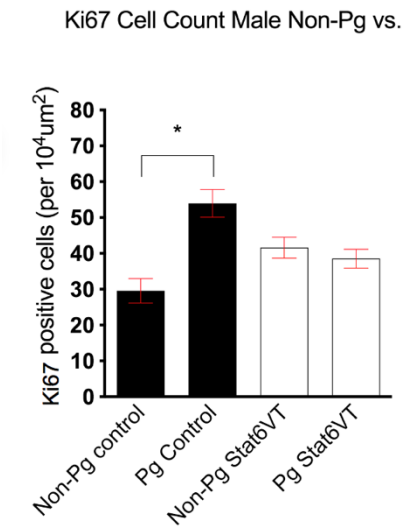

Figure 90. Cell count analysis of Ki67 positive cells, comparing uninfected and *Pg*-infected control and Stat6VT mice. *p<0.0001.

4.4.5 CK1 immunofluorescence

CK1 positive cells were detected in the basal and granular layers in the palates of *Pg*-infected male control mice (Figure 91). The fluorescence intensity was much greater in the cells of the granular layer. The palates of *Pg*-infected male Stat6VT mice showed CK1 positive cells only in the granular layer; the fluorescence intensity of these cells was less than control.

Figure 91. CK1 positive cells in the palates of male *Pg*-infected A: control and B: Stat6VT mice. C: Secondary-antibody alone control to show non-specific staining. The white dashed line demarcates the basal layer for reference. Scale bar 20µm.

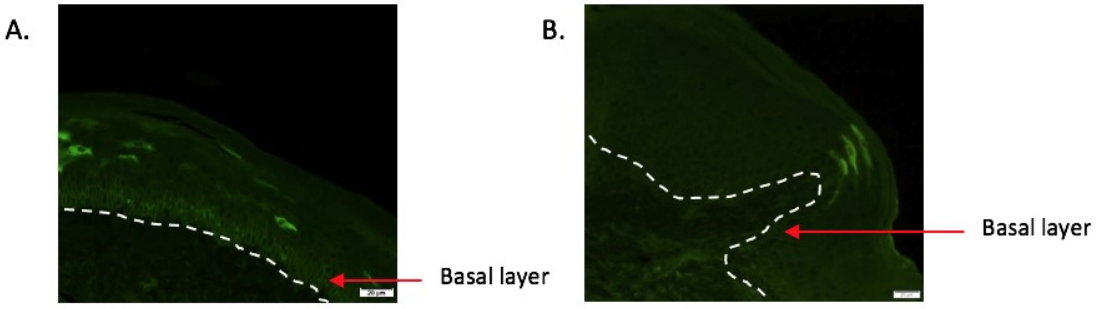

4.4.6 CK14 immunofluorescence

Pg-infected male control and Stat6VT mice both demonstrated CK14 expression localized to the basal layer (Figure 92). However, the control mice seemed to have greater expression as evidenced by slightly brighter staining.

Figure 92. CK14 positive cells in the palates of male *Pg*-infected A: control and B: Stat6VT mice. C: Secondary-antibody alone control to show non-specific staining. Scale bar 20µm.

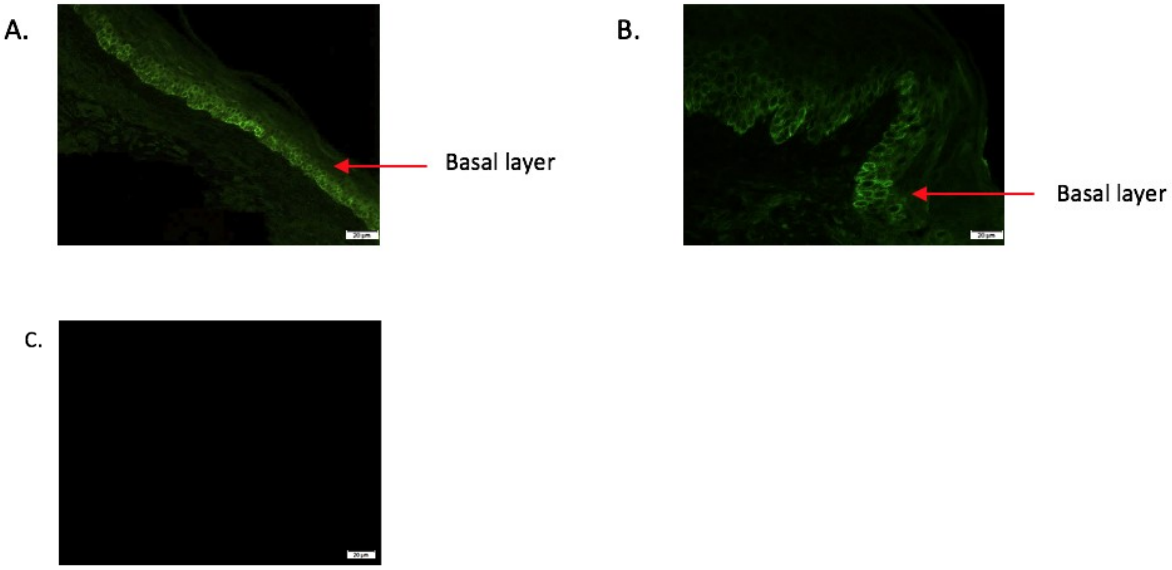

4.5 Histological findings of the hard tissues consistently demonstrated signs of heightened inflammation upon *Pg* infection

The lower right mandibles of *Pg*-infected control and Stat6VT mice were collected and prepared for histology in the same fashion as the palate samples. We performed H&E and immunofluorescence staining for loricrin and CD45 on hard tissue samples from 3 mice per group. Additionally, CD45 positive cells were counted at a standardized site, the distal gingiva adjacent to the sulcus of the third molar. The gingival tissue at this site is attached gingiva, which means that the tissue is keratinized and directly attached to the bone structure of the tooth (Cekici *et al*., 2014). Findings in this site are comparable to what may be observed in periodontal disease (Cekici *et al*., 2014) and will allow us to investigate the effects of *Pg* infection and changes in loricrin expression on inflammation in a more relevant to human disease location.

4.5.1 H&E staining

Pg-infected Stat6VT mice qualitatively showed greater number of rete pegs, and clear cells in the spinous and granular layer of the gingiva, when compared to controls (Figure 93). Additionally, all along the rete pegs in the epithelium of Stat6VT mice, there were clusters of inflammatory cells. These were also present in *Pg*-infected control mice, but to a lesser extent. These findings suggest an increased inflammatory response in the gingiva of Stat6VT mice compared to controls.

Figure 93. H&E staining of the gingivae of male *Pg*-infected A: control and B: Stat6VT mice. Sulcus, clear cells, rete pegs, and sites of inflammation are identified. Scale bar 50µm.

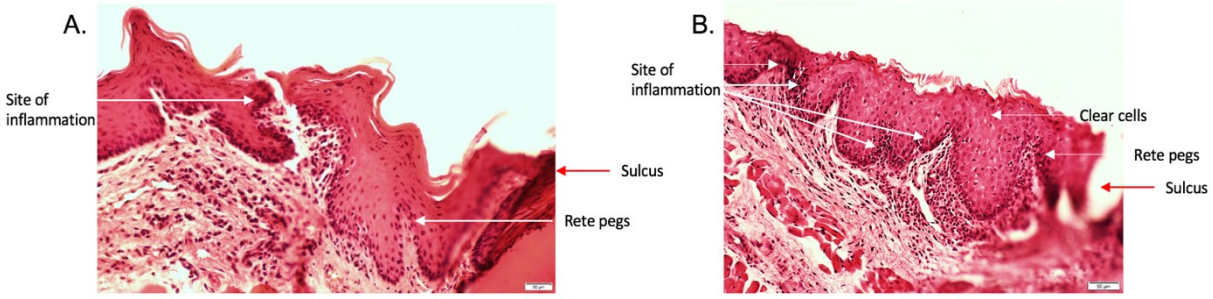

4.5.2 Loricrin immunofluorescence

Loricrin was localized to the granular layer in the gingivae of both control and Stat6VT mice, however, expression was significantly reduced in Stat6VT mice compared to controls (Figure 94). This is evidenced by the brighter staining observed in the controls and the minimal, faint staining observed in the Stat6VT mice. These findings further support our hypothesis that reduced expression of loricrin may lead to an impaired barrier, which may in turn increase the inflammatory response in the presence of a periodontal disease pathogen.

Figure 94. Loricrin immunofluorescence in the gingivae of male *Pg*-infected A: control and B: Stat6VT mice. C: Secondary-antibody alone control to show non-specific staining. The keratinized and granular layers were labeled for identification purposes. The white dashed line demarcates the keratinized layer for reference. Scale bar 20µm.

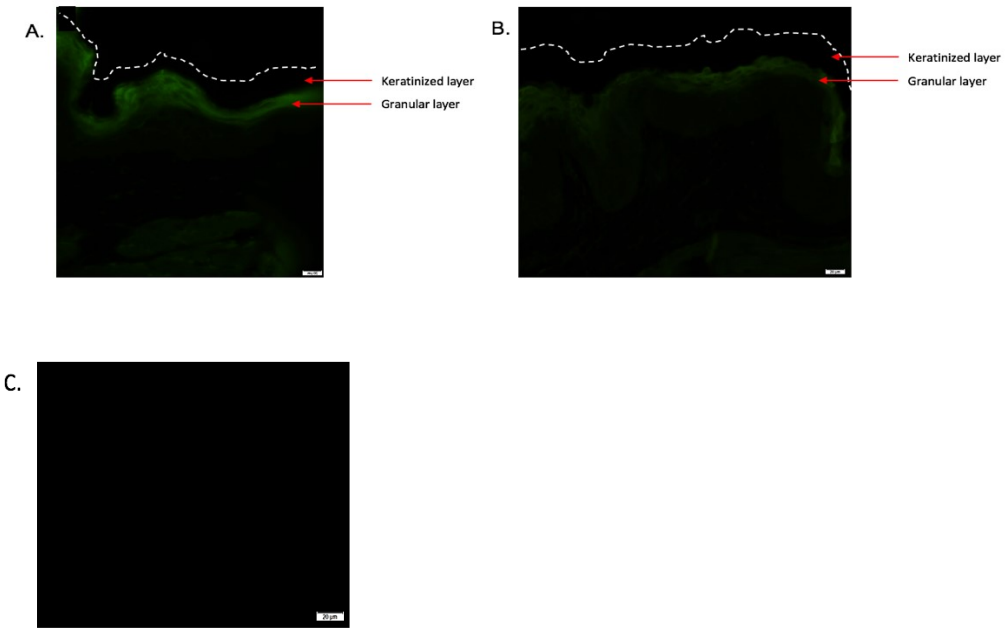

4.5.3 CD45 immunofluorescence

CD45 positive cells were more numerous and found across all layers of the epithelium in the Stat6VT mice, whereas control mice demonstrated CD45 positive cells mainly in the spinous and granular layers (Figure 95). Cell count analysis confirmed these observations (Figure 96).

There were significantly more CD45 positive cells in the gingivae of Stat6VT mice compared with control (control: 29.55 ± 4.397 vs. Stat6VT: 58.11 ± 5.301, n=3/group, p=0.0006). These findings support our hypothesis that the Stat6 mutation and effects of *Pg* would result in a heightened inflammatory response in the oral cavity of Stat6VT mice.

Figure 95. CD45 positive cells in the gingivae of male *Pg*-infected A: control and B: Stat6VT mice. C: Secondary-antibody alone control to show non-specific staining. The white dashed line demarcates the keratinized layer for reference. Scale bar 20µm.

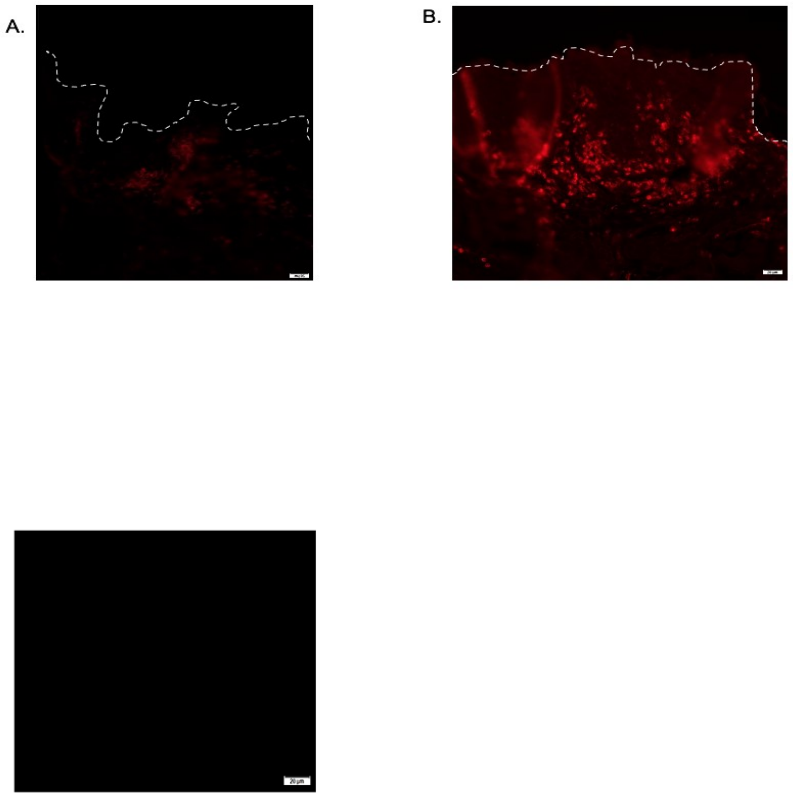

Figure 96. CD45 cell count in control and Stat6VT hard tissues. *p=0.0006.

4.6 ELISA revealed similar amounts of loricrin in the gingivae of *Pg*-infected and uninfected mice

To quantitatively measure loricrin in the gingiva, we performed an ELISA (Cloud Clone Corp, SEC658Mu). Gingival tissue samples from 3 mice within the same group were pooled. In order to quantify the amount of protein in each sample, the Pierce Bicinchoninic Acid Kit was used (23227, Thermo Fisher Scientific).

Our results showed similar amounts of loricrin/total protein in *Pg*-infected control and Stat6VT male mice (Figure 97). Amounts were also similar to uninfected control and Stat6VT male mice (Figure 64). We had the same challenges in achieving accurate ELISA results here as in the longitudinal study. This will be further discussed in the "discussion" section.

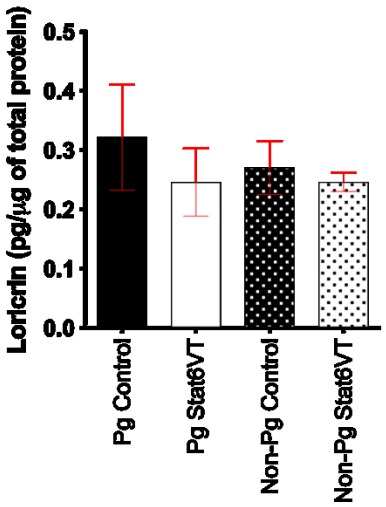

Figure 97. Gingival loricrin concentration, comparing uninfected and *Pg*-infected control and Stat6VT mice.

4.7 Plasma cytokine profiling revealed 3 cytokines were significantly increased in *Pg*-infected Stat6VT mice compared to controls

We performed a cytokine array on plasma collected at sacrifice. (AB193659, Mouse Cytokine Antibody Array). Three cytokines were increased by at least 1-fold in both *Pg*-infected Stat6VT and control mice: Osteopontin (OPN), Insulin-like Growth Factor Binding Protein 2 (IGFBP2), and Intercellular Adhesion Molecule 1 (ICAM1) (Figure98). IGFBP2 was the most increased cytokine.

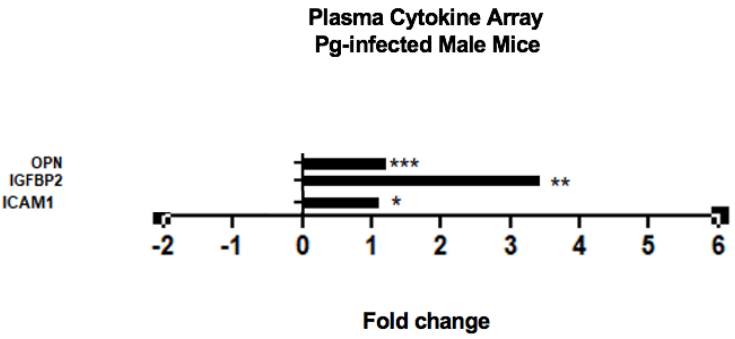

Figure 98. Plasma cytokine array results expressed as fold change *Pg*-infected male Stat6VT mice/control.

CHAPTER 5: DISCUSSION

5.1 Rational

The goal of our study was to investigate loricrin deficiency in the oral epithelium and its impact on the periodontal health of Stat6VT transgenic mice, with and without periodontal disease pathogen challenge. The overall literature indicates that defects in CE proteins affecting skin can lead to a heightened host inflammatory response to bacteria involved in disease (Agrawal & Woodfolk, 2014; Guttman-Yassky *et al*., 2009; Pyun 2015). Furthermore, downregulation of loricrin gene expression has been shown to be associated with SvP Guzeldeimir-Akcakanat *et al*., 2015; Nowak *et al*., 2013). However, a causal linkage to SvP remains inconclusive. With evidence that points to loricrin being one of the most profoundly downregulated CE proteins in SvP, the Stat6VT mouse model was ideal for our study. Since the oral cavity has not been explored before in this mouse model, this warranted further investigation.

5.2 Phenotype of Stat6VT

Excluding the oral cavity, the phenotype of the Stat6VT mouse model has been described in the literature (DaSilva-Arnold *et al*., 2018; Kaplan *et al*., 2007; Sehra *et al*., 2016). One of the most common phenotypical findings of this mouse model is the presentation of blepharitis (Sehra *et al*., 2008). Blepharitis is inflammation of the eyelids, where the borders of the eyes present with redness, swelling and may become visually impairing and painful (Sehra *et al*., 2008). One study found that approximately 1 in every 4 Stat6VT transgenic mice that were under the age of 12 weeks old had blepharitis, and all mice over 12 weeks of age had blepharitis (Sehra *et al*., 2008). This study had even found blepharitis in Stat6VT transgenic mice as early as 4 weeks of age. Although blepharitis can be caused by various factors, in the case of Stat6VT, blepharitis is

caused by increased scratching behavior, resulting in hyperkeratosis and thickening of the dermis and epidermis around the borders of the eyes (Sehra *et al*., 2008). Blepharitis seen in Stat6VT transgenics is indicative of allergic inflammation, evidenced by the lymphocytes and eosinophilic infiltration of the dermis (Kaplan *et al*., 2007; Sehra *et al*., 2008). This phenotype has been seen in other mouse models with a hyper Th2 cytokine production, including IL-4 transgenic and NFATc2/c4-double-deficient mice (Sehra *et al*., 2008). The literature suggests that by 20 weeks, Stat6VT mice develop periocular edema and eyelid erythema, as well as loss of hair, similar to our observations. It has also been confirmed by a study that increased scratching does indeed lead to the ocular inflammation observed (Sehra *et al*., 2008; Turner *et al*., 2014). These investigators showed that Stat6VT mice had an increased rate of scratching in comparison to wild-type controls (Sehra *et al*., 2008; Turner *et al*., 2014). Our study confirms these findings since, by the 18-week time point, all Stat6VT mice had some degree of edema and inflammation around the eyes, some even with a loss of hair around the face, neck and ear region.

Other studies have also noted keratitis in 35% of mice by 20 weeks of age, which is an inflammation of the cornea (Turner *et al*., 2014). Keratitis was confirmed in these studies by slit-lamp examination (an exam that validates peripheral neovascularization of the cornea) (Turner *et al*., 2014); we did not perform this examination on our mice. Other studies have confirmed the presence of corneal disease and uveitis in Stat6VT mice (Turner *et al*., 2014). These conditions were all confirmed to have been caused by allergic inflammation, by measuring Th2 cytokines via quantitative real-time PCR (Turner *et al*., 2014). As we did not perform quantitative real-time PCR nor immunoblotting, we could not definitively confirm these findings in our mice by observation. Additionally, Stat6VT mice have been found to develop pulmonary inflammation

around the ages of 12-16-weeks (DaSilva-Arnold *et al*., 2018; Sehra *et al*., 2008). Pulmonary inflammation has been characterized by immune cell infiltration and pulmonary tissue destruction (DaSilva-Arnold *et al*., 2018; Sehra *et al*., 2008). In our study, we did not test for pulmonary inflammation.

Other more common phenotypical findings of this mouse model are most notably the AD-like lesions (DaSilva-Arnold *et al*., 2018; Sehra *et al*., 2008). The Stat6VT AD-like lesions are caused by their constant scratching behavior and present as dermatitic plaques with alopecia on the face, back or other areas of the body (DaSilva-Arnold *et al*., 2018; Sehra *et al*., 2008). Some studies showed AD-like lesions only after a 24-week time point (DaSilva-Arnold *et al*., 2018). Within our 18-week time period, we began seeing early signs of these dermatitic plaque lesions around the ears and a loss of fur within the neck region. Studies that examined the ear tissue of Stat6VT mice via histology, discovered that they were considerably thickened at the dermis and epidermis layers, with cellular infiltration of eosinophils and lymphocytes (DaSilva-Arnold *et al*., 2018).

Although unconfirmed in our study, a rare phenotypical finding in Stat6VT mice was the development of lymphoproliferative disease (LPD) that results in dramatic splenomegaly (Kaplan *et al*., 2007). The phenotype of cells in LPD can be divided into being predominately T cells or B cells (Kaplan *et al*., 2007). In Stat6VT mice, the spleen size, by mass, can increase 40-fold and leukocyte cell numbers can increase on average 5-fold (Kaplan *et al*., 2007).

Although our experiments did not reveal any gross, superficial, phenotypical findings in the oral cavity at 6-18 weeks, the presentation of oral disease may be different in mice than what we would expect in humans. It is clear that Stat6VT mice and their heightened Th2 immune response have consequential effects to not only the outer layer of skin but also systemically, such

as pulmonary and lymphoproliferative diseases (DaSilva-Arnold *et al*., 2018; Kaplan *et al*., 2007; Sehra *et al*., 2008). These conditions can cause significant stress to the mice at an early age, which in turn can predispose them to problems related to maturation and bone development. In fact, studies have confirmed this in mice and human studies (Azuma *et al*., 2015; Cizza *et al*., 2010; Furlan *et al*., 2005; Mezuk *et al*., 2008; Williams *et al*., 2016). Mice that were exposed to early life stresses revealed a significant decrease in osteoblast growth factors, higher innervation density in bone and increased serum levels of CTX-I (blood marker associated with bone resorption) (Wippert *et al*., 2017; Wuertz-Kozak *et al*., 2020). The heightened Th2 immune response and loricrin downregulation that elicits a barrier dysfunction, complimented by the constant scratching and possible medical conditions, can play a role in irregular growth and development.

5.3 MicroCT results

5.3.1 Successful use of the microCT approach

Although there have been various linear measurement approaches used in assessing alveolar bone height in the periodontium of mice, there is no standardized universal approach. This is a concern that may hinder the accuracy of our alveolar bone height analysis. By utilizing the protocol developed by Dr. Catunda, we were able to achieve consistent landmarks that were highly reproducible and accurate. Furthermore, the advantage that this protocol has over the other protocols in the available literature is that landmarks are achieved by 2 planes rather than 1 plane, which enables greater accuracy in angulation and orientation. Take for example, our male microCT measurements collected in the longitudinal study at the 10-13-week time point. Male Stat6VT when compared to controls demonstrated greater CEJ-ABC measurements in a total of 5 sites on the first and second molar teeth. 4 out of 5 of these sites were found on the coronal

plane. Had this plane not been utilized, the accuracy and representation of alveolar bone levels would not have been as telling.

Inter-rater reliability was measured via Cohen's kappa and the results were interpreted as follows: ≤0 as no agreement, 0.01-0.20 as none to slight, 0.21-0.40 as fair, 0.41-0.60 as moderate, 0.61-0.80 as substantial, and 0.81-1.00 as almost perfect agreement (McHugh 2012). Across the 3 examiners involved in the microCT analysis, the scores were indicative of "substantial" to "strong" agreement. This suggests that the protocol not only produced calibrated measurements for this study but can also be a protocol adapted in future periodontal research experiments as it has proven to be reproducible.

The protocol used in this study is dissimilar to other bone measurement protocols in the literature because our study demonstrated alveolar bone loss on the sagittal and coronal lingual plane, which is a plane not often included in other linear measurement approaches (Park *et al*., 2007; Marchesan *et al*., 2018; Wilensky *et al*., 2005). Studies that do include the coronal plane (buccal and lingual aspect) often present the results as an average (Ebbers *et al*., 2018; Li *et al*., 2011; Lübcke, *et al*., 2019; Myneni *et al*., 2011; Settem *et al*., 2014; Srinivasan *et al*., 2010; Yuan *et al*., 2013; Zhang *et al*., 2014).

5.3.2 MicroCT Pg results

Across all the comparisons, *Pg*-infected male mice demonstrated a reduction in alveolar bone levels compared to uninfected male mice. More specifically, the *Pg*-infected Stat6VT male mice compared to *Pg*-infected control mice demonstrated a significant reduction in alveolar bone levels across various different sites. These findings are aligned with our hypothesis, as we expected an increased inflammatory response caused by the pathogenic bacteria, and an even greater response seen due to the barrier defect in the Stat6VT mice. Additionally, the reduction

in alveolar bone levels seen in the *Pg*-infected controls versus the uninfected controls suggests that periodontal infection in male mice was achieved. Similar to the longitudinal study, the female *Pg* microCT results were inconsistent. This novel finding in our study suggests that female Stat6VT and control mice may have hormonal and physiological factors that can possibly contribute to the variance seen in the phenotypical findings, BMC/BMD results and the microCT analysis.

5.4 Cytokine profiling

5.4.1 Cytokine profiling of uninfected Stat6VT male mice

For the uninfected mice cytokine profiling, cytokines identified as increased in Stat6VTmice were: CD30L, Eotaxin2, MCP5, MIG, ad BLC.

CD30L is a membrane-bound cytokine that is a member of the tumor necrosis factor receptor superfamily (Van Der Weyden *et al*., 2017). Studies have shown that CD30L expression is higher in Th2-type cytokine responses (Agrawal *et al*., 1996; Del Prete *et al*., 1995; Ellis *et al*., 1993; Manetti *et al*., 1994; Smith *et al*., 1993). Furthermore, CD30L is highly expressed in cases of acute myeloid leukemias, B-lineage acute lymphoblastic leukemia and B-cell lymphoproliferative disorders (Gattei *et al*., 1997). In the case of the Stat6VT mouse model, CD30L may have been found to be significant in the cytokine profiling results due to their risk of developing LPD. In addition, another study investigated the role of CD30L signal transduction in inflammatory responses mediated by the skin and showed that CD30L gene deletion (CD30LKO mice) led to psoriasis and aggravated skin inflammation (Yue *et al*., 2019). This suggests that CD30L may play an important role in maintenance of the skin barrier.

Eotaxin2, or CCL24, is among 1 of 3 chemokine subfamilies of eosinophil chemotactic proteins (Van Coillie *et al*., 1999). An allergic reaction, similar to that of AD, is commonly

found to be associated with the induction of Eotaxins (Eberle *et al*., 2019; Menzies-Gow *et al*., 2002; Owczarek *et al*., 2010; Sabroe & Williams, 2006). It is known that Th2 cells regulate infiltration of eosinophils in allergic reactions by secreting IL-4, which switches on the genes for the Eotaxins in other cells of the tissue (Eberle *et al*., 2019; Menzies-Gow *et al*., 2002; Owczarek *et al*., 2010; Sabroe & Williams, 2006). When there are phenotypical changes, such as that in the Stat6VT mice, IL-4 regulation may become disrupted and induction of CCL24 generation in macrophages may occur. Additionally, studies in the literature suggest that Stat6 mediates the transcriptional activation of M2 macrophage-specific genes such as CCL24 (Yu *et al*., 2019). Because Stat6VT has a constitutive activation of Stat6, this may lead to the significant difference in CCL24 seen. Interestingly, Eotaxin2 has been investigated and found to be associated with bone loss disorders, such as osteopenia and osteoporosis (Ahmadi *et al*., 2020; Hoshino *et al*., 2014). In a study that investigated osteoporotic and osteopenic patients, circulating levels of CCL24 were increased in patients with these conditions compared to healthy subjects (Ahmadi *et al*., 2020). In an *in vitro* study, spinal tuberculosis infection by *Mycobacterium tuberculosis* was investigated, and CCL24 was among a variety of chemokines that was found to be produced that led to a disturbed pattern of osteoclast activation (Hoshino *et al*., 2014). These studies suggest that CCL24 may be associated with normal bone remodeling, and greater expression can lead to bone loss via increased transcriptional activation of M2 macrophage-specific genes.

MCP5, also known as CCL12, is a CCL2 homologue (Tsui *et al*., 2007). The human CCL2 chemokine is implicated in many chronic inflammatory conditions (Tsui *et al*., 2007). Humans express CCL2 (MCP1), but not CCL12 (MCP5), while mice have both homologues of CCL2 (Tsui *et al*., 2007). Interestingly, a study investigated cardiac wound healing and its association with periodontal-induced chronic inflammation in mice (Deleon-Pennell *et al*.,

2017). The study found that CCL12 prevented initiation of the reparative response by prolonging inflammation and inhibiting fibroblasts necessary for scar formation (Deleon-Pennell *et al*., 2017). Since MCP5 was found in Stat6VT mice to be significantly increased, it is possible that the periodontal bone loss may be cytokine-driven.

MIG, also known as CXCL9, is a chemokine that belongs to the CXC chemokine subfamily (a different family than the CC chemokine subfamily) (Cekici *et al*., 2014). CXCL9 expression is commonly found to be highly expressed in AD patients and contact dermatitis patients (Hulshof *et al*., 2018; Shimada *et al*, 2004). Interestingly, CXCL9 has been shown to be elevated in various inflammatory bone diseases (Amarasekara *et al*., 2018; Cekici *et al*., 2014; Kuan *et al*., 2010; Liu *et al*., 2020). A study by Hasegawa *et al*. (2021), found that CXCL9, which acts through chemokine receptor CXCR3, is recruited in apical periodontitis (inflammation and destruction of the peri-radicular tissues). By using an apical periodontitis mouse model and inhibiting CXCL9, the apical periodontal lesion size in the mice was reduced. Their study revealed that CXCL9 can regulate the function of macrophages that contribute to apical periodontal pathogenesis and by blocking CXCL9 expression, suppression of apical periodontal progression can occur. In another study by Green (2018), CXCL9 and CXCL10 were found to be significantly expressed in a high bone loss (C57Bl/6J) mouse strain compared to bone loss resistant (A/J) strain. They reported that both chemokines play a key role in the maintenance and amplification of inflammatory pathways. Research has shown that IL-4 stimulates the secretion of CXCL9 to increase endocytic activity, cell growth and tissue repair (Muñoz *et al*., 2020). Due to the Stat6VT-mediated increased Th2 immune response, there is an overproduction of IL-4, which may be a factor that contributes to the increased expression of CXCL9.

BLC, also known as CXCL13, is also a chemokine that belongs to the CXC chemokine subfamily (Kim *et al*., 2018; Park *et al*., 2011). CXCL13 has also been shown to be highly expressed in individuals with AD (Kim *et al*., 2018; Park *et al*., 2011). In mice, CXCL13 is known to attract B lymphocytes (Carlsen *et al*., 2002; Silva *et al*., 2007). Interestingly, B lymphocytes are the dominant infiltrating cell type in periodontitis lesions and CXCL13 is essential for B-cell trafficking (Nakajima *et al*., 2008). A study by Nakajima *et al*., (2008) discovered a significantly greater number of CXCL13 positive cells in periodontitis and in gingivitis patients, which suggests that CXCL13 may be involved in B cell recruitment and distribution in inflammatory periodontal lesions.

In our study, the cytokines that were significantly expressed in Stat6VT mice were those that play a role in allergic reactions and periodontal bone loss. Undoubtfully, it has been shown that Stat6VT mice may present with an increased inflammatory response due to the down regulation of loricrin gene transcription, thereby contributing to a barrier defect (Bao *et al*., 2017; Kim *et al*., 2008). This response was most likely responsible for the alveolar bone loss and histological signs of inflammation in the oral cavity observed in our study's Stat6VT mice compared to controls; however, it is possible that these cytokines may have also partially contributed to some of the inflammation.

5.4.2 Cytokine profiling of Pg-infected Stat6VT male mice

Cytokine profiling was performed on the *Pg*-infected 10-13-week Stat6VT and control male mice. The cytokines that were significantly increased in the Stat6VT mice were OPN, IGFBP2 and ICAM1.

OPN, also known as bone sialoprotein 1 (BSP1), is a protein expressed in bone and other tissues (Lund *et al*., 2009). OPN is known to mediate diverse biological functions, including cell

migration, adhesion and survival in many cell types. OPN plays a role in chronic inflammatory and autoimmune diseases (Lund *et al*., 2009). OPN has been shown to be an essential cytokine in inflammatory skin disorders, such as AD, contact dermatitis, psoriasis and skin cancer (American Journal of Pathology, 2010; Bassyouni *et al*., 2016; Buommino *et al*., 2009). Studies have shown skin cells and immune cells in inflammatory skin disorders over-secrete OPN (Forootan *et al*., 2006). In skin cancer, such as in metastatic melanoma, one study found that 14 genes out of 190 were more than 20-fold overexpressed, and within this group, OPN was the most overexpressed gene (Forootan *et al*., 2006). In our cytokine array, OPN had the second greatest expression and this may suggest that OPN not only contributed to the inflammation seen in the skin but also periodontally. Indeed, OPN is also known to play a crucial role in periodontitis, as this protein is essential for bone remodeling, biomineralization and periodontal remodeling during mechanical tensions and stress (Singh *et al*., 2018). In a study by Sharma & Pradeep (2006), 45 subjects were categorized as either healthy, or having gingivitis or periodontitis, and the highest mean OPN concentration within the gingival crevicular fluid was found in those with periodontitis. Another study also demonstrated that osteoclast proliferation and differentiation were increased with increased OPN expression in patients with periapical periodontitis (Dong *et al*., 2018). One *in vitro* study even investigated *Pg* and its effects on calcification of smooth muscle cells and found that OPN expression was significantly promoted in the presence of *Pg* infection (Liu *et al*., 2016). Our microCT results suggest that the *Pg*-infected Stat6VT mice experienced a degree of bone loss that may have been impacted by the increased expression of OPN. Our results seem to align with the implications of overexpression of OPN.

IGFBP2 is an insulin growth factor binding protein and supports the regulation of insulin growth factor proteins in the body (Allard & Duan, 2018). Additionally, IGFBP2 is important for the acquisition of normal bone mass in mice (Xi *et al*., 2014). This has been investigated in IGFBP2 knockout mice, which demonstrated a substantial delay in osteoblast differentiation and reduced osteocalcin expression (Allard & Duan, 2018). Interestingly, IGFBP2 was found to be one of the proteins differentially expressed in human monocytes when induced by *Pg* (Nakka 2016; Zhou & Amar, 2006). In addition, IGFBP2 expression has a strong association with bone loss in animal and human studies (Amin *et al*., 2004). A human clinical study by Amin *et al*., (2004), discovered that higher IGFBP2 levels were associated with lower BMD. IGFBP2, which increases in expression with age in both men and women, was the greatest predictor of BMD among the other IGF and IGFBPs investigated in their study. In an animal study, IGFBP2 overexpression impairs long bone development (Fisher *et al*., 2005). Although the association between IGFBP2 and skin disorders may be minimally reported in literature, research seems to suggest an essential involvement of IGFBP2 with bone loss. In our cytokine profiling, IGFBP2 had the greatest expression, with a fold change greater than 4. Although BMD of the femur was measured in our mice, this was not measured after *Pg*-infection. However, microCT results of bone loss in our *Pg*-infection reflect bone loss that could be cytokine-driven, such as by the expression of IGFBP2.

ICAM1, also known as CD54, is a protein that has been implicated in a variety of immune and inflammatory responses (Figenschau *et al*., 2018, Müller 2019). In fact, ICAM1 has been suggested to be overexpressed in inflamed gingival tissues, and its expression by human gingival fibroblasts is crucial for regulating local inflammatory responses in inflamed periodontal tissues (Chang *et al*., 2013). Other studies have investigated *Pg* infection and

atherosclerosis and discovered that ICAM1 expression is increased in the presence of *Pg* in endothelial cells and monocyte-endothelial cell adhesion (Xu *et al*., 2018). Similarly, another study investigated adhesion molecule expression in chronic inflammatory periodontal disease tissue and discovered ICAM1 to be significantly increased in expression in endothelial cells of periodontal tissues (Gemmell *et al*., 1994). In addition, this study also showed that keratinocyte expression of ICAM1 increased with the increasing size of infiltrate. In consideration of our experiment, the *Pg* infection was designed to induce a periodontal state in the Stat6VT mice. The increased ICAM1 cytokine expression in the Stat6VT mice suggests an increased inflammatory response similar to that seen in inflamed periodontal tissues.

Our goal of infecting the mice with *Pg* was to elicit an increased Th2 response that would mimic periodontal disease. By doing this, we would be able to investigate the oral epithelium, alveolar bone levels and tissue structures in a heightened inflammatory environment. Our *Pg* study demonstrated that loricrin downregulation occurred most likely as a result of the Stat6VT mutant as well as from the effects of *Pg*. Furthermore, the cytokines identified in our array match the kind of cytokines that would be overexpressed in conditions of inflammation and bone loss. This suggests that inflammation may have also been partially contributed by these cytokines as well.

5.5 BMD/BMC

In the literature, there are reports of BMC and BMD in humans and mice across different parts of the body, such as the tibiae, femurs, lumbar spine and entire body (Akhter *et al*., 2000; Dengler-Crish *et al*., 2018; Halloran *et al*., 2002; Payne *et al*., 1999). In addition, BMC and BMD are commonly reported as combined values of different body parts, which makes it difficult to compare our values with what is available (Akhter *et al*., 2000; Dengler-Crish *et al*.,

2018; Halloran *et al*., 2002; Payne *et al*., 1999). However, there is evidence in the literature that helps explain the significant differences seen in BMD and BMC in 6-8 week and 18-week Stat6VT and control male mice. Regarding the significant difference seen in BMD and BMC of the 6-8-week Stat6VT and control mice, research suggests that mice in normal conditions tend to reach bone maturation at a time point after 6-8 weeks (Ferguson *et al*., 2003; Gargiulo *et al*., 2014; Halloran *et al*., 2002; Jilka 2013), which may suggest that growth and development are still inconsistent prior to this time. One study by Ferguson *et al*., (2003) investigated the bone development and age-related bone loss in long bones of male C57Bl/6J mice by measuring bone size, mineral mass and mechanical properties. They found that bone maturity, in which maintenance of bone and mechanical properties was kept constant, occurred only after 12 weeks of age. Additionally, previous research investigated the calcium content of the entire skeleton of 32 inbred strains of mice (one of which was the C57Bl/6J) via dual-energy X-ray absorptiometry, and they found that peak bone mass was achieved after 16 weeks of age (Ackert-Bicknell *et al*., 2008; Jilka 2013). In addition, they found that bone acquisition and longitudinal bone growth continue in mice even after sexual maturity, which occurs at 6-8 weeks. Another study by Gargiulo *et al*., (2014) investigated BMD of the entire body in female C57Bl/6J mice via dual energy X-ray absorptiometry and found that BMD peaked at 17 weeks. These studies suggest that at the 6-8-week time point, the bone maturation of the femur may not yet be complete, leading to potential differences seen between the Stat6VT and control mice. Therefore, these differences may be within the normal range leading into the later stages of complete maturation.

At the 10-13-week time point, male Stat6VT and control mice were found to have no significant differences in BMC and BMD. As suggested by the study conducted by Ferguson *et*

al., (2003), bone maturity occurs between 12 and 42 weeks of age. Additionally, another study by Klein *et al*., (1998) also suggested that female C57Bl/6J peak whole-body BMD (via Faxitron) occurred at approximately 12 weeks. Nonetheless, the general pattern of age-related BMD maturation in C57Bl/6J mice has not been clearly delineated.

At the 18-week time point, BMC and BMD was greater in male control mice compared to Stat6VT. There is reason to believe that Stat6VT mice at this time point were undergoing an increased amount of inflammation that was cytokine-driven. As seen phenotypically, the Stat6VT had severe swelling of the eyes and skin lesions around the face and ears. Upon exposure to the heightened inflammatory response, the secreted cytokines may have played a role in the reduced BMC and BMD seen in the Stat6VT mice compared to control. According to the literature, almost all of the significantly increased cytokines that were identified in the uninfected Stat6VT mice have evidence of some association with bone loss (namely CCL2/Eotaxin2, MIG/CXCL9, and BLC/CXCL13). It is possible that due to the increased expression of these cytokines, a reduction in BMD and BMC occurred in Stat6VT mice.

Interestingly, studies have looked into the similarities and differences seen between bone loss seen in mice as compared to humans (Jilka 2013). Research suggests that the characteristics and timing of age-related bone loss in mice are quite similar to that of humans. More specifically, both humans and mice begin to exhibit similar loss of cancellous bone, thinning of cortical bone and increase cortical porosity in early adulthood (Khosla 2013). However, longitudinal bone growth tends to cease at sexual maturity in humans, whereas slow growth continues after sexual maturity for mice.

The same cytokines found in our study have been suggested to have cytokine-driven BMD/BMC effects in human studies. For example, a study that was conducted on the femurs of

62 postmenopausal osteoporotic female patients found that elevated CCL2 levels were linked with decreased BMD (Yang *et al*., 2016). In another study by Wu *et al*., (2020), plasma inflammatory cytokines were investigated in postmenopausal women with osteoporosis and it was discovered that CXCL13 was significantly greater in those with low BMD compared to those with high BMD. These studies, along with previously mentioned studies that link these cytokines to inflammatory and bone-related disorders, suggest that the BMD and BMC reduction seen in the femurs of the Stat6VT mice may have also been cytokine-driven.

5.6 Limitations and future research directions

There were a few pitfalls during the ELISA that we believe contributed to its outcomes. Firstly, we suspect that the small size of the gingival tissue may have led to inaccurate readings. As we were primarily collecting only from the buccal left molar region, we did not maximize our collection of gingival keratinized tissues throughout the entire oral cavity of the mouth. During collection, although the collection was done with the aid of a 2.5 magnifying light microscope, there was also a possibility that non-keratinized tissues were collected as part of the gingival sample, which can lead to unequal amounts of keratinized tissues collected per sample. Furthermore, loricrin is a highly cross-linked protein that can make complete solubilization more difficult to achieve. To ensure the next ELISA experiment will provide more reliable results, future collections should involve all quadrants on the buccal aspect to ensure enough keratinized gingival tissue has been collected. In addition, an alternative homogenizer should be used in order to achieve complete lysis of the tissue sample while still maintaining high protein efficiency.

Our histological investigations helped advance our hypothesis and provided some evidence that supported our theory. More specifically, the loricrin immunofluorescence in both

the longitudinal study and *Pg* study demonstrated a reduced expression in the Stat6VT mice when compared to controls. Cell count analyses of Ki67 and CD45 positive cells enabled us to gain a more accurate understanding of the Ki67 and CD45 immunofluorescence-stained images. Through this work, we were able to more accurately draw the conclusion of an increased inflammatory response occurring in the Stat6VT mice compared to the controls. Future research directions should include a cell count analyses of clear cells and rete pegs for the H&E images. This would enable us to quantify the data, instead of solely relying on a qualitative interpretation. Aside from loricrin, filaggrin would be an ideal CE protein to further investigate the theory of dysfunctional barrier eliciting a heightened immune response, and therefore, future research directions will involve assessing changes in filaggrin in the CE via immunofluorescence. AD has been shown to not only be caused by defects in loricrin but also filaggrin (Bussmann *et al*., 2011; Ishida-Yamamoto *et al*., 1998; O'Regan *et al*., 2008; Schmuth *et al*., 2004). Similar to loricrin, changes in filaggrin can lead to a Th2 response directed towards bacteria as a result of a defect in epidermal barrier function. Furthermore, studies have shown that filaggrin is downregulated in patients with SvP, but not to as great of an extent as loricrin (Guzeldemir-Akcakanat *et al*., 2015; Nowak *et al*., 2013). In the less severe forms of periodontal disease, both loricrin and filaggrin were shown to be downregulated, but again, filaggrin to a lesser extent (Guzeldemir-Akcakanat *et al*., 2015; Nowak *et al*., 2013). These studies suggest that filaggrin is similar to loricrin, in that they both may contribute to a barrier defect that promotes a host inflammatory response to periodontitis.

The microCT protocol utilized in this study has never been used before, therefore, some of the results could not be compared to other available results. MicroCT was used to obtain linear measurements that can only account for isolated bone loss and not intra-bone loss,

therefore, future research can incorporate measurement of volume and density to assess the internal alveolar bone.

A murine model was used to carry out our investigation of loricrin downregulation and its impact on barrier dysfunction in periodontal disease. Although Stat6VT was the most ideal animal model to use for our study, it will not perfectly mimic the conditions of a human oral cavity. Other factors that contribute to periodontal disease in humans, such as plaque and calculus, are not possible to duplicate in a mouse model.

CHAPTER 6: CONCLUSION

Our study aimed to compare the periodontal health of Stat6VT mice with littermate controls and investigate whether loricrin deficiency impacts the oral epithelium, with and without periodontal disease pathogen challenge. Our hypothesis was that the Stat6VT mice, with an impaired epithelial barrier due to loricrin deficiency, would develop an exaggerated immune response and much greater bone loss compared to control mice. To the best of our knowledge, this is the first study using the Stat6VT transgenic mouse model for periodontal research. Our investigations included a cohort of unchallenged mice and *Pg* challenged mice. Both cohorts were subject to bone measurement analyses, cytokine profiling, histology and ELISA. We found that the time points we established (6-8 weeks, 10-13 weeks and 18 weeks) were appropriate for the purpose of our study. Furthermore, our results suggest that *Pg* infection was successfully induced in the Stat6VT and control mice. Overall, Stat6VT male mice demonstrated significantly lower alveolar bone levels and greater signs of inflammation when compared to littermate controls.

Although we gathered a great deal of insightful results, there were limitations in our study and other findings that were gathered along the way that may assist in navigation of future research directions. ELISA required a larger sample of standardized tissue collection in order to accurately quantify the protein amount. We would recommend standardizing collection of tissues from all buccal quadrants of the mouth instead of just one buccal quadrant. We would also recommend using a homogenizer that can achieve complete lysis of the sample. Although both female and male mice were investigated for phenotypical changes, microCT and Faxitron analysis, future research should include ELISA, histology and cytokine profiling for female Stat6VT and control mice.

Despite the limitations faced in the study, Stat6VT when compared to controls, demonstrated increased alveolar bone loss and signs of inflammation in periodontal pathogen challenged and unchallenged conditions. This suggests that loricrin deficiency and its consequentially reduced epithelial barrier may play a vital role in bringing about an overexaggerated host response in the oral cavity. The results suggest that Stat6VT transgenic may be a suitable mouse model for periodontal research and future studies should continue to incorporate this mouse model for investigations that pertain to barrier dysfunction in the oral epithelium and its association to SvP.

REFERENCES

Ackert-Bicknell, C., Beamer, W.G., Rosen, C.J., Sundberg, J.P. (2008). Aging study: Bone mineral density and body composition of 32 inbred strains of mice. *Mouse Phenome Database Web Site. Bar Harbor, ME: The Jackson Laboratory,* https://phenome.jax.org/projects/Ackert1

Agrawal, B., Reddish, M., Longenecker, B.M. (1996). CD30 expression on human CD8+ T cells isolated from peripheral blood lymphocytes of normal donors. *Journal of Immunology, 157*(8), 3229–3234.

Agrawal, R., Woodfolk, J.A. (2014). Skin barrier defects in atopic dermatitis. *Current Allergy Asthma Reports*, 14(5), 433.

Ahmadi, H., Khorramdelazad, H., Hassanshahi, G., Abbasi Fard, M., Ahmadi, Z., Noroozi Karimabad, M., Mollahosseini, M. (2020). Involvement of eotaxins (CCL11, CCL24, CCL26) in pathogenesis of osteopenia and osteoporosis. *Iranian Journal of Public Health*, *49*(9), 1769–1775.

Akhter, M.P., Iwaniec, U.T., Covey, M.A., Cullen, D.M., Kimmel, D.B., Recker, R.R. (2000). Genetic variations in bone density, histomorphometry, and strength in mice. *Calcified Tissue International*, *67*(4), 337–344.

Alam, H., Sehgal, L., Kundu, S.T., Dalal, S.N., Vaidya, M.M. (2011). Novel function of keratins 5 and 14 in proliferation and differentiation of stratified epithelial cells. *Molecular Biology of the Cell*, *22*(21), 4068–4078.

Albandar, J.M. (2014). Aggressive periodontitis: Case definition and diagnostic criteria. *Periodontology 2000*, 65, 13-26.

Allard, J.B., Duan, C. (2018). IGF-binding proteins: Why do they exist and why are there so many?. *Frontiers in Endocrinology*, *9*, 117.

Altin, J. G., & Sloan, E. K. (1997). The role of CD45 and CD45-associated molecules in T cell activation. *Immunology and Cell Biology*, *75*(5), 430–445.

Amano, A., Nakagawa, I., Kataoka, K., Morisaki, I., Hamada, S. (1999). Distribution of Porphyromonas gingivalis strains with fimA genotypes in periodontitis patients. *Journal of Clinical Microbiology*, *37*(5), 1426–1430.

Amarasekara, D.S., Yun, H., Kim, S., Lee, N., Kim, H., Rho, J. (2018). Regulation of osteoclast differentiation by cytokine networks. *Immune Network*, *18*(1), e8.

American Journal of Pathology. (2010). Osteopontin contributes to allergic contact dermatitis. *ScienceDaily*, www.sciencedaily.com/releases/2009/12/091230193136.htm

Amin, S., Riggs, B.L., Atkinson, E.J., Oberg, A.L., Melton, L.J., 3rd, Khosla, S. (2004). A potentially deleterious role of IGFBP-2 on bone density in aging men and women. *Journal of bone and Mineral Research, 19*(7), 1075–1083.

Armitage, G.C. (2002). Classifying periodontal diseases-A long-standing dilemma. *Periodontology 2000*, 30, 9–23.

Armitage, G.C., Cullinan, M.P. (2010) Comparison of the clinical features of chronic and aggressive periodontitis. *Periodontology 2000*, 53, 12–27.

Armstrong, A.W., Read C. (2020). Pathophysiology, clinical presentation, and treatment of psoriasis: A review. *Journal of American Medical Association*, 323(19), 1945–1960.

Azuma, K., Adachi, Y., Hayashi, H., Kubo, K.Y. (2015). Chronic psychological stress as a risk factor of osteoporosis. *Journal of UOEH*, *37*(4), 245–253.

Badersten, A., Nilveus, R., Egelberg, J. (1981). Effect of nonsurgical periodontal therapy in Moderately advanced periodontitis. *Journal of Clinical Periodontology*, 8(1), 57–72.

Bao, L., Mohan, G.C., Alexander, J.B., Doo, C., Shen, K., Bao, J., Chan, L.S. (2017). A molecular mechanism for IL-4 suppression of loricrin transcription in epidermal keratinocytes: implication for atopic dermatitis pathogenesis. *Innate Immunity*, 23(8), 641-647.

Bartova, J., Kratka-Opatrna, Z., Prochazkova J., Krejsa, O., Duskova, J., Mrklas, J., Tlaskalova, H., Cukrowska, B. (2000). Th1 and Th2 cytokine profile in patients with early onset periodontitis and their healthy siblings. *Mediators of Inflammation,* 9(2), 115-120.

Bassyouni, R.H., Ibrehem, E.G., Abd, E.l., Raheem, T.A., Abd El-Malek, M. (2016). The role of osteopontin in skin diseases. *Global Vaccines Immunology*, 1, DOI: 10.15761/GVI.1000114

Berlin-Broner, Y. (2018). *Apical periodontitis as a contributive risk factor for atherosclerosis.* [Master dissertation, University of Alberta]. Education & Research Archives. https://doi.org/10.7939/R38G8G02Z

Bilal, J., Malik, S.U., Riaz, I.B., Kurtzman, D.J.B. (2018). Psoriasis and psoriatic spectrum disease: A primer for the primary care physician. *American Journal of Medicine*. S0002-9343(18)30500-X.

Birajdar, S.S., Radhika, M., Paremala, K., Sudhakara, M., Soumya, M., Gadivan, M. (2014). Expression of Ki-67 in normal oral epithelium, leukoplakic oral epithelium and oral squamous cell carcinoma. *Journal of Oral and Maxillofacial Pathology*, *18*(2), 169–176.

Bruns, H.A., Schindler, U., Kaplan, M.H. (2003). Expression of a constitutively active Stat6 in vivo alters lymphocyte homeostasis with distinct effects in T and B cells. *Journal of Immunology*, 170(7), 3478-87.

Buommino, E., Tufano, M.A., Balato, N., Canozo, N., Donnarumma, M., Gallo, L., Balato, A., & Ayala, F. (2009). Osteopontin: A new emerging role in psoriasis. *Archives of Dermatological Research*, *301*(6), 397–404.

Bussmann, C., Weidinger, S., Novak, N. (2011). Genetics of atopic dermatitis. *Journal der Deutschen Dermatologischen Gesellschaft*, *9*(9), 670–676.

Candi, E., Schmidt, R., Melino, G. (2005). The cornified envelope: A model of cell death in the skin. *Nature Reviews Molecular Cell Biology*, 6, 328-340.

Carlsen, H.S., Baekkevold, E.S., Johansen, F.E., Haraldsen, G., & Brandtzaeg, P. (2002). B cell attracting chemokine 1 (CXCL13) and its receptor CXCR5 are expressed in normal and aberrant gut associated lymphoid tissue. *Gut*, *51*(3), 364–371.

Casarin, R.C.V., Del, P.R., Mariano, F.S., Nociti, F.H., Casati, M.Z., Goncalves, R.B. (2010). Levels of aggregatibacter actinomycetemcomitans, porphyromonas gingivalis, inflammatory cytokines and species-specific immunoglobulin G in generalized aggressive and chronic periodontitis. *Journal of Periodontal Research*, 5, 635-642.

Caton, J., Armitage, G., Berglundh, T., Chapple, I., Jepsen, S., Kornman, K., Mealey, B., Papapanou, P., Sanz, M. (2018). A new classification scheme for periodontal and peri-implant diseases and conditions– Introduction and key changes from the 1999 classification. *Journal of Clinical Periodontology,* 45(Suppl 20), S1–S8.

Caton, J., & Nyman, S. (1980). Histometric evaluation of periodontal surgery. I. The modified Widman flap procedure. *Journal of Clinical Periodontology,* 7(3), 212–23.

Cekici, A., Kantarci, A., Hasturk, H., Van Dyke, T.E. (2014). Inflammatory and immune pathways in the pathogenesis of periodontal disease. *Periodontology 2000,* 64, 57-80.

Chahboun, H., Arnau, M.M., Herrera, D., Sanz, M., Ennibi, O.K. (2015). Bacterial profile of aggressive periodontitis in Morocco: A cross-sectional study. *BMC Oral Health*, 15(25).

Chang, L.C., Kuo, H.C., Chang, S.F., Chen, H.J., Lee, K.F., Lin, T.H., Huang, T.Y., Choe, C.S., Lin, L.T., Chen, C.N. (2013). Regulation of ICAM-1 expression in gingival fibroblasts infected with high-glucose-treated P. gingivalis. *Cellular Microbiology*, *15*(10), 1722–1734.

Chovatiya, R., & Silverberg, J. I. (2019). Pathophysiology of atopic dermatitis and psoriasis: Implications for management in children. *Children (Basel, Switzerland)*, *6*(10), 108.

Christodoulou, N., Weberling, A., Strathdee, D., Anderson, K., Timpson, P., Zernicka-Goets, M. (2019). Morphogenesis of extra-embryogenic tissues directs the remodeling of the mouse embryo at implantation. *Nature Communications,* 10(1), 1-12.

Cizza, G., Primma, S., Coyle, M., Gourgiotis, L., Csako, G. (2010). Depression and osteoporosis: a research synthesis with meta-analysis. *Hormone and Metabolic Research*, *42*(7), 467–482.

Clark, D., Febbraio, M., Levin, L. (2017). Aggressive periodontitis: The unsolved mystery *Quintessence Int*ernational, 48, 103-111

Darlenski, R.K.J., & Tsankov, N. (2011). Skin barrier function: Morphological basis and regulatory mechanisms. *Journal of Clinical Medicine*, 4, 36-45.

DaSilva-Arnold, S.C., Thyagarajan, A., Seymour, L.J., Yi, Q., Bradish, J.R., Al-Hassani, M., Zhou, H., Perdue, N.J., Nemeth, V., Krbanjevic, A., Serezani, A., Olson, M., Spandau, D., Travers, J., Kaplan, M. (2018). Phenotyping acute and chronic atopic dermatitis-like lesions in Stat6VT mice identifies a role for IL-33 in disease pathogenesis. *Archives of Dermatological Research*, 310(3), 197-207.

Del Prete, G., De Carli, M., D'Elios, M.M., Daniel, K.C., Almerigogna, F., Alderson, M., Smith, C.A., Thomas, E., Romagnani, S. (1995). CD30-mediated signaling promotes the development of human T helper type 2-like T cells. *The Journal of Experimental Medicine*, *182*(6), 1655–1661.

DeLeon-Pennell, K.Y., Iyer, R.P., Ero, O.K., Cates, C.A., Flynn, E.R., Cannon, P.L., Jung, M., Shannon, D., Garrett, M.R., Buchanan, W., Hall, M.E., Ma, Y., Lindsey, M.L. (2017). Periodontal-induced chronic inflammation triggers macrophage secretion of Ccl12 to inhibit fibroblast-mediated cardiac wound healing. *JCI insight*, *2*(18), e94207.

Deng, H.W., Xu, F.H., Davies, K.M., Heaney, R., Recker, R.R. (2002). Differences in bone mineral density, bone mineral content, and bone areal size in fracturing and non-fracturing women, and their interrelationships at the spine and hip. *Journal of Bone and Mineral Metabolism*, *20*(6), 358–366.

Dengler-Crish, C.M., Ball, H.C., Lin, L., Novak, K.M., Cooper, L.N. (2018). Evidence of Wnt/β-catenin alterations in brain and bone of a tauopathy mouse model of Alzheimer's disease. *Neurobiology of Aging*, *67*, 148–158.

Dong, M., Yu, X., Chen, W., Guo, Z., Sui, L., Xu, Y., Shang, Y., Niu, W., Kong, Y. (2018). Osteopontin promotes bone destruction in periapical periodontitis by activating the NF-κB pathway. *Cellular Physiology and Biochemistry, 49*(3), 884–898.

Ebbers, M., Lubcke, P., Volzke, J., Kriebel, K., Hieke, C., Engelmann, R., Lang, H., Kreikemeyer, B., Hilke, B. (2018). Interplay between P. gingivalis, F. nucleatum and A. actinomycetemcomitans in murine alveolar bone loss, arthritis onset and progression. *Scientific Reports*, 8(1), p. 15129.

Eberle, J.U., Radtke, D., Nimmerjahn, F., Voehringer, D. (2019). Eosinophils mediate basophil-dependent allergic skin inflammation in mice. *The Journal of Investigative Dermatology*.

Ellis, T.M., Simms, P.E., Slivnick, D.J., Jäck, H.M., Fisher, R.I. (1993). CD30 is a signal-transducing molecule that defines a subset of human activated CD45RO+ T cells. *Journal of Immunology, 151*(5), 2380–2389.

Famili, P., Short, E. (2010). Compliance with periodontal maintenance at the university of Pittsburgh: retrospective analysis of 315 cases. *General Dentistry*, 58(1), e42-e47.

Fang, D. (2020). *A peptide coating preventing the attachment of Porphyromonas gingivalis on the surfaces of dental implants*. [Master dissertation, University of Alberta]. Education & Research Archives. https://doi.org/10.7939/r3-4s5a-5b40

Ferguson, V.L., Ayers, R.A., Bateman, T.A., Simske, S.J. (2003). Bone development and age-related bone loss in male C57BL/6J mice. *Bone*, *33*(3), 387–398.

Figenschau, S.L., Knutsen, E.S., Urbarova, I., Fenton, C., Elston, B., Perander, M., Mortensen, E., & Fenton, K. (2018). ICAM1 expression is induced by proinflammatory cytokines and associated with TLS formation in aggressive breast cancer subtypes. *Scientific Reports, 8*.

Figueredo, C.M., Lira-Junior, R., Love, R.M. (2019). T and B Cells in Periodontal Disease: New Functions in A Complex Scenario. *International Journal of Molecular Sciences*, *20*(16), 3949.

Fisher, M.C., Meyer, C., Garber, G., Dealy, C.N. (2005). Role of IGFBP2, IGF-I and IGF-II in regulating long bone growth. *Bone*, *37*(6), 741–750.

Forootan, S.S., Foster, C.S., Aachi, V.R., Adamson, J., Smith, P.H., Lin, K., Ke, Y. (2006). Prognostic significance of osteopontin expression in human prostate cancer. *International Journal of Cancer*, *118*(9), 2255–2261.

Furlan, P.M., TenHave, T., Cary, M., Zemel, B., Wehrli, F., Katz, I.R., Gettes, D.R., Evans, D.L. (2005). The role of stress-induced cortisol in the relationship between depression and decreased bone mineral density. *Biological Psychiatry*, *57*(8), 911–917.

Gandhi, M., Kothiwale S. (2012). Association of periodontal diseases with genetic polymorphisms. *International Journal of Genetic Engineering and Biotechnology*, 2(3), 19-27.

Gargiulo, S., Gramanzini, M., Megna, R., Greco, A., Albanese, S., Manfredi, C., Brunetti, A. (2014). Evaluation of growth patterns and body composition in C57Bl/6J mice using dual energy X-ray absorptiometry. *BioMed Research International*, *2014*, 253067.

Garlet, G., Martins, W., Ferreira, B., Milanezi. C., Silva, J. (2003). Patterns of chemokines and chemokine receptors expression in different forms of human periodontal disease. *Journal of Periodontal Research,* 38(2), 210-217.

Gattei, V., Degan, M., Gloghini, A., De Iuliis, A., Improta, S., Rossi, F.M., Aldinucci, D., Perin, V., Serraino, D., Babare, R., Zagonel, V., Gruss, H.J., Carbone, A., Pinto, A. (1997). CD30 ligand is frequently expressed in human hematopoietic malignancies of myeloid and lymphoid origin. *Blood*, *89*(6), 2048–2059.

Gautier, J., Slaoui, M., Bauchet, A., Fiette, L., Walker, J. M. (2017). Tissue sampling and processing for histopathology evaluation. *Drug Safety Evaluation*, 1641, 101-114.

Gemmell, E., Walsh, L.J., Savage, N.W., & Seymour, G.J. (1994). Adhesion molecule expression in chronic inflammatory periodontal disease tissue. *Journal of Periodontal Research*, *29*(1), 46–53.

Gonzales, J. R., Gröger, S., Haley, G., Bödeker, R. H., & Meyle, J. (2010). The interleukin-4 -34TT and -590TT genotype is correlated with increased expression and protein production in aggressive periodontitis. *Molecular Immunology*, *47*(4), 701–705.

Gonzales, J. R., Mann, M., Stelzig, J., Bödeker, R. H., & Meyle, J. (2007). Single-nucleotide polymorphisms in the IL-4 and IL-13 promoter region in aggressive periodontitis. *Journal of Clinical Periodontology*, *34*(6), 473–479.

Green, E.B. (2018). The role of CXCL9 and CXCL10 in periodontal bone loss. *UCLA*. ProQuest ID: Green_ucla_0031N_17004. Merritt ID: ark:/13030/m5x39tws. Retrieved from https://escholarship.org/uc/item/8bx4t2gv

Guttman-Yassky, E., Suarez-Farinas, M., Chiricozzi, A., Nograles, K.E., Shemer, A., Fuentes-Duculan, J., Cardinale, I., Lin, P., Bergman, R., Bowcock, A., Kruger, J. (2009). Broad defects in epidermal cornification in atopic dermatitis identified through genomic analysis. *The Journal of Allergy and Clinical Immunology*, 6,1235.

Guzeldemir-Akcakanat, E., Sunnetci-Akkoyunlu, D., Orucguney, B., Cine, N., Kan, B., Yılmaz, E.B., Gümüşlü, E., Savli, H. (2015). Gene Expression Profiles in Generalized Aggressive Periodontitis: A Gene Network-Based Microarray Analysis. *Journal of Periodontology Online*, doi:10.1902/jop.2015.150175.

Hahn, M., & Ghoreschi, K. (2017). The role of IL-4 in psoriasis. *Expert Review of Clinical Immunology*, 13:3,171-173.

Halloran, B., Ferguson, V., Simske, S., Burghardt, A., Venton, L., Majumdar, S. (2002). Changes in bone structure and mass with advancing age in the male C57BL/6J mouse. *Journal of Bone and Mineral Research, 17*.

Harnden, P., Southgate, J. (1997). Cytokeratin 14 as a marker of squamous differentiation in transitional cell carcinomas. *Journal of clinical pathology*, *50*(12), 1032–1033.

Hasegawa, T., Venkata Suresh, V., Yahata, Y., Nakano, M., Suzuki, S., Suzuki, S., Yamada, S., Kitaura, H., Mizoguchi, I., Noiri, Y., Handa, K., & Saito, M. (2021). Inhibition of the CXCL9-CXCR3 axis suppresses the progression of experimental apical periodontitis by blocking macrophage migration and activation. *Scientific Reports*, *11*(1), 2613.

Herbert, B.A., Novince, C.M., Kirkwood, K.L. (2016). Aggregatibacter actinomycetemcomitans, a potent immunoregulator of the periodontal host defense system and alveolar bone homeostasis. *Molecular Oral Microbiology*, 31(3), 207-227.

Hohl, D., Mehrel, T., Lichti, U., Turner, M.L., Roop, D.R., Steinert, P.M. (1991). Characterization of human loricrin. structure and function of a new class of epidermal cell envelope proteins. *Journal of Biological Chemistry*, 266, 6626-36.

Holmstrup, P., Damgaard, C., Olsen, I., Klinge, B., Flyvbjerg, A., Nielsen, C.H., Hansen, P.R. (2017). Comorbidity of periodontal disease: two sides of the same coin? An introduction for the clinician. *Journal of Oral Microbiology*, 14, 9(1), 1332710.

Hoshino, A., Hanada, S., Yamada, H., Mii, S., Takahashi, M., Mitarai, S., Yamamoto, K., Manome, Y. (2014). Mycobacterium tuberculosis escapes from the phagosomes of infected human osteoclasts reprograms osteoclast development via dysregulation of cytokines and chemokines. *Pathogens and Disease*, *70*(1), 28–39.

Hoste, E., Denecker, G., Gilbert, B., Van Nieuwerburgh, F., van der Fits, L., Asselbergh, B., De Rycke, R., Hachem, J.P., Deforce, D., Prens, E.P., Vandenabeele, P., Declercq, W. (2013). Caspase-14-deficient mice are more prone to the development of parakeratosis. *The Journal of Investigative Dermatology*, *133*(3), 742–750.

Hou, J., Schindler, U., Henzel, W.J., Ho, T., Brasseur, M., McKnight, M.L. (1994). An interleukin-4-induced transcription factor: IL-4 Stat. *Science,* 265, 1701.

Howell, M.D., Gao, P., Kim, B.E., Lesley, L.J., Streib, J.E., Taylor, P.A., Zaccaro, D.J., Boguniewicz, M., Beck, L.A., Hanifin, J.M., Schneider, L.C., Hata, T.R., Gallo, R.L., Kaplan, M.H., Barnes, K.C., Leung, D.Y. (2011). The signal transducer and activator of transcription 6 gene (STAT6) increases the propensity of patients with atopic dermatitis toward disseminated viral skin infections. *The Journal of Allergy and Clinical Immunology*, *128*(5), 1006–1014.

Hulshof, L., Overbeek, S.A., Wyllie, A.L., Chu, M., Bogaert, D., De Jager, W., Knippels, L., Sanders, E., Van Aalderen, W., Garssen, J., Van't Land, B., Sprikkelman, A.B., Clinical Study Group (2018). Exploring immune development in infants with moderate to severe atopic dermatitis. *Frontiers in Immunology*, *9*, 630.

Ishida-Yamamoto, A., Takahashi, H., Iizuka, H. (1998). Loricrin and human skin diseases: Molecular basis of loricrin keratodermas. *Histology and Histopathology*, *13*(3), 819–826.

Jacob, J.T., Coulombe, P.A., Kwan, R., Omary, M.B. (2018). Types I and II keratin intermediate filaments. *Cold Spring Harbor Perspectives in Biology*, *10*(4), a018275.

Jambu, M. (1991). *Exploratory and multivariate data analysis*. Academic Press (Statistical Modelling and Decision Science).

Jarnik, M., de Viragh, P.A., Scharer, E., Bundman, D., Simon, M.N., Roop, D.R., Steven, A.C. (2002). Quasi-normal cornified cell envelopes in loricrin knockout mice imply the existence of a loricrin backup system. *Journal of Investigative Dermatology,* 118(1), 102-109.

Jeong, Y. H., Oh, Y.C., Cho, W.K., Yim, N.H., Ma, J.Y. (2019). Hoveniae semen seu fructus ethanol extract exhibits anti-inflammatory activity *via* MAPK, AP-1, and STAT signaling pathways in LPS-stimulated RAW 264.7 and mouse peritoneal macrophages. *Mediators of inflammation*, *2019*, 9184769.

Jilka R.L. (2013). The relevance of mouse models for investigating age-related bone loss in humans. *The Journals of Gerontology, 68*(10), 1209–1217.

Kantarci, A., Nseir, Z., Kim, Y.S., Sume, S.S., Trackman, P.C. (2011). Loss of basement membrane integrity in human gingival overgrowth. *Journal of Dental Research*, *90*(7), 887–893.

Kaplan, M.H., Sehra, S., Chang, H.C., O'Malley, J.T., Mathur, A.N., Bruns, H.A. (2007). Constitutively active STAT6 predisposes toward a lymphoproliferative disorder. *Blood.* 110(13), 4367-4369.

Kalinin, A., Marekov, L.N., Steinert, P.M. (2001). Assembly of the epidermal cornified cell envelope. *Journal of Cell Science*. 114, 3069-70.

Kayal, R.A. (2013). The role of osteoimmunology in periodontal disease. *BioMed research international*, *2013*, 639368.

Khosla S. (2013). Pathogenesis of age-related bone loss in humans. *The Journals of Gerontology*, *68*(10), 1226–1235.

Kim, B.E., Leung, D.Y., Boguniewicz, M., Howell, M.D. (2008). Loricrin and involucrin expression is down-regulated by Th2 cytokines through STAT-6. *Clinical Immunology,* 126(3), 332–337.

Kim, M., Lee, S.H., Kim, Y., Kwon, Y., Park, Y., Lee, H.K., Jung, H.S., & Jeoung, D. (2018). Human adipose tissue-derived mesenchymal stem cells attenuate atopic dermatitis by regulating the expression of MIP-2, miR-122a-SOCS1 axis, and Th1/Th2 responses. *Frontiers in Pharmacology*, *9*, 1175.

Kim, S., Park, S., Park, Y., Myung, D., Rew, J., Joo, Y. (2017). Chlorogenic acid suppresses lipopolysaccharide-induced nitric oxide and interleukin-1β expression by inhibiting

JAK2/STAT3 activation in RAW264.7 cells. *Molecular Medicine Reports*, 16, 9224-9232.

Klein, R.F., Mitchell, S.R., Phillips, T.J., Belknap, J.K., Orwoll, E.S. (1998). Quantitative trait loci affecting peak bone mineral density in mice. *Journal of Bone and Mineral Research*, *13*(11), 1648–1656.

Koch, P.J., Viragh, P.A., Scharer, E., Bundman, D., Longley, M.A., Bickenbach, J., Kawachi, Y., Suga, Y., Zhou, Z., Huber, M., Hohl, D., Kartasova, T., Jarnik, M., Steven, A., Roop. (2000). Lessons from loricrin-deficient mice: Compensatory mechanisms maintaining skin barrier function in the abscence of a major cornified envelope protein. *Journal of Cell Biology,* 151:389-400.

Kotanides, H., Reich, N. (1993). Requirement of tyrosine phosphorylation for rapid activation of a DNA binding factor by IL-4. *Science,* 262, 1265.

Kuan, W.P., Tam, L.S., Wong, C.K., Ko, F.W., Li, T., Zhu, T., Li, E. K. (2010). CXCL 9 and CXCL 10 as sensitive markers of disease activity in patients with rheumatoid arthritis. *The Journal of Rheumatology*, *37*(2), 257–264.

Kumar, K.V., Chaithanya, K.H., Punde, P., Thorat, A., Jangam, A.G., Deepthi, S. (2015) Comparative evaluation of immunohistochemical expression of Ki-67 in oral lichen planus, oral leukoplakia and normal mucosa cases. *Journal of International Oral Health, 7(10), 82-87.*

Lappin, D.., Macleod, C., Kerr, A., Mitchell, T., Kinane, D. (2001). Anti-inflammatory cytokine IL-10 and T cell cytokine profile in periodontitis granulation tissue. *Clinical & Experimental Immunology*, 123(2), 294-300.

Lee, E.N., Park, J.K., Lee, J.R., Oh, S.O., Baek, S.Y., Kim, B.S., Yoon, S. (2011). Characterization of the expression of cytokeratins 5, 8, and 14 in mouse thymic epithelial cells during thymus regeneration following acute thymic involution. *Anatomy & Cell Biology*, *44*(1), 14–24.

Li, D., Feng, Y., Tang, H., Huang, L., Tong, Z., Hu, C., Chen, X., Tan, J. (2020). A simplified and effective method for generation of experimental murine periodontitis model. *Frontiers in Bioengineering and Biotechnology*, *8*, 444.

Liu, G., Deng, J., Zhang, Q., Song, W., Chen, S., Lou, X., Zhang, P., Pan, K. (2016). Porphyromonas gingivalis lipopolysaccharide stimulation of vascular smooth muscle cells activates proliferation and calcification. *Journal of Periodontology*, *87*(7), 828–836.

Liu, Z., Liang, W., Kang, D., Chen, Q., Ouyang, Z., Yan, H., Huang, B., Jin, D., Chen, Y., & Li, Q. (2020). Increased osteoblastic Cxcl9 contributes to the uncoupled bone formation and resorption in postmenopausal osteoporosis. *Clinical Interventions in Aging*, *15*, 1201–1212.

Lübcke, P.M., Ebbers, M.N.B., Volzke, J., Kneitz, S., Engelmann, R., Lang, H., Kreikemeyer, B., Hilk, B. (2019). Periodontal treatment prevents arthritis in mice and methotrexate ameliorates periodontal bone loss. *Scientific Reports,* 9, 8128(2019)

Lund, S.A., Giachelli, C.M., Scatena, M. (2009). The role of osteopontin in inflammatory processes. *Journal of Cell Communication and Signaling*, *3*(3-4), 311–322.

Manetti, R., Annunziato, F., Biagiotti, R., Giudizi, M.G., Piccinni, M.P., Giannarini, L., Sampognaro, S., Parronchi, P., Vinante, F., Pizzolo, G., Maggi, E., Romagnani, S. (1994). CD30 expression by CD8+ T cells producing type 2 helper cytokines. Evidence for large numbers of CD8+CD30+ T cell clones in human immunodeficiency virus infection. *The Journal of Experimental Medicine*, *180*(6), 2407–2411.

Manhart, S.S., Reinhardt, R.A., Payne, J.B., Seymour, G.J., Gemmell, E., Dyer JK, Pretro, T.M. (1994). Gingival cell IL-2 and IL-4 in early-onset periodontitis. *Journal of Periodontology*, 65(9), 807–813.

Marchesan, J., Girnary, M.S., Jing, L., Miao, M.Z., Zhang, S., Sun, L., Morelli, T., Schoenfisch, M.H., Inohara, N., Offenbacher, S., Jiao, Y. (2018). An experimental murine model to study periodontitis. *Nature Protocols*, *13*(10), 2247–2267.

McHugh M.L. (2012). Interrater reliability: the kappa statistic. *Biochemia Medica*, *22*(3), 276–282.

Menzies-Gow, A., Ying, S., Sabroe, I., Stubbs, V.L., Soler, D., Williams, T. J., Kay, A.B. (2002). Eotaxin (CCL11) and eotaxin-2 (CCL24) induce recruitment of eosinophils, basophils, neutrophils, and macrophages as well as features of early- and late-phase allergic reactions following cutaneous injection in human atopic and nonatopic volunteers. *Journal of Immunology, 169*(5), 2712–2718.

Mezuk, B., Eaton, W.W., Golden, S.H. (2008). Depression and osteoporosis: epidemiology and potential mediating pathways. *Osteoporosis International*, *19*(1), 1–12.

Müller N. (2019). The Role of intercellular adhesion molecule-1 in the pathogenesis of psychiatric disorders. *Frontiers in Pharmacology*, *10*, 1251.

Muñoz, J., Akhavan, N.S., Mullins, A.P., & Arjmandi, B.H. (2020). Macrophage polarization and osteoporosis: A review. *Nutrients*, *12*(10), 2999.

Myneni, S. R., Settem, R. P., Connell, T. D., Keegan, A. D., Gaffen, S. L., & Sharma, A. (2011). TLR2 signaling and Th2 responses drive Tannerella forsythia-induced periodontal bone loss. *Journal of Immunology, 187*(1), 501–509.

Nakka, S.S. (2016). Development of novel tools for prevention and diagnosis of Porphyromonas gingivalis infection and periodontitis, *Örebro university*.

Nakajima, T., Amanuma, R., Ueki-Maruyama, K., Oda, T., Honda, T., Ito, H., Yamazaki, K. (2008). CXCL13 expression and follicular dendritic cells in relation to B-cell infiltration in periodontal disease tissues. *Journal of Periodontal Research*, *43*(6), 635–641.

Nakib, S., Han, J., Li, T., Joshipura, K., Qureshi, A.A. (2013). Periodontal disease and risk of psoriasis among nurses in the United States. *Acta Odontologica Scandinavica*, 71(6), 1423-9.

Nemes, Z., Steinert, P.M. (1999). Bricks and mortar of the epidermal barrier. *Experimental & Molecular Medicine*. 31(1), 5-19.

Nibali, L. (2015). Aggressive Periodontitis: microbes and host response, who to blame? *Virulence*. 6(3), 223-228.

Nithya, S., Radhika, T., Jeddy, N. (2015). Loricrin - An overview. *Journal Oral Maxillofacial Pathology.* 19(1),64-68.

Nowak, M., Kramer, B., Haupt, M., Papapanou, P.N., Kebschull, J., Hoffmann, P., Schmidt-Wolf, I.G., Jepsen, S., Brossart, P., Perner, S., Kebschull, K. (2013). Activation of Invariant NK T Cells in Periodontitis Lesions. *Journal of Immunology*, 190, 2282-2291.

Nutten, S. (2015). Atopic dermatitis: Global epidemiology and risk factors. *Annals of Nutrition and Metabolism*. 66, Suppl, 1, 8-16.

O'Driscoll, J., Muston, G.C., McGrath, J.A., Lam, H.M., Ashworth, J., Christiano, A.M. (2002). A recurrent mutation in the loricrin gene underlies the ichthyotic variant of vohwinkel syndrome. *Clinical Experimental Dermatology*, 27, 243-46.

O'Regan, G.M., Sandilands, A., McLean, W., Irvine, A.D. (2008). Filaggrin in atopic dermatitis. *The Journal of Allergy and Clinical Immunology*, *122*(4), 689–693.

Owczarek, W., Paplińska, M., Targowski, T., Jahnz-Rózyk, K., Paluchowska, E., Kucharczyk, A., Kasztalewicz, B. (2010). Analysis of eotaxin 1/CCL11, eotaxin 2/CCL24 and eotaxin 3/CCL26 expression in lesional and non-lesional skin of patients with atopic dermatitis. Cytokine, 50(2), 181–185.

Painsi, C., Hirtenfelder, A., Lange-Asschenfeldt, B., Quehenberger, F., Wolf, P. (2017). The prevalence of periodontitis is increased in psoriasis and linked to its inverse subtype. Skin Pharmacology and Physiology, 30(6), 324-328, doi: 10.1159/000481544.

Pan, W., Wang, Q. & Chen, Q. (2019). The cytokine network involved in the host immune response to periodontitis. *International Journal of Oral Science,* 11, 30, https://doi.org/10.1038/s41368-019-0064-z

Park, C.H., Abramson, Z.R., Taba, M., Jr, Jin, Q., Chang, J., Kreider, J.M., Goldstein, S.A., Giannobile, W.V. (2007). Three-dimensional micro-computed tomographic imaging of

alveolar bone in experimental bone loss or repair. *Journal of Periodontology*, *78*(2), 273–281.

Park, H., Park, Y., Hong, J., Kim, K., & Sohn, M. (2011). Clinical implication of serum CXCL13 in children with atopic dermatitis: 522. *The Journal of Allergy and Clinical Immunology*, 127(2 Suppl), AB138.

Payne, J.B., Reinhardt, R.A., Nummikoski, P.V., Patil, K.D. (1999). Longitudinal alveolar bone loss in postmenopausal osteoporotic/osteopenic women. *Osteoporosis International, 10*(1), 34–40.

Proksch, E., Brandner, J.M., Jensen, J. (2008). The skin: An indispensable barrier. *Experimental Dermatology*. 17, 1063-72.

Pyun, B.Y. (2015). Natural history and risk factors of atopic dermatitis in children. *Allergy Asthma Immunology Research*, 7(2), 101-105.

Reichrath, J., Holick, M. (2011). *Vitamin D*. Academic Press. https://doi.org/10.1016/B978-0-12-381978-9.10097-6

Rice, R.H., Durbin-Johnson, B.P., Ishitsuka, Y., Salemi, M., Phinney, B.S., Rocke, D.M., Roop, D.R. (2016). Proteomic Analysis of Loricrin Knockout Mouse Epidermis. *Journal of Proteome Research,* 15(8), 2560-2566.

Ross, M. (2006). *Histology: A text and atlas: With correlated cell and molecular biology*. Lippincott Wiliams & Wilkins. 10.26641/1997-9665.2019.4.76-89

Roth, W., Kumar, V., Beer, H.D., Richter, M., Wohlenberg, C., Reuter, U., Thiering, S., Staratschek-Jox, A., Hofmann, A., Kreusch, F., Schultze, J.L., Vogl, T., Roth, J., Reichelt, J., Hausser, I., Magin, T.M. (2012). Keratin 1 maintains skin integrity and participates in an inflammatory network in skin through interleukin-18. *Journal of Cell Science*, *125*(Pt 22), 5269–5279.

Sabroe, I., Williams, P. (2006). EOTAXINS. *Encyclopedia of Respiratory Medicine*, Four-Volume Set, 125–129.

Saito, T., Nakajima, T., Mogi, K. (1999). Immunohistochemical analysis of cell cycle-associated proteins p16, pRb, p53, p27 and Ki-67 in oral cancer and precancer with special reference to verrucous carcinomas. *Journal of Oral Pathology & Medicine*, *28*(5), 226–232.

Sarac, G., Kapicioglu, Y., Cayli ,S., Altas, A., Yologlu, S. (2017). Is the periodontal status a risk factor for the development of psoriasis? *Nigerian Journal of Clinical Practice*, 20(4), 474-478.

Schenkein, H.A., Best, A.M., Brooks, C.N., Burmeister, J.A., Arrowood, J.A., Kontos, M.C., Tew, J.G. (2007). Anti-cardiolipin and increased serum adhesion molecule levels in patients with aggressive periodontitis. *Journal of Periodontology*, *78*(3), 459–466.

Schmuth, M., Fluhr, J.W., Crumrine, D.C., Uchida, Y., Hachem, J.P., Behne, M., Moskowitz, D.G., Christiano, A.M., Feingold, K.R., Elias, P.M. (2004). Structural and functional consequences of loricrin mutations in human loricrin keratoderma (Vohwinkel syndrome with ichthyosis). *The Journal of Investigative Dermatology*, *122*(4), 909–922.

Schork, N.J., Fallin, D., Lanchbury, J.S. (2000). Single nucleotide polymorphisms and the future of genetic epidemiology. *Clinical Genetics*, 58(4), 250-64.

Sehra, S., Bruns, H.A., Ahyi, A.N., Nguyen, E.T., Schmidt, N.W., Michels, E.G., Bulow, G.U., Kaplan, M.H. (2008). IL-4 is a critical determinant in the generation of allergic inflammation initiated by a constitutively active Stat6. *Journal of Immunology,* 180, 3551-3559.

Sehra, S., Krishnamurthy, P., Koh, B., Zhou, H., Seymour, L., Akhtar, N, Travers, J., Tuner, M., Kaplan, M. (2016). Increased Th2 activity and diminished skin barrier function cooperates in allergic skin inflammation. *European Journal of Immunology*, 46(11):2609-2613.

Settem, R.P., Honma, K., Sharma, A. (2014). Neutrophil mobilization by surface-glycan altered Th17-skewing bacteria mitigates periodontal pathogen persistence and associated alveolar bone loss. *PLoS ONE,* 9(9), e108030.

Seymour, G.J., Gemmell, E., Reinhardt, R.A. (1993). Immunopathogenesis of chronic inflammatory periodontal disease: cellular and molecular mechanisms. *Journal of Periodontal Research,* 28, 478-486.

Sharma, C.G., Pradeep, A.R. (2006). Gingival crevicular fluid osteopontin levels in periodontal health and disease. *Journal of Periodontology*, *77*(10), 1674–1680.

Shimada, Y., Takehara, K., Sato, S. (2004). Both Th2 and Th1 chemokines (TARC/CCL17, MDC/CCL22, and Mig/CXCL9) are elevated in sera from patients with atopic dermatitis. Journal of Dermatological Science, 34(3), 201–208.

Silva, T.A., Garlet, G.P., Fukada, S.Y., Silva, J.S., Cunha, F.Q. (2007). Chemokines in oral inflammatory diseases: Apical periodontitis and periodontal disease. *Journal of Dental Research*, *86*(4), 306–319.

Singh, A., Gill, G., Kaur, H., Amhmed, M., Jakhu, H. (2018). Role of osteopontin in bone remodeling and orthodontic tooth movement: a review. *Progress in Orthodontics*, *19*(1), 18.

Smith, C.A., Gruss, H.J., Davis, T., Anderson, D., Farrah, T., Baker, E., Sutherland, G.R., Brannan, C.I., Copeland, N.G., Jenkins, N.A. (1993). CD30 antigen, a marker for Hodgkin's lymphoma, is a receptor whose ligand defines an emerging family of cytokines with homology to TNF. *Cell*, *73*(7), 1349–1360.

Son, E.D., Kim, H.J., Kim, K.H., Bin, B.H., Bae, I.H., Lim, K.M., Yu, S.J., Cho, E.G., Lee, T.R. (2016). S100A7 (psoriasin) inhibits human epidermal differentiation by enhanced IL-6 secretion through IκB/NF-κB signalling. *Experimental Dermatology*, 25(8), 636-41.

Srinivasan, M., Kodumudi, K.N., Galli, D.M. (2010). Aggregatibacter actinomycetemcomitans modulates toll-like receptors 2 and 4 in gingival epithelial cells in experimental periodontitis. *Journal of International Clinical Dental Research Organisation*, 2, 24-9.

Steinert, P.M., Kartasova, T., Marekov, L. (1998). Biochemical evidence that small proline-rich proteins and trichohyalin function in epithelia by modulation of the biomechanical properties of their cornified cell envelopes. *Journal of Biological Chemistry*, 273:11758-69.

Steinert, P.M., Marekov, L.N. (1995). The proteins elafin, filaggrin, keratin intermediate filaments, loricrin, and small proline-rich proteins 1 and 2 are isodipeptide cross-linked components of the human epidermal cornified cell envelope. *Journal of Biological Chemistry*, 17702-11.

Steven, A.C., Steinert, P.M. (1994). Protein composition of cornified cell envelopes of epidermal keratinocytes. *Journal of Cell Science*, 107:693-700.

Su, N.Y., Huang, J.Y., Hu, C.J., Yu, H.C., Chang, Y.C. (2017). Increased risk of periodontitis in patients with psoriatic disease: a nationwide population-based retrospective cohort study. *Peer Journal,* doi: 10.7717/peerj.4064.

Susin, C., Haas, A.N., Albandar, J.M. (2014). Epidemiology and demographics of aggressive periodontitis. *Periodontology 2000*. 65, 27-45.

Suzuki, N., Yoneda, M., Hirofuji, T. (2013). Mixed red-complex bacterial infection in periodontitis. *International Journal of Dentistry*, 587279. https://doi.org/10.1155/2013/587279

Takkem, A., Barakat, C., Zakaraia, S., Zaid, K., Najmeh, J., Ayoub, M., Seirawan, M.Y. (2018). Ki-67 Prognostic value in different histological grades of oral epithelial dysplasia and oral Squamous cell carcinoma. *Asian Pacific Journal of Cancer Prevention*, *19*(11), 3279–3286.

Tapashetti, R.P., Sharma, S., Patil, S.R., Guvva, S. (2013). Potential effect of neutrophil functional disorders on pathogenesis of aggressive periodontitis. *Journal of Contemporary Dental Practice*, 14(3), 387-393.

Tonetti, M.S., Jepsen, S., Jin, L., Otomo-Corgel, J. (2017). Impact of the global burden of periodontal diseases on health, nutrition and wellbeing of mankind: A call for global action. *Journal of Clinical Periodontology,* 44(5), 456–62.

Turner, M.J., DaSilva-Arnold, S., Luo, N., Hu, X., West, C.C., Sun, L., Hill, C., Bradish, J., Kaplan, M.H., Travers, J.B., Sun, Y. (2014). STAT6-mediated keratitis and blepharitis: a

novel murine model of ocular atopic dermatitis. *Investigative Ophthalmology & Visual Science*, *55*(6), 3803–3808. https://doi.org/10.1167/iovs.13-13685

Van Coillie, E., Van Damme, J., Opdenakker, G. (1999). The MCP/eotaxin subfamily of CC chemokines. *Cytokine & growth Factor Reviews*, *10*(1), 61–86.

Van Der Weyden, C.A., Pileri, S.A., Feldman, A.L., Whisstock, J., Prince, H.M. (2017). Understanding CD30 biology and therapeutic targeting: a historical perspective providing insight into future directions. *Blood Cancer Journal*, *7*(9), e603.

Vieira, A.R., Albandar, J.M. (2014). Role of genetic factors in the pathogenesis of aggressive periodontitis. *Periodontology 2000,* 65:92-106.

Wilensky, A., Gabet, Y., Yumoto, H., Houri-Haddad, Y., Shapira, L. (2005). Three-dimensional quantification of alveolar bone loss in Porphyromonas gingivalis-infected mice using micro-computed tomography. *Journal of periodontology*, *76*(8), 1282–1286.

Williams, L., Pasco, J., Jackson, H., Kiropoulos, L.A., Stuart, A.L., Jacka, F., & Berk, M. (2016). Depression as a risk factor for fracture in women: A 10-year longitudinal study. *Journal of Affective Disorders, 192*, 34-40.

Wippert, P.M., Rector, M., Kuhn, G., Wuertz-Kozak, K. (2017). Stress and Alterations in Bones: An Interdisciplinary Perspective. *Frontiers in Endocrinology*, *8*, 96.

Wu, L.F., Wang, W.Y., Zhu, D.C., He, P., Zhu, K., Gui, G.P., Gao, H.Q., Mo, X.B., Lu, X., Deng, F.Y., & Lei, S.F. (2020). Protein array test detected three osteoporosis related plasma inflammatory cytokines in Chinese postmenopausal women. *Cytokine*, *133*, 155166.

Wu, Y.H., Kuraji, R., Taya, Y., Ito, H., Numabe, Y. (2018). Effects of theaflavins on tissue inflammation and bone resorption on experimental periodontitis in rats. *Journal of Periodontal Research*, *53*(6), 1009–1019.

Wuertz-Kozak, K., Roszkowski, M., Cambria, E., Block, A., Kuhn, G. A., Abele, T., Hitzl, W., Drießlein, D., Müller, R., Rapp, M.A., Mansuy, I.M., Peters, E., Wippert, P.M. (2020). Effects of Early Life Stress on Bone Homeostasis in Mice and Humans. *International Journal of Molecular Sciences*, *21*(18), 6634.

Xi, G., Wai, C., DeMambro, V., Rosen, C.J., & Clemmons, D.R. (2014). IGFBP-2 directly stimulates osteoblast differentiation. *Journal of Bone and Mineral Research*, *29*(11), 2427–2438.

Xu, W., Pan, Y., Xu, Q., Wu, Y., Pan, J., Hou, J., Lin, L., Tang, X., Li, C., Liu, J., Zhang, D. (2018). Porphyromonas gingivalis ATCC 33277 promotes intercellular adhesion molecule-1 expression in endothelial cells and monocyte-endothelial cell adhesion through macrophage migration inhibitory factor. *BMC Microbiology*, *18*(1), 16

Yang, X.W., Wang, X.S., Cheng, F.B., Wang, F., Wan, L., Wang, F., Huang, H.X. (2016). Elevated CCL2/MCP-1 levels are related to disease severity in postmenopausal osteoporotic patients. *Clinical Laboratory*, *62*(11), 2173–2181.

Yamazaki, K., Nakajima, T., Gemmell, E., Polak, B., Seymour, G., Hara, K. (1992). Il-4- and IL-6-producing cells in human periodontal disease tissue. *Journal of Oral Pathological Medicine*. 23(8), 347-353.

Yoshida, K., Sato, K., Tonogi, M., Tanaka, Y., Yamane, G.Y., Katakura, A. (2015). Expression of cytokeratin 14 and 19 in process of oral carcinogenesis. *The Bulletin of Tokyo Dental College*, *56*(2), 105–111.

Yu, T., Gan, S., Zhu, Q., Dai, D., Li, N., Wang, H., Chen, X., Hou, D., Wang, Y., Pan, Q., Xu, J., Zhang, X., Liu, J., Pei, S., Peng, C., Wu, P., Romano, S., Mao, C., Huang, M., Zhu, X., Xiao, Y. (2019). Modulation of M2 macrophage polarization by the crosstalk between Stat6 and Trim24. *Nature Communications*, *10*(1), 4353.

Yuan, H., Zelkha, S., Burkatovskaya, M., Gupte, R., Leeman, S.E., Amar, S. (2013). Pivotal role of NOD2 in inflammatory processes affecting atherosclerosis and periodontal bone loss. *Proceedings of the National Academy of Sciences of the United States of America*, *110*(52), E5059–E5068.

Yue, D., You, Y., Zhang, X., Wang, B., Wang, X., Qi, R., Yang, F., Meng, X., Yoshikai, Y., Wang, Y., Sun, X. (2019). CD30L/CD30 protects against psoriasiform skin inflammation by suppressing Th17-related cytokine production by Vγ4+ γδ T cells. *Journal of Autoimmunity, 101*, 70-85.

Zein Elabdeen, H. R., Mustafa, M., Ali, R., & Bolstad, A. I. (2017). Cytokine profile in gingival crevicular fluid and plasma of patients with aggressive periodontitis. *Acta odontologica Scandinavica*, 75(8), 616–622. https://doi.org/10.1080/00016357.2017.137262

Zhang, L., Meng, S., Tu, Q., Yu, L., Tang, Y., Dard, M.M., Kim, S.H., Valverde, P., Zhou, X., Chen, J. (2014). Adiponectin ameliorates experimental periodontitis in diet-induced obesity mice. *PloS One*, *9*(5), e97824.

Zhang, Y., Syed, R., Hart, T., Uygar, C., Pallos, D., Gorry, M., Firatli, E., Cortelli, J., VanDyke, T., Hart, P. (2003). Evaluation of human leukocyte N-formylpeptide receptor (FPR1) SNPs in aggressive periodontitis patients. *Genes Immunology*, 4(1), 22-29.

Zheng, C., Wu, J., & Xie, H. (2011). Differential expression and adherence of Porphyromonas gingivalis FimA genotypes. *Molecular Oral Microbiology*, *26*(6), 388–395.

Zhou, Q., Amar, S. (2006). Identification of proteins differentially expressed in human monocytes exposed to Porphyromonas gingivalis and its purified components by high-throughput immunoblotting. *Infection and Immunity*, *74*(2), 1204–1214.